Analysis of hydro-pneumatic interconnected suspension struts in the roll plane vehicle model

Liwen Wu

A Thesis

in

The Department

of

Mechanical and Industrial Engineering

Presented in Partial Fulfillment of the Requirements
for the Degree of Master of Applied Science (Mechanical Engineering)
at Concordia University
Montreal, Quebec, Canada

May 2003

Your file Votre référence
ISBN: 0-612-83887-0
Our file Notre référence
ISBN: 0-612-83887-0

ABSTRACT

ANALYSIS OF HYDRO-PNEUMATIC INTERCONNECTED SUSPENSION STRUTS IN THE ROLL PLANE VEHICLE MODEL

Liwen Wu

Design of passive suspension systems for road vehicles invariably involves complex compromise between ride, handling and directional control performance characteristics. While a soft suspension is desired to enhance ride quality, hard suspension springs are required to achieve good handling and directional control performance. Auxiliary roll stiffness, in conjunction with soft suspension, are frequently used to attain an acceptable compromise between ride and handling performance of a vehicle. Alternatively, hydro-pneumatic suspension struts interconnected in the roll plane have been proposed to realize soft vertical ride and enhanced anti-roll properties. Such hydro-pneumatic struts often require high charge pressure and large working area to achieve desired load carrying capacity, and vertical and roll properties. This dissertation research is focussed on analysis of a compact strut design with considerably larger working area to reduce the design pressure requirement. Furthermore, unlike the reported configurations with an external gas accumulator, the strut design considered in this study integrates the gas chamber within main cylinders.

A four-degrees-of-freedom roll plane model of a heavy highway vehicle is developed to investigate the ride and anti-roll properties of two different hydro-pneumatic strut designs, unconnected and interconnected in the roll plane. Three different interconnections, involving flows across different chambers of the right-

and left- compact struts, are realized for the analyses. The analytical models are solved to derive the static and dynamic properties of various unconnected and interconnected configurations in terms of vertical spring rate, effective vertical mode damping, effective roll stiffness and roll mode damping. From the results it is concluded that roll plane interconnection of the suspension struts offers considerably potential for enhancing the anti-roll properties, with insignificant influence on the vertical ride properties.

The analytical models are further analyzed under deterministic and random vertical road and roll moment arising from directional maneuvers. The relative performance potentials of interconnected suspensions are presented in terms of vertical and roll acceleration transmissibility under a harmonic excitation transient vertical and roll responses under a transient road bump and roll moment excitations, and power spectral densities and RMS values of the sprung mass responses to random road excitation. The results show that interconnecting the lower chamber of right-strut to the upper chamber of the left strut, and vice versa, offers considerably potential for realizing improved anti-roll and ride performances.

ACKNOWLEDGEMENTS

The work described in this thesis was carried out in the Concordia University Mechanical Engineering department between January 2001 and May 2003.

I would like to thank Dr. Subhash Rakheja, who suggested and supervised this thesis, and who contribute his ideas, experience, encouragement and energy.

I am also very grateful to Chunyi Su, my co-supervisor, who enthusiastically and generously sharing his knowledge.

The author would also like to thank the members of the faculty, staff and students of the CONCAVE Research Centre, Department of Mechanical Engineering, Concordia University, for their time and assistance during the evolution of this work.

I would also like to thank my family and all my good friends, whose friendship and support throughout this thesis were invaluable.

TABLE OF CONTENTS

LIST OF FIGURES

LIST OF TABLES

NOMENCLATURE

SYMBOL	DESCRIPTION
$a_\ell; a_r$	orifice area of the left and right struts.
$a_{12\ell}; a_{12r}$	orifice area between chamber 1 and 2 of the left and right struts.
$a_{13\ell}; a_{13r}$	orifice area between chamber 1 and 3 of the left and right struts.
a_y	lateral acceleration of the roll motion.
$A_{1j}\ (j = \ell, r)$	piston head areas on the chamber 1 sides of the left and right struts
$A_{2j}\ (j = \ell, r)$	piston head area on the chamber 2
A_2	effective working area of the strut
$A_{3j}\ (j = \ell, r)$	piston head areas on the chamber 3 side of the left and right struts
A_r	piston rod area
$c_{t\ell}, c_{tr}$	viscous damping coefficient of left and right tire, respectively
C_d	discharge coefficient
d	diameter of the anti-roll bar
di	distance along the road
F_1, F_2	forces developed by the actuators
F_b	vertical elastic force of the anti-roll bar
$F_\ell; F_r$	dynamic forces developed by the left and right struts
$F_{d\ell}; F_{dr}$	damping force of left and right strut
$F_{s\ell}; F_{sr}$	restoring force of left and right strut
g	acceleration due to gravity
G	shear modulus of the anti-roll bar
h_1	vertical distance between unsprung mass c.g. and its roll

	center
h_2	distance between sprung mass c.g. height and the roll center
I_s	moment of inertia of the sprung mass
I_u	moment of inertia of the unsprung mass
k_a	auxiliary roll stiffness of the anti-roll bar
k_b	spring constant of the anti-roll bar
k_r	The effective roll stiffness of the unconnected suspension
$k_r^{'}$	total roll stiffness of the unconnected suspension with anti-roll bar
$k_{t\ell};k_{tr}$	stiffness coefficients of the left and right tires
k_{vu}^0	static stiffness
K	active anti-roll bar linkage gear ratio distribution
l	length of the trailing lever of the anti-roll bar
l_b	distance between the two ends of the anti-roll bar
$\ell_\ell;\ell_r$	lateral distances between left and right suspension to the c.g. of the sprung mass
$L_{t\ell};L_{tr}$	lateral distances between left and right tires to the c.g. of the unsprung mass
m_s	sprung mass of vehicle
m_u	unsprung mass of vehicle
M	restore moment
M_θ	sprung mass roll moment caused by a centrifugal force
n	polytropic exponent
N_u	number of struts used on each track
$P_{0\ell};P_{0r}$	left and right absolute internal pressures of suspension struts
$P_{1\ell};P_{1r}$	instantaneous pressures in chamber 1 of left and right strut, respectively

$P_{12\ell}$; P_{12r}	pressure drop between chambers 1 and 2
$P_{2\ell 1r}$; $P_{2r1\ell}$	pressure drops across the connecting chambers 2 and 1
P_{1j0} $(j=\ell, r)$	absolute internal pressures of fluid in chamber 1 on the left and right suspension struts
$P_{2\ell}$; P_{2r}	instantaneous pressures in chamber 2 of left and right strut, respectively
$P_{23\ell}$; P_{23r}	pressure differential across the damping restriction
$P_{3\ell}$; P_{3r}	instantaneous pressures in chamber 3 of left and right strut, respectively
$P_{3s\ell}$; P_{3sr}	static gas pressure of strut of left and right strut, respectively
P_{3j0} ; P_{4j0} $(j=\ell, r)$	pressures of fluid chambers 3 and 4 on the left and right suspension struts
P_{4j} $(j=\ell, r)$	instantaneous gas pressures in chamber 4 in strut j.
V_{4j} $(j=\ell, r)$	instantaneous gas volumes in chamber 4 in strut j.
P_a	atmosphere pressure
P_c	initial charge pressure
$P_{c\ell}$; P_{cr}	initial charge pressure and initial charge volume of the left and right suspension respectively.
$P_{s\ell}$; P_{sr}	the static absolute internal pressure of left and right strut, respectively
Q_{1j} $(j=\ell, r)$	volume flow rate of left and right in chamber 1
Q_{12j} $(j=\ell, r)$	rates of fluid flows between chambers 1 and 2
Q_{13j} $(j=\ell, r)$	flow rates between chambers 1 and 3
$Q_{2\ell}$; Q_{2r}	rate of change of fluid volume in chamber 2 of the left and right suspension struts
$Q_{23\ell}$; Q_{23r}	the fluid flow through the damping restriction
$Q_{2\ell 1r}$; $Q_{2r1\ell}$	volume flow rate of left and right from chambers 2 to 1

$Q_{1\ell 3r}; Q_{1r3\ell}$	volume flow rate of right and left struts from chambers 1 to 3
r	length of the trailing lever
$S(f)$	The 'double sided' power spectral density
$S(\Omega)$	spatial spectral density of the road profile
v	vehicle forward speed
$V_{0\ell}; V_{0r}$	static volumes of gas in the left and right suspensions
$V_{3\ell}; V_{3r}$	left and right instantaneous gas volume in chamber 3 of strut
$V_{3j0}; V_{3cj}\ (j = \ell, r)$	static and initial volumes of gas in chamber 3
$V_{3s\ell}; V_{3sr}$	the left and right static gas volume of strut
V_c	initial charge volume of gas in accumulator
$V_{c\ell}; V_{cr}$	initial charge volumes of gas in the left and right struts
$V_{s\ell}; V_{sr}$	nominal gas volume of left and right strut
$w_\ell; w_r$	static loads acting on the left and right suspension struts
w	load supported by one strut
W	the total load carrying capacity
$x_i(d)$	road profile
$x(t)$	The temporal variations in the road roughness,
$x_s,\ x_u$	the vertical motions of the sprung and unsprung masses
$x_{f\ell}(d)$,	time-histories of the left--tracks
$x_{fr}(d)$	time-histories of the right-tracks
$x_\ell; x_r$	relative displacements of the left and right struts
$x_{\ell 0}; x_{r0}$	the static deflections of the suspension struts
$\dot{x}_\ell; \dot{x}_r$	relative velocities across the left and right struts
$\ddot{x}_\ell; \ddot{x}_r$	relative acceleration across the left and right struts
$x_{t\ell}; x_{tr}$	vertical motion at the left and right tire-terrain interface
T_b	restore moment due to anti-roll bar

T_R	roll moment due to an anti-roll bar
T_s	time duration of the response
T_θ	total roll moment due to lateral acceleration
θ	relative roll deflection
$\theta(d)$	relative roll angle of the road profile
$\theta_s;\theta_u$	roll angles of the sprung mass and unsprung mass
ρ	mass density of the fluid
Ω	spatial frequency variable
$\overline{\ddot{x}}_s$	RMS value of the sprung mass vertical acceleration
$\overline{\ddot{\theta}}_s$	RMS value of the sprung mass roll acceleration
$\overline{\theta}_s$	RMS value of the sprung mass roll angle
γ	pulse severity parameter
τ_s	duration of pulse.
λ	road profile of wavelength

CHAPTER 1

INTRODUCTION & LITERATURE REVIEW

1.1 GENERAL

The ride, handling and roll dynamics of a road vehicle are complex functions of vehicle weight and dimensions, weight distribution, and static and dynamic properties of the suspension and tires. Heavy vehicles, in general, are designed to conform with the weights and dimensional regulations, while all other important design variables are derived within the constraints of the regulations. These include the drive train, suspension, tires and the brake system. Among these, the static and dynamic properties of suspension and tire are known to affect the vehicle dynamic responses or measures related to ride, handling and roll, most significantly. Such measures, however, pose conflicting requirements for the suspension design. A soft and lightly damped suspension is considered desirable for smooth ride, while adequate handling and directional performance necessitates relatively hard suspension. The suspension design is thus invariably realized as a compromise among the varying conflicting requirements.

The roll and lateral stability performance of road vehicles are achieved through auxiliary roll stiffness, such as an anti-roll bar and Pan-hard rod, such that relatively soft springs could be employed to achieve adequate bounce ride. Concepts in mechanically or hydraulically connected wheel suspensions have also evolved to achieve relatively soft vertical ride, and anti-pitch and anti-roll performance. The interconnection of suspension on different wheels tends to equalize the loads on the connected wheels, thereby, reducing the magnitudes of

pitch and roll motions. An interconnection between the front and rear wheels tends to reduce the magnitude of pitch response encountered under braking, acceleration or road wheel interactions with a bump. The interconnections in the roll plane, connecting the right and left suspension units of an axle, would yield equalization under the actions of steering induced centrifugal force or the road bump on one of the tire tracks, thereby, reducing the roll motion of the sprung weight.

The interconnection between suspension units may be realized either through mechanical means or through hydraulic means. Such suspension, interconnected in the roll plane, offers considerable potential to realize soft vertical mode stiffness for adequate ride, and variable high roll stiffness in the presence of roll motion to achieve improved roll dynamics performance. The hydro-pneumatic suspension struts comprise of hydraulic chamber for damping control and pneumatic chamber to provide the load carrying and restoring properties, within a single unit. Such struts thus offer considerable potential for interconnection through the hydraulic flows.

Although the designs of interconnected hydro-pneumatic suspension have been developed for over 20 years (Moulton, 1979; Felez and Vera, 1987; Fraser, 1982; Rosam and Darling, 1997), only a few studies have investigated their static and dynamic properties through modeling and analysis tools (Fraser, 1982; Felez and Vera, 1987; Liu, 1994; Chaudhary, 1998). The reported analytical studies have explored the hydro-pneumatic suspension strut, which provide the load carrying capacity related to the rod area (Liu, 1994). Such struts, therefore,

require a large rod area or extremely high pressure to meet the load carrying demand. The use of large rod area would yield a relatively large size strut, while the use of high pressure would pose considerable challenge in the design of seals. Alternatively, smaller size hydro-pneumatic struts interconnected in the roll plane in conjunction with passive unconnected springs have also been investigated in a recent study in an attempt to reduce the high pressure requirement (Chaudhary, 1998). The study showed that sharing the load with unconnected springs tends to reduce the effectiveness of the interconnected suspension considerably.

This dissertation research explores two different configurations of hydro-pneumatic struts interconnected in the roll plane. The static and dynamic properties of both configurations with different interconnected chambers are investigated to assess their anti-roll and ride performance potential. The first configuration considers the struts reported in an earlier study (Liu, 1994), where the relatively small piston rod area requires very high fluid pressure to support the static load. The second configuration proposes an alternate strut design, where the volume within the large size piston rod acts as the pneumatic spring. Unlike the first configuration, which utilizes an external pneumatic reservoir, the latter configuration is a compact design, which comprises both the hydraulic and the pneumatic chambers. The roll-plane analytical models developed are analyzed under both the steering induced centrifugal force, and road roughness induced vertical and roll motions.

1.2 LITERATURE REVIEW

In the last three decades, extensive developments in passive, semi-active, and active vehicle suspensions have been realized on the basis of results attained from conceptual and total vehicle models, and laboratory and field measurements. Many studies have demonstrated that the performance characteristics of suspension concepts and the control systems can be effectively investigated using simplified vehicle models (King, 1998; Sayers, 1996; Suresh, 1994). The studies of vehicle suspension dynamics include those related to ride dynamic responses to road roughness induced excitations, roll dynamics and handling characteristics. The majority of the studies on suspension dynamics are conducted with an objective to achieve improved design compromise between the ride, handling and directional dynamics performance. These studies include the classical passive, semi-active and active suspension units or components, while only a few studies have explored different types of interconnected suspension. The reported studies on interconnected suspension are briefly reviewed in the following sections in order to build a background on the concepts and methods of analysis, and to formulate the scope of this dissertation.

1.3 INTERCONNECTED ROLL CONTROL SUSPENSION SYSTEM

The vast developments in advanced suspension systems, including fully active, semi-active and slow active suspensions, have been documented in a number of articles (Rosam and Darling, 1997; Horton and Crolla, 1986; Ei-Demerdash, 1996). The majority of the reported studies concentrate on solving for the design conflict between the ride comfort, and handling performance

requirements. While the majority of the studies focus more on the ride dynamics aspects using independent suspension, a few studies have also explored roll control through interconnected suspension (Felez and Vera, 1987; Rosam and Darling, 1997). Several studies have investigated the use of active roll control to reduce the body roll of heavy vehicles (Felez, and Vera, 1987; Lang and Walz, 1991 and Sharp and Pan, 1993). On the basis of the results attained through computer simulation of models or experiments, it is generally shown that the maneuver induced roll dynamic motions could be either reduced or eliminated using feedback controlled hydraulic actuators with only moderate power consumption and cost. Many other earlier studies have explored the performance characteristics of mechanically interconnected suspension units to achieve enhanced anti-roll and anti-pitch response (Pevsner, 1957; Bastow, 1987; Newton, 1989). The relevant studies in the field of interconnected suspension (passive, semi-active, and active) for attenuation of roll or pitch motion are discussed in the following subsections.

1.3.1 Mechanically interconnected suspension system

The roll and pitch properties of a suspension system can be varied considerably by interconnecting the different wheel suspensions of a vehicle. The well-known French Citroen 2CV Saloons employed interconnected suspension system, which permitted the use of soft springs for adequate ride quality, while maintaining good vehicle handling and control through mechanical interconnections (Newton, 1989). The effect of mechanical coupling on the pitch and bounce frequency of the suspension can be best seen from Figure 1.1 (a).

Under a pure vertical excitation at the front and rear wheels, the vehicle body D and the connecting lever C remain parallel to the ground surface. The corresponding suspension rate thus depends on the stiffness of springs A, which are chosen to be relatively soft to achieve good ride quality. Under motions around the oscillation center O, the pitch oscillation frequency of the body would depend on the stiffness of the spring B. The rate of springs A and B can be thus selected to achieve desirable pitch and bounce natural frequencies. Earlier designs employed a soft pitch spring B and a hard bounce spring A to achieve the lower pitch frequency than the bounce frequency. Such suspensions thus resulted in poor anti-pitch performance and low resistance to attitude changes caused by dynamic load transfers. Figure 1.1(b) and 1.1 (c) illustrate different design configurations of mechanically interconnect suspensions (Newton, 1989).

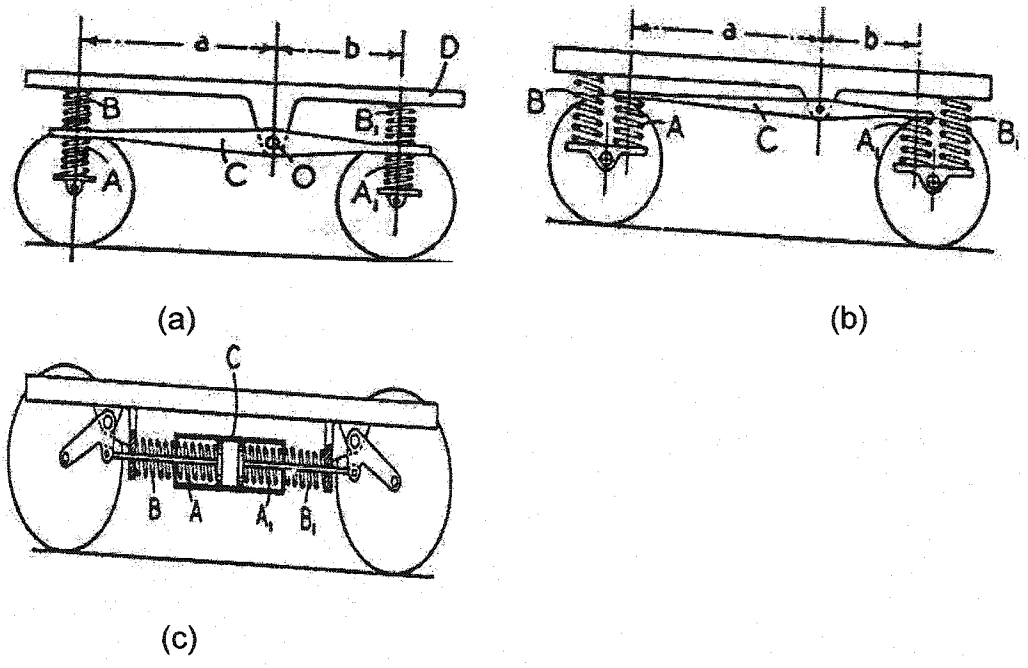

Figure 1.1: Schematics of mechanically interconnected suspension systems (Newton, 1989)

1.3.2 Hydro-mechanical interconnected suspension

Control of body roll motion in vehicles is mostly achieved through anti-roll bars, which provide additional roll stiffness. Actively controlled roll bar mechanisms have also been investigated to realize improved lateral and roll stability of vehicles. Darling and Hickson (2000) conducted an experimental study of a prototype vehicle with actuation of a roll bar. Figure 1.2 illustrates a schematic of the roll plane of the vehicle with an active roll bar. In this study the active roll bar was mounted forward of the front axle, while the end levers were cranked backwards. The transverse section was mounted in bushes fixed to the chassis section running across the front of the vehicle. A vertical drop link and a linear actuator were used to connect the roll bar ends to the suspension tie rods.

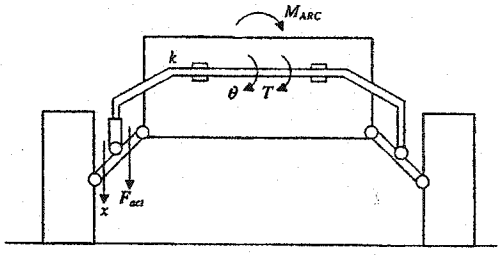

Figure 1.2: A schematic of an actively controlled anti-roll bar.

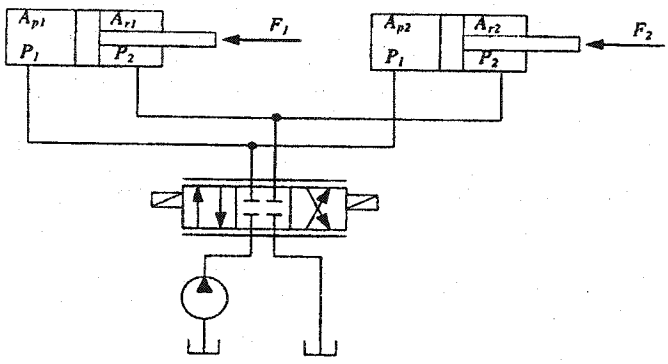

Figure 1.3: Schematic layout of the hydraulic actuators and the valve.

The prototype system consisted of two single ended linear hydraulic actuators, connected in parallel to the same valve as illustrated in Figure 1.3. The forces, $F_1 = P_1 A_{p1} - P_2 A_{r1}$, and $F_2 = P_1 A_{p2} - P_2 A_{r2}$, must remain proportional to each other on both extension and retraction.

$$F_1 = KF_2 \text{ and } K = \frac{A_{r1}}{A_{r2}} = \frac{A_{p1}}{A_{p2}} \tag{1.1}$$

where F_1 and F_2 are the forces developed by the actuators, and K represents the active anti-roll bar linkage gear ratio distribution. Since the front and rear actuators were supplied through a single control valve, the two actuators incurred identical fluid pressures. High pressure of fluid flows from a pump driven by the engine was supplied to two linear hydraulic actuators connected in parallel, which produced twist in the front and rear roll bars.

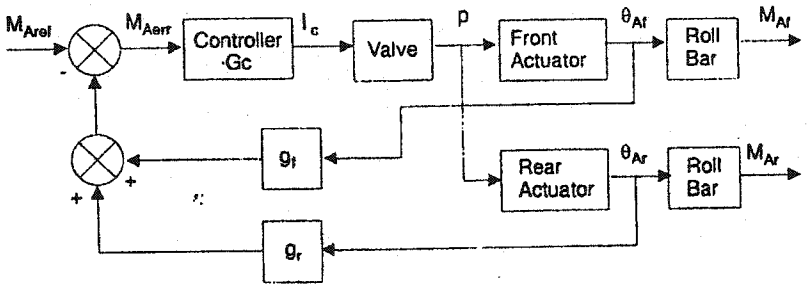

Figure 1.4: Block diagram of the active roll moment control system.

Figure 1.4 illustrates the roll moment control block diagram. A simple PID controller (G_c) is implemented using the roll angle feedback (θ_{Af} and θ_{Ar}) to track the target roll moment (M_{Arel}). The output of the PID controller is the desired electric current signal (I_c), which permits the desired fluid flow to the

front and rear actuators. The roll and warp modes of the roll bars can be eliminated by a suitable choice of feedback gains, g_f and g_r.

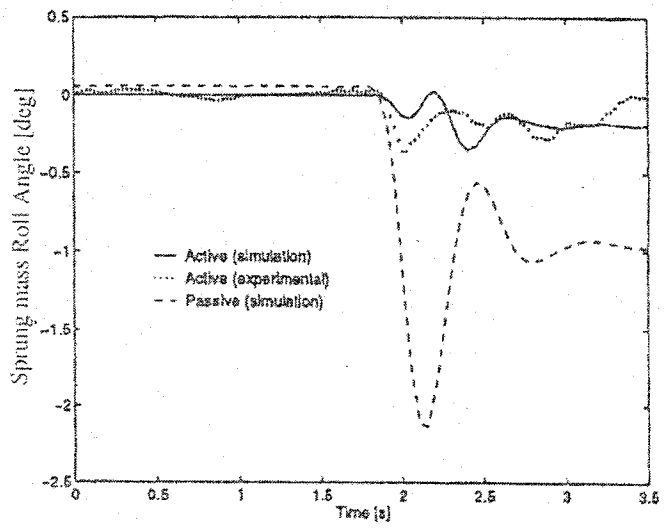

Figure 1.5: Comparison of roll displacement responses of active and passive suspension under a step steer input.

Dynamic handling performance tests were conducted under a clockwise steer input of ramp type, where the steering wheel angle increased to 120^0 over a period of 0.3 *s* at a vehicle speed of 6.5 *m/s*. The measurement of the handling response In terms of the roll angle revealed that the active roll bar could considerably reduce the magnitude of sprung mass roll displacement when compared to that of the vehicle with a passive roll bar, as presented in Figure 1.5, for a step steer input. It was estimated that the peak roll angle could be reduced by approximately *80%* under lateral acceleration of up to 0.5 *g*, but the selection of feedback gains was strongly influenced by the properties of the front and rear suspension system, actuator dimensions, roll bar stiffness, actuator lever arm linkage length and secondary suspension stiffness.

Sharp and Pan (1992, 1993) investigated the potential performance gains of an active roll control system for a luxury car. The car was fitted with rotary actuators within the anti-roll bars at the front and rear axles. The lateral acceleration, and the actuator displacement and velocity signals served as feedback for the controller. The study suggested that the control performance deteriorated with valves with a bandwidth lower than 40 *Hz*. Furthermore, the high power consumption (peak power consumption of around 2 *kW*) was a clear disadvantage of the fully active system. A similar controller developed on the basis of active roll bar technology and lateral acceleration as the control input was developed and successfully implemented by Lang and Walz (1991).

1.3.3 Hydro-pneumatic interconnected suspension

Moulton (1979) developed a hydro-pneumatic suspension, referred to as hydrogas suspension, to improve the ride quality of small cars, which combines the nitrogen gas as the springing medium and the hydraulic fluid pressure drop across the flow path served as a damping mechanism within a single unit, as shown in Figure 1.6. The hydraulic and pneumatic chambers are separated from a flexible separator. The suspension also employs a tapered aluminium piston and different orifice flow paths to achieve variable spring rates and damping coefficients.

The damping fluid chambers of the front and rear wheels on each track could be connected via hydraulic lines to realize pitch plane interconnection. Such an interconnection permitted load equalization and thus the pitch control through fluid flows through the interconnected pipe, whenever either the front or

the rear wheel encountered an excitation, or when the vehicle experienced pitch motion during braking and acceleration. An excitation at the front wheel alone would yield an increase in the fluid pressure within the rear suspension unit, thereby creating an upward force on the sprung mass and, thus reducing the differential between the suspension forces acting on the front and rear of the car body.

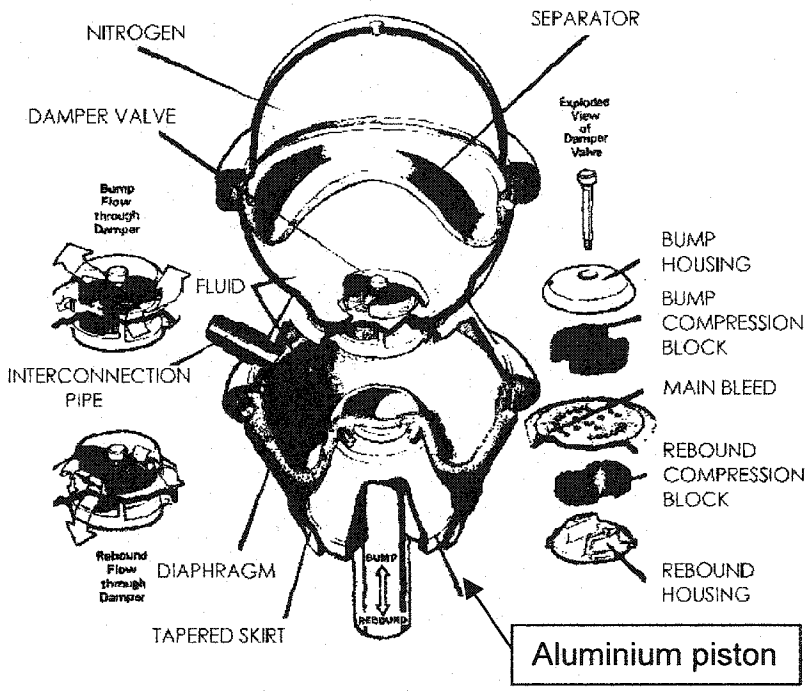

Figure 1.6: A cutaway section of the hydra-gas suspension unit (Moulton, 1989)

As shown on Figure 1.6, the upward vertical movement of the tapered aluminium piston tends to vary the effective area of the chamber against which fluid pressure acts, which yields variable spring rate. Sufficient pressure differential between the upper and lower chambers compresses either the bump or rebound compression block, increasing fluid flow as a function of the pressure difference. Under pitch motions, the fluid flows occur between the interconnected front and rear suspension, which tend to reduce further compression of the gas,

as shown in Figure 1.7 (a). The front wheel is lifted in relation to the car body, while the rear wheel is lowered. The interconnection thus minimizes the differential of the forces at the two ends of the sprung mass, thereby, reducing the pitch motions.

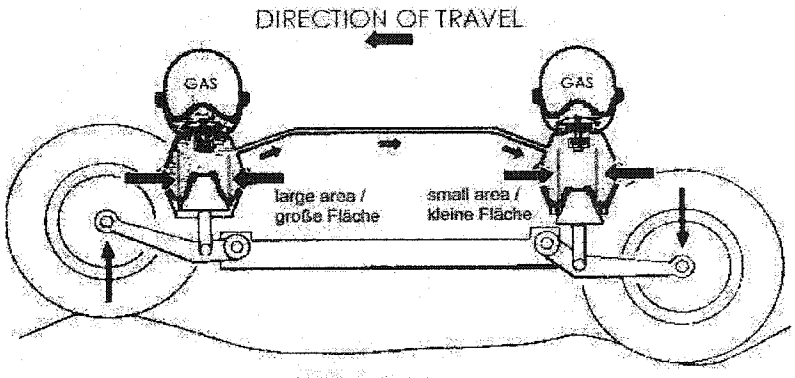

(a. Pitch)

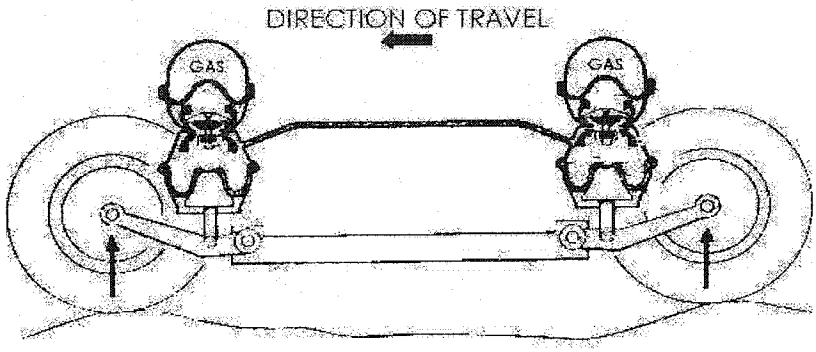

(b. Bounce and Roll)

Figure 1.7: Interconnected hydra-gas suspension systems in the pitch and roll plane.

Figure 1.7 (b) shows that the flows through the interconnected pipes do not occur under pure bounce motion. Fluid flows occur only between the upper and lower chambers of individual units through the damper valves. The suspension units with higher fluid pressures and increasing piston areas with increasing

bounce and roll motions yield higher stiffness in bounce and roll, which may obviate the need for an anti-roll bar.

Rideout (2003) performed experimental and analytical study of the interconnected hydra-gas suspension system. The study proposed a linear model of the suspension system derived from measured suspension characteristics. The model suggested that the simplest possible representation of an interconnected hydra-gas suspension would be a mass-spring-damper system with linear time-invariant coefficient matrices, $[M]$, $[C]$ and $[K]$. The forces F_1 and F_2 developed by the constrained front and rear hydra-gas units and transmitted to the test frames were thus expressed as:

$$\begin{Bmatrix} F_1 \\ F_2 \end{Bmatrix} = \begin{bmatrix} M_{11} & M_{12} \\ M_{21} & M_{22} \end{bmatrix} \begin{Bmatrix} \ddot{x}_1 \\ \ddot{x}_2 \end{Bmatrix} + \begin{bmatrix} C_{11} & C_{12} \\ C_{21} & C_{22} \end{bmatrix} \begin{Bmatrix} \dot{x}_1 \\ \dot{x}_2 \end{Bmatrix} + \begin{bmatrix} K_{11} & K_{12} \\ K_{21} & K_{22} \end{bmatrix} \begin{Bmatrix} x_1 \\ x_2 \end{Bmatrix} \tag{1.2}$$

where M_{ij}, C_{ij}, K_{ij} ($i = 1,2$ and $j = 1,2$) are the constant mass, damping and stiffness coefficients, respectively, identified from the measured data and suspension characteristics, x_1 and x_2 represent the motions of the front and rear suspension units. The mass matrix in the above formulation was assumed to be negligible, given the lighter weight of the lower piston and small fluid inertia. An alternate model was also proposed incorporating the bilinear damping matrix elements that were estimated from the bounce and rebound characteristics of the suspension units. The study concluded that the linear model for interconnected units can return reasonable amplitude predictions for restricted frequency ranges of interest. An expanded model with bilinear spring and bilinear damping coefficients was constructed such that a common set of parameters could

accurately predict the forces. However the phase lag of the coupled forces could not be predicted (Rideout, 2003).

Rosam and Darling (1997) proposed a low cost roll control system comprising the interconnected hydra-gas suspension. The system is similar to that proposed earlier by Karnopp et al. (1992). The proposed active roll control system consists of a sealed 'shuttle' device which effectively transmits the hydra-gas fluid from the suspension units on the inside track of the vehicle to the outside track during cornering. The study outlined the design of a fluid displacer or 'shuttle', as shown in Figure 1.8. The shuttle control system included a 4 port-3 position proportional valve, a D.C. electric motor, pump, tank, accumulator and the relief valve. Additional flow requirements were supplied by a 1 liter accumulator. An accelerometer mounted laterally on the car body below the front bumper, and an LVDT position transducer mounted on the outer case of the shuttle served as the feedback for the control system illustrated in Figure 1.9.

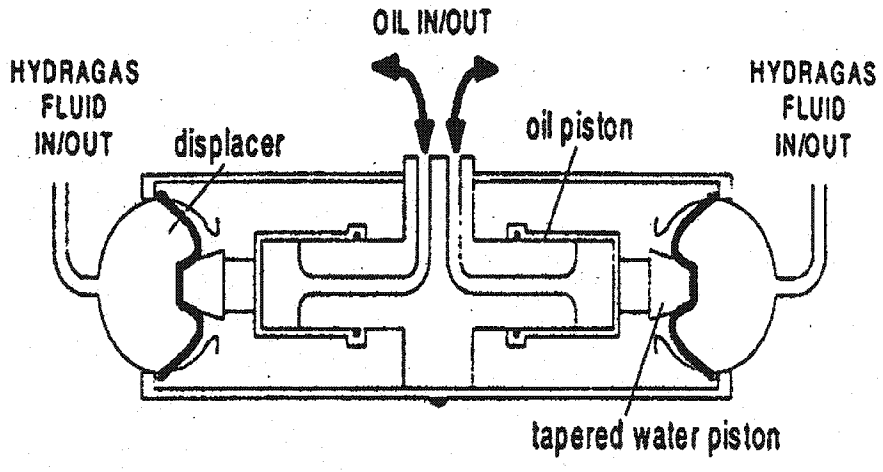

Figure 1.8: Schematic representation of the hydra-gas roll control shuttle.

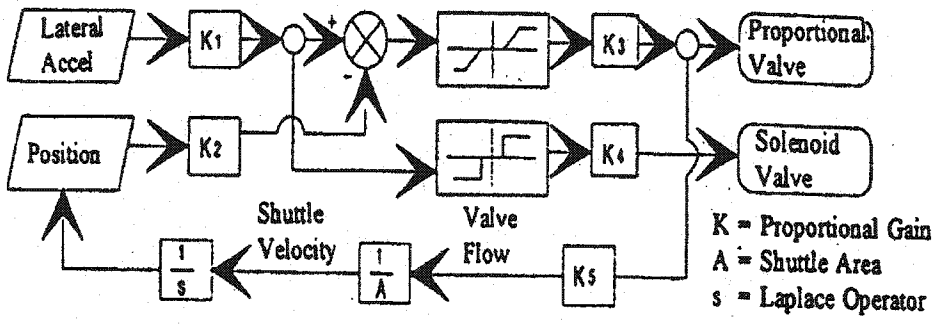

Figure 1.9: The block diagram representation of the hydra-gas roll control shuttle.

The study also presented the actively roll controlled vehicle model, where the hydra-gas suspension units were modeled as three components: the fluid displacer, the damper valve and the gas chambers. The component models were presented by a combination of analytical functions and empirical functions. The simulation and experimental response in terms of lateral acceleration and roll motion were attained under a step steer input and a forward speed of 13 m/s. The study showed reasonably good correlation between the experimental and simulation results, as shown in Figure 1.10.

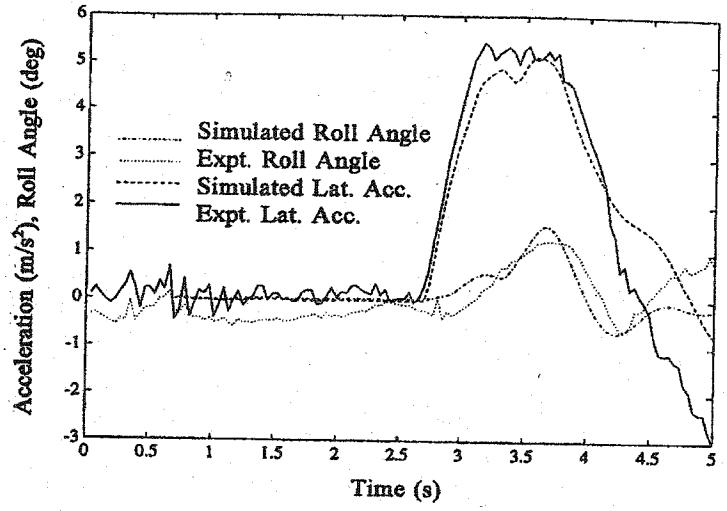

Figure 1.10: Comparison of simulation and measured response of the side-to-side ride hydra-gas units during steer pad test (Rosam and Darling, 1997).

The study showed that the active system could reduce the body roll substantially. At the same time, relatively high magnitude of lateral acceleration were obtained, which was argued to be beneficial since it could provide a feedback to the drives of the maneuvers severity. Only a modest control system bandwidth was required for effective roll control during fast transient maneuvers.

A hydro-pneumatic suspension unit serves as the primary load carrying element as well as the suspension damper, similar to the hydra-gas unit developed by Moulton (1989). The hydro-pneumatic suspension unit comprises a hydraulic actuator, a gas reservoir that serves as the restoring force element, and a damping valve, inserted between the gas reservoir and the strut, as shown in Figure 1.11. The strut thus serves as a compact suspension design with potential for realizing interconnection between the hydraulic or pneumatic chambers of the struts mounted either on the front and rear axles, or on the right and left tracks of the vehicle.

Horton and Crolla (1986) proposed a semi-active hydro-pneumatic suspension interconnected in the roll as well as pitch planes (Figure 1.12) to control both the roll and pitch stiffness properties. The proposed suspension concept offered considerable potential to enhance vertical ride comfort performance, since it permitted the selection of lower vertical spring rates. The pitch and roll suspension rates were controlled by diagonally connecting the upper chambers of front suspension struts to the lower chambers of rear suspension struts, and by laterally connecting the upper chambers of the rear suspension struts. Figure 1.13 illustrates detailed schematic of single suspension

unit that comprises and inertial control valve, and a pendulum based angular position sensor, under application of braking, accelerating, or cornering forces on the body, the pendulum arm pivot will move relative to the pendulum, and permit hydraulic flows to minimize the pitch and roll motion.

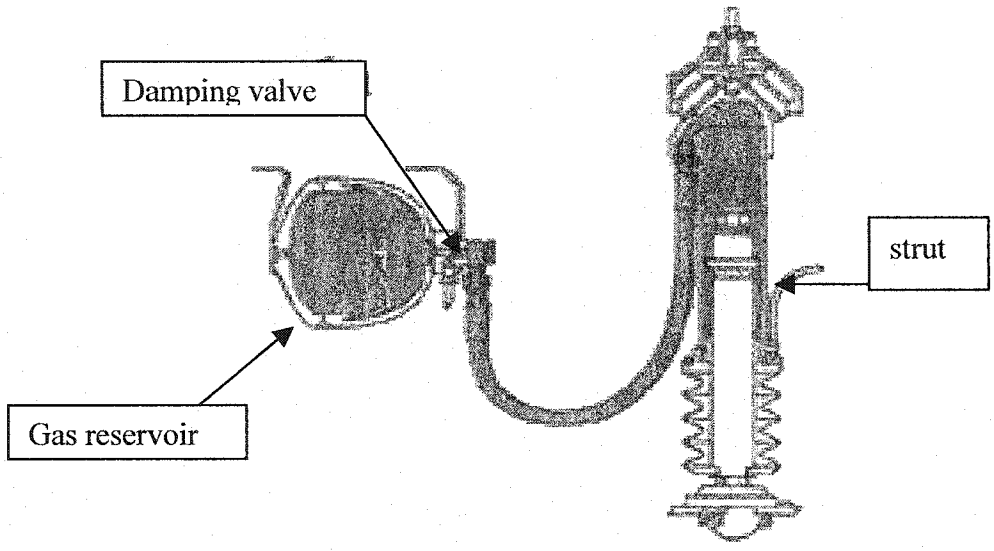

Figure 1.11: Schematic illustration of a hydro-pneumatic suspension [www.m-100.org].

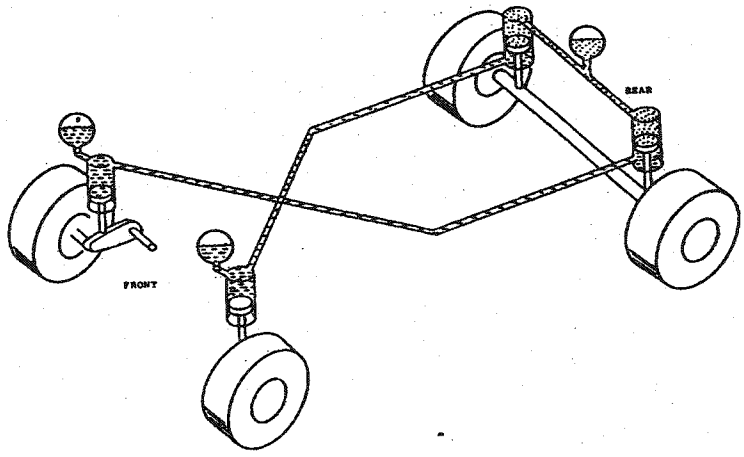

Figure 1.12: Schematic of the interconnected suspension in the pitch and roll planes. Horton and Crolla (1986)

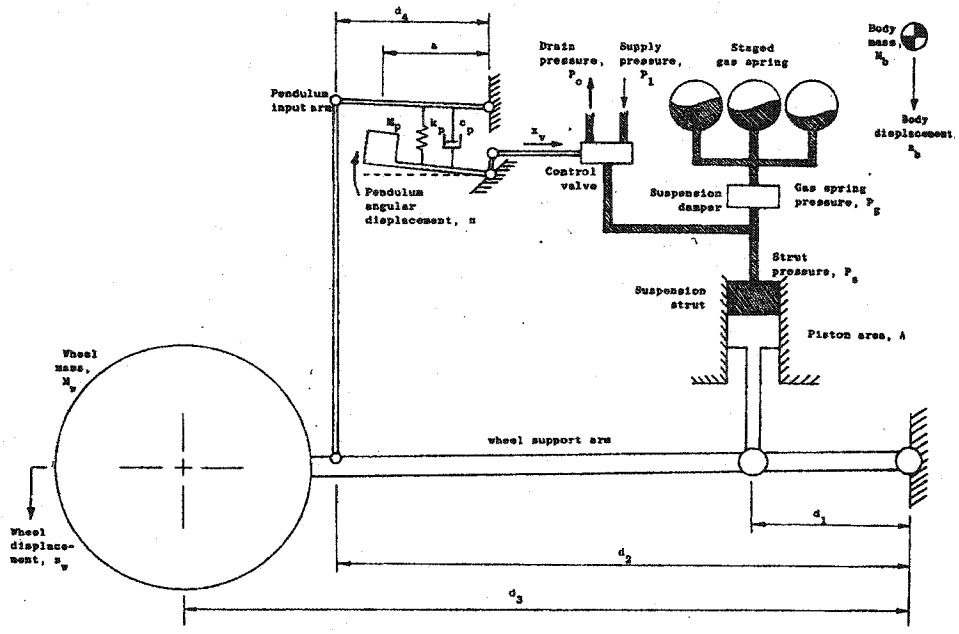

Figure 1.13: Schematic diagram of a single wheel station of the above suspension.

The semi-active suspension system proposed by Horton and Crolla (1986) has been referred to as 'AP' suspension, and has been described in more details in earlier studies (Packer, 1978 and Pitcher et al, 1977). The first published analysis was presented by Cotterell, (1975), for application to a double-decker bus. Fraser (1982) developed a mathematical model of the single wheel station, shown in Figure 1.13.

Felez and Vera (1987) developed a simplified roll plane model of a multi-wheeled crane vehicle incorporating roll connected hydro-pneumatic struts, as shown in Figure 1.14 (a). The study applied the bond graph technique to develop the model. The study also investigated an active roll-plane connected suspension shown in Figure 1.14 (b), where each suspension strut consisted of an external gas reservoir, while a pump with a control valve was used to modulate the flows

to and from the struts on the basis of pressure differential between the interconnected struts.

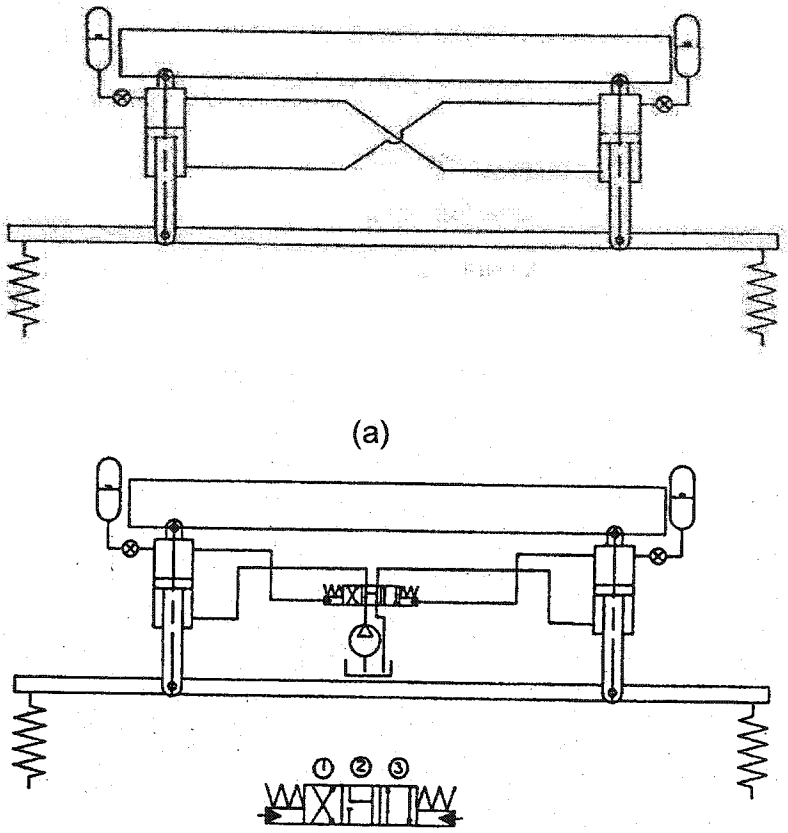

Figure1.14: Schematic representations of interconnected hydro-pneumatic suspension (a) passive suspension; (b) active interconnected suspension.

The struts mounted on the same track of the vehicle have their upper chambers connected, while the upper chamber of each strut is connected to a gas charged accumulator through a damping valve. The lower chambers of these struts on the same track are also interconnected. The upper and lower chambers of struts on one track are linked to lower and upper chamber of struts on the other track through a valve. A pressure increase in the upper chambers of left track struts caused by a roll motion of the chassis, leads flows from these

chambers to the lower chambers of the right track struts. The resulting increases in pressure of fluid of upper chambers of the right struts tend to stabilize the chassis level. The simulation results of the active interconnected suspension revealed nearly 80% reduction in the chassis roll motion. The relatively small working area of the struts, however, required very high-pressure fluid in order to support the static load.

1.4 SCOPE OF PRESENT INVESTIGATION

Although a number of active roll control systems proposed in the literature have demonstrated their superior performance potentials, the high power requirements deter their general application. Furthermore, the high cost associated with the use of sensors and high bandwidth valves in most cases would justify their implementation, where such high cost could offset the performance gains. Alternatively, hydro-pneumatic suspension systems interconnected in the roll plane could be applied to realize high roll stiffness and thus the roll control in a reliable passive manner.

The modern highway buses and heavy vehicles exhibit poor roll stability due to their high center of sprung mass. The static and dynamic roll performance of such vehicles could be enhanced by increasing the effective roll stiffness through anti-roll bars or alternated auxiliary roll stiffness. Alternatively, compact design of interconnected suspensions may be realized to achieve high roll stiffness, without affecting the vertical stiffness and thus the ride performance of the vehicle. Only a few studies, however, have investigated the performance potentials of passively interconnected hydro-pneumatic struts. These studies

have mostly considered hydro-pneumatic struts with relatively small working area, represented by the piston rod area, and external gas charge accumulator with damping valves. The small working area would require high fluid pressures in realizing the desired load carrying capacity, and would thus pose challenge in the design of seals. Alternate configurations of the hydro-pneumatic struts with relatively larger working area would thus be desirable. Moreover, the inclusion of the gas chamber within the struts would yield more compact designs, and would allow interconnection between both pneumatic and hydraulic fluid chambers. This dissertation research focused and analysis of two types of interconnected hydro-pneumatic struts. The Type I struts represent lower working area, similar to these considered in the reported studies. The Type II strut is compact design containing the gas chamber within the strut, while the working area is considerably enhanced to reduce the operating fluid pressure.

1.5 OBJECTIVE OF PRESENT INVESTIGATION

The primary objective of this dissertation research is to investigate the roll control performance potentials of three laterally interconnected hydro-pneumatic suspension configurations in the roll plane, through development and analysis of analytical models. The specific objectives include the following:

Identify a hydro-pneumatic suspension strut layout to achieve adequate load carrying capacity under pressures lower than those required in the reported concepts.

Develop roll plane models of vehicles employing conventional unconnected and interconnected hydro-pneumatic suspensions employing the struts identified in the study and reported in earlier studies.

Perform analysis to derive the static and dynamic characteristics of different unconnected and interconnected suspensions configurations in terms of suspension spring rate, roll stiffness, and vertical and roll damping.

Study the potential performance benefits of the interconnected hydro-pneumatic suspension configurations under centrifugal force and road roughness excitations.

1.6 ORGANIZATION OF THE THESIS

In chapter 2, two different configurations of hydro-pneumatic suspension struts are presented and discussed in view of their load carrying capabilities and pressure requirement. Three different roll plane interconnection concepts are introduced under different configurations of the struts. The generalized suspension forces are derived for the unconnected and the interconnected configuration assuming incompressible fluid in hydraulic struts, turbulent flows through the orifice restrictions, polytropic process of the gas in accumulators, and laminar flows within the interconnecting pipes.

In chapter 3, the static and dynamic properties (load carry capacity, suspension spring rate, roll stiffness, vertical and roll damping) are derived from the force-moment-displacement, and force-moment-velocity characteristics of the unconnected as well as interconnected suspension configurations. The resulting

properties are discussed in view of the potential performance benefits of different suspension configurations.

In chapter 4, the ride and handling performance characteristics of different hydro-pneumatic suspension configurations are investigated under deterministic excitations using numerical integration approach. The nature of excitations arising from tire-terrain interactions and steering inputs are described. The roll performance characteristics of the suspension struts are evaluated in terms of transient and steady state roll response of the sprung and unsprung masses subject to constant radius turn and lane change maneuvers. The dynamic ride performance characteristics are established in terms of both the heave and roll response characteristics under road excitations. Vibration transmissibility characteristics of different suspension struts are also investigated and compared.

In chapter 5, the vibration isolation performances of the vehicle suspension employing three different configurations are further investigated for actual road excitations.

CHAPTER 2

THE DEVELOPMENT OF ANALYTICAL MODELS OF INTERCONNECTED HYDRO-PNEUMATIC SUSPENSION SYSTEMS

2.1 INTRODUCTION

Hydro-pneumatic suspension systems offer both advantages and disadvantages compared to conventional vehicle suspension systems. The light weight and compact high pressure gas spring generates high restoring forces to support the vehicle load and provide a low natural frequency for the vehicle system. The low suspension weight helps reduce the unsprung mass of the vehicle, and the compact size permits the designer with increased flexibility for suspension packaging and design. Due to the nonlinear progressively stiffening spring rate provided by the gas, it would be possible to design a vehicle suspension system with a fairly constant natural frequency over a wide range of vehicle loading conditions (Joo, 1991). Hydro-pneumatic suspension further offers the potential to achieve standing height control and self-leveling in a relatively simple manner. Although a number of designs and concepts in interconnected suspension, including those with active roll control, have been realized (Felez and Vera, 1987; Rosam, 1997; Sharp and Pan, 1991), a few studies have attempted a thorough analysis of the suspension units and the interconnections (Moulton, 1979; Fraser, 1982; Liu, 1994; Chaudhary, 1998; Darling, 2000). The hydro-pneumatic suspension strut employed in these studies mostly comprises a separated gas reservoir, a piston cylinder arrangement and a damping valve. The effective working area of the strut is represented as the relatively small piston rod area. The suspension units thus require either a large

size piston rod or very high fluid pressure in order to support the vehicle load. Moreover, the external gas reservoir and damping valve would require added space for their installation.

In this chapter, an alternative configuration of a more compact hydro-pneumatic suspension strut is considered to achieve roll-plane interconnected suspension. The compact design comprises the gas chamber as well as the damper orifice control within the same unit. Moreover, the configuration affords a relatively large working area to permit the design and implementation with pressure considerably lower than that required for the actuators reported in earlier studies (Liu, 1994; Chaudhary, 1998). The reported as well as the identified suspension struts are initially modeled to study their static and dynamic characteristics. Different configurations of interconnected suspension are then created and analytically modeled for the response analysis.

2.2 MODELING HYDRO-PNEUMATIC SUSPENSION UNITS

Hydro-pneumatic suspensions invariably comprise a gas chamber, hydraulic chambers and damping valves within a single unit. A floating piston is often employed to separate the gas chamber from the hydraulic fluid chambers. The gas chamber can be contained within the same unit or can be realized using a separate reservoir. Two different types of struts are considered for the analysis, Type I, and Type II. The Type I strut employs a separate gas reservoir as reported in earlier studies (Liu, 1994; Chaudhary, 1998; Felez & Vera, 1987), while Type II contains the gas chamber within the same unit. The Type II

configuration offers a considerably larger working area than Type I and thus requires lower pressure to attain the same load carrying capacity.

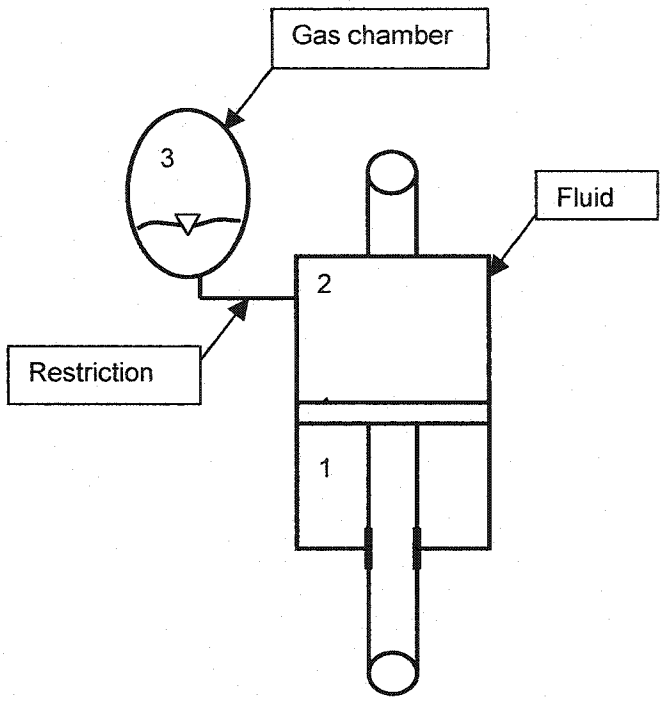

Figure 2.1: An idealized representation of the hydro-pneumatic suspension strut (Type I)

This idealized hydro-pneumatic suspension strut of Type I consists of two chambers within the cylinder (an upper chamber and a lower chamber), as illustrated in Figure 2.1. An external gas charged accumulator is connected to the upper chamber through a damping valve. The compression/expansion of the nitrogen gas in the accumulator is assumed to follow a polytropic process leading to nonlinear, progressively stiffening spring characteristics. For the purposes of model formulation, the lower and upper chambers of the strut are referred to as 'chamber 1' and 'chamber 2,' respectively. The gas charged chamber is referred to as 'chamber 3.' The seal friction force is assumed to be negligible in relation to

the total force developed by the strut, while the hydraulic fluid is considered to be incompressible. The flows through the damping orifice are assumed to constitute turbulent flow. Furthermore, the damping restriction is considered as a constant area orifice, resulting in damping force proportional to the square of the velocity. The influences of variations in the temperature on the thermal expansion of the fluid and the strut components have been neglected.

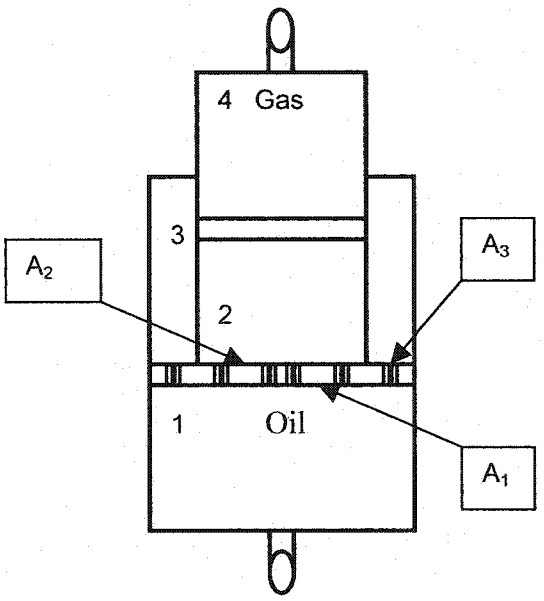

Figure 2.2: Schematic of an alternative configuration of the hydro-pneumatic suspension strut (Type II)

The Type II suspension strut encompasses the gas chamber within the same unit and consists of four chambers, as illustrated in Figure 2.2. A number of damping orifices are introduced in the piston, separating chamber 1 from chambers 2 and 3. A floating piston separates the hydraulic fluid of chamber 2 from the nitrogen gas of chamber 4. This alternate design offers a compact configuration, which eliminates the external bladder (accumulator) and throttle restriction. The configuration also offers far more flexibility in realizing a larger working area than

the Type I strut. The suspension strut could thus be operated with lower fluid pressure corresponding to the desired load carrying capacity.

2.3 ROLL PLANE MODELS OF A VEHICLE WITH UNCONNECTED HYDRO-PNEUMATIC SUSPENSION STRUTS

A large number of vehicle models of varying complexities ranging from simple two degrees-of-freedom (DOF) quarter vehicle models to several DOF three-dimentional models, have been developed for analysis of ride, handling and directional control characteristics of road vehicles. The simple two-DOF quarter vehicle models are frequently employed to study different concepts in vehicle suspension components and their responses under vertical excitations alone (Wong, 1978). Alternatively, either pitch or roll-plane models have also been developed to study the vehicle and suspension responses in the bounce-pitch or bounce-roll planes. Such models in the pitch plane primarily possess four-DOF involving vertical and pitch motions of the sprung masses, and vertical motion of the unsprung masses. A similar model may also be applied to study the roll-plane dynamics, when the wheel suspensions are independent. Heavy vehicle with high center of gravity location employ dependent suspension in the roll plane, such as beam axles, and experience considerably large roll motions under road of steering induced excitations. The vertical and roll dynamics of such vehicles can be effectively investigated using four-DOF a roll plane model including vertical and roll motions of sprung and unsprung masses (Su, 1990). Such a model would allow for analysis of independent as well as roll-connected hydro-pneumatic suspension in a highly convenient manner. In this dissertation

research, a four-DOF roll-plane model of heavy road vehicle is considered for the analysis of Type I and Type II hydro-pneumatic suspension systems.

2.3.1 Unconnected hydro-pneumatic struts (Type I) model in roll plane

Figure 2.3 illustrate the roll plane model of a road vehicle, where ms represent the sprung mass, and all the vehicle axles lumped together are represented by unsprung mass mu. A single track are lumped together and represented by linear stiffness and viscous damping arrangement assuming point contact with the road (Dulac, 1992). The hydro-pneumatic suspension struts are represented by two-point force elements, where the forces are derived from the relationships governing the fluid flows.

The coupled differential equations of motion for the vehicle model, derived using Newton's second law of motion, are presented below:

Bounce motion of the sprung mass

$$m_s \ddot{x}_s = F_\ell + F_r \tag{2.1}$$

Roll motion of the sprung mass

$$I_s \ddot{\theta}_s = -F_\ell \ell_\ell + F_r \ell_r + T_\theta - T_R \tag{2.2}$$

Bounce motion of the unsprung mass

$$\begin{aligned} m_u \ddot{x}_u = &-(c_{t\ell} + c_{tr})\dot{x}_u + (c_{t\ell}\ell_{t\ell} - c_{tr}\ell_{tr})\dot{\theta}_u - (k_{t\ell} + k_{tr})x_u - F_\ell - F_r \\ &+ (k_{t\ell} l_{t\ell} - k_{tr}\ell_{tr})\theta_u + c_{t\ell}\dot{x}_{i\ell} + k_{t\ell}x_{t\ell} + c_{tr}\dot{x}_{ir} + k_{tr}x_{ir} \end{aligned} \tag{2.3}$$

Roll motion of the unsprung mass

$$\begin{aligned} I_u \ddot{\theta}_u = &(c_{t\ell}\ell_{t\ell} - c_{tr}\ell_{tr})\dot{x}_u - (c_{t\ell}\ell_{t\ell}^2 + c_{tr}\ell_{tr}^2)\dot{\theta}_u + (k_{t\ell}\ell_{t\ell} - k_{tr}\ell_{tr})x_u + F_\ell \ell_\ell - F_r \ell_r \\ &- (k_{t\ell} l_{t\ell}^2 + k_{tr}\ell_{tr}^2)\theta_u + c_{tr}\ell_{tr}\dot{x}_{ir} + k_{tr}\ell_{tr}x_{ir} - c_{t\ell}\ell_{t\ell}\dot{x}_{i\ell} - k_{t\ell}\ell_{t\ell}x_{i\ell} + T_R \end{aligned} \tag{2.4}$$

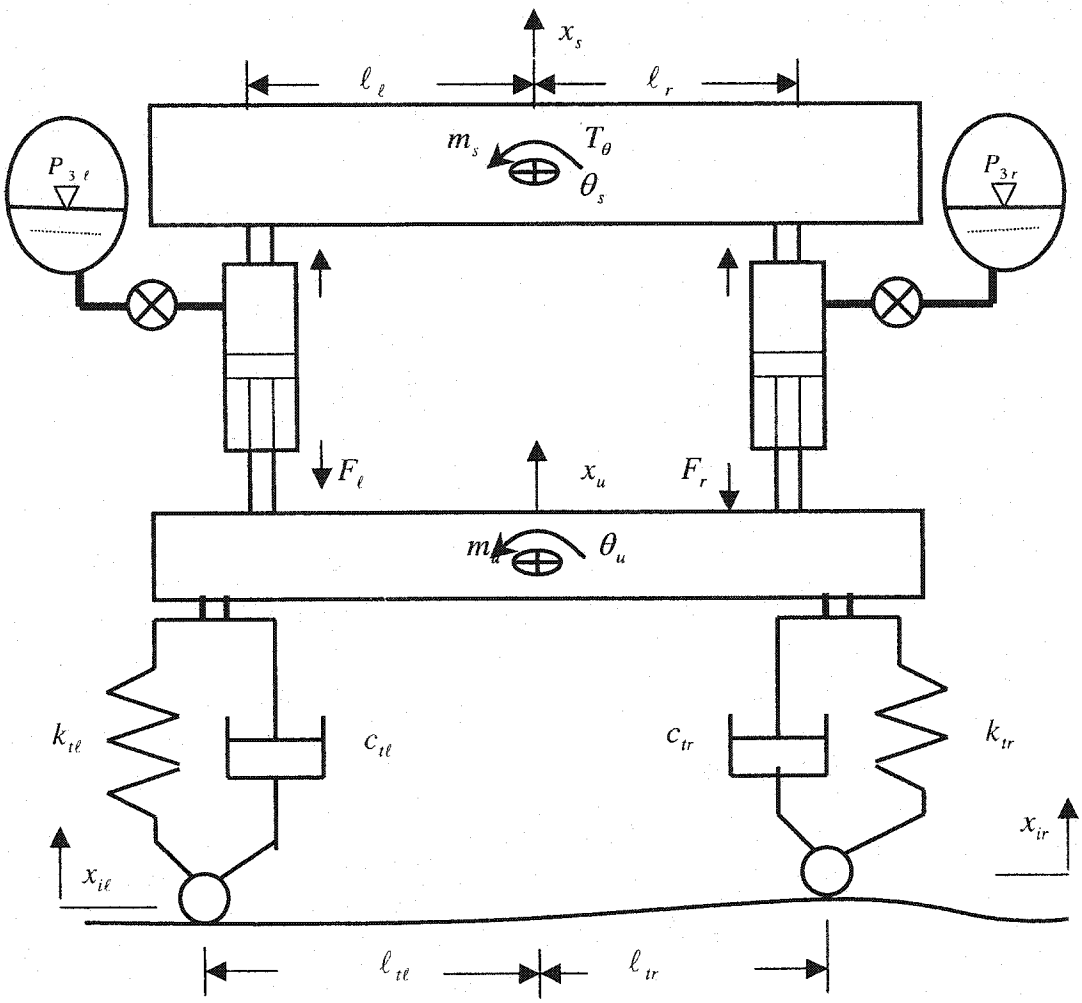

Figure 2.3: A four-DOF roll plane model of a vehicle supported on unconnected (Type I) hydro-pneumatic suspension struts

In the above equations, x_s and x_u represent the vertical motions of the sprung and unsprung masses with respect to their static equilibriums. θ_s and θ_u are the roll displacements of the sprung and unsprung masses, respectively; F_ℓ and F_r are the dynamic forces developed by the left and right suspension struts, respectively; $k_{t\ell}$ and k_{tr} are the linear spring rates due to left and right tires, and $c_{t\ell}$ and c_{tr} are the respective viscous damping coefficients. The horizontal spacing of the left and right struts with respect to the sprung mass center c.g. are

represented by ℓ_ℓ and ℓ_r, respectively. The horizontal spacing of the tires contact points with the road with respect to unsprung mass c.g. are represented by $\ell_{t\ell}$ and ℓ_{tr}; $x_{i\ell}$ and x_{ir} represent the elevations of the road surface at the contact points between the left and right tires, respectively, with the road. T_R represents the roll moment due to an anti-roll bar, which presents a suspension configuration.

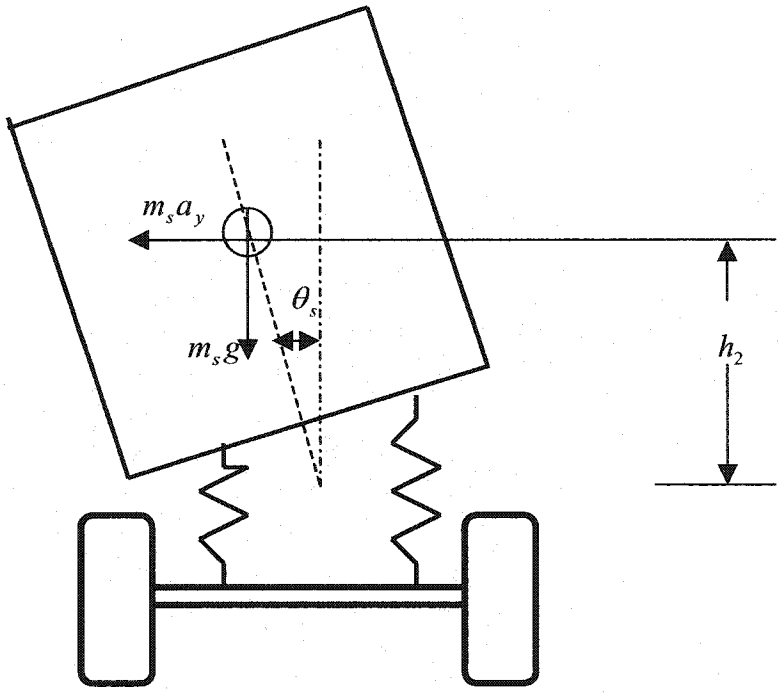

Figure 2.4: Simplified roll plane model of a vehicle

T_θ is the effective roll moment imposed on the sprung mass under a directional maneuver. The effective roll moment excitation of the sprung mass can be characterized using a simplified roll plane model of a vehicle, as shown in Figure 2.4. During a turning or steering maneuver, the tires generate lateral forces at the tire-ground interface and impose roll deflections and lateral acceleration a_y on the sprung and unsprung masses. Assuming that the roll center of the unsprung

mass lies at its c.g., the overturning moment acting on a vehicle during steady steer or lane change maneuver can be expressed as a combination of the following:

1. The primary overturning moment, $m_s a_y h_2$, due to the lateral acceleration.

2. The lateral displacement moment, $m_s g h_2 \theta_s$, arising from the roll motion that displaces the center of the mass laterally from the nominal center of the vehicle. The effective roll moment can thus be expressed as:

$$T_\theta = m_s a_y h_2 + m_s g \theta_s h_2 \tag{2.5}$$

where g is the acceleration due to gravity, and h_2 is the distance between sprung mass c.g. height and the roll center.

2.3.2 Unconnected hydro-pneumatic suspension forces (Type I)

Each strut of hydro-pneumatic suspension system, shown in Figure 2.5, comprises an accumulator and a damping restriction (throttle valve). Chamber 1 of the hydraulic strut is open to the atmosphere, while the chamber 2 contains pressurized hydraulic fluid. Chamber 3, the accumulator, contains a membrane to prevent the gas from diffusing into the fluid.

The dynamic suspension forces, F_ℓ and F_r, can be derived assuming incompressible fluid in the struts, turbulent flows through the orifice restrictions, and a polytropic and the adiabatic gas law carried out by the accumulators. $A_{2\ell}$ and A_{2r} are piston head areas; $A_{1\ell}$ and A_{1r} are piston rod side areas of the left and right struts, respectively. Let $P_{2\ell}$ and P_{2r} denote fluid pressures in chamber 2

of the left and right suspension struts, respectively, and $P_{3\ell}$ and P_{3r} be the pressure of gas chambers on the left and right struts, respectively.

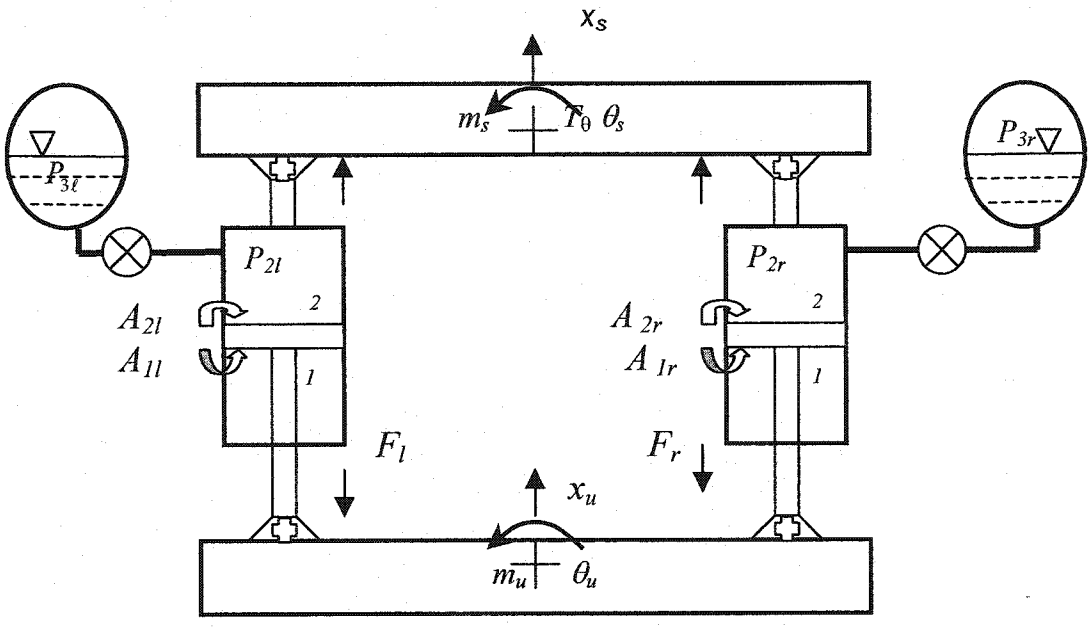

Figure 2.5: Schematic of conventional unconnected hydro-pneumatic suspension in the roll plane (Type I)

The Static Equilibrium Equation

The pressure of the fluid within each strut under static equilibrium is related to the static load acting on the strut:

$$w_\ell = (P_{0\ell} - P_a)A_{2\ell} \; ; \; w_r = (P_{0r} - P_a)A_{2r} \tag{2.6}$$

where $P_{0\ell}$ and P_{0r} are the left and right absolute internal pressures of suspension struts under static equilibrium conditions; P_a is atmospheric pressure; w_ℓ and w_r are the static loads acting on the left and right suspension struts, respectively, given by (Liu, 1994):

$$w_\ell = \frac{m_s g \ell_r}{N_u(\ell_\ell + \ell_r)} \; ; \; w_r = \frac{m_s g \ell_\ell}{N_u(\ell_\ell + \ell_r)} \tag{2.7}$$

where N_u is the number of struts used on each track in the roll plane model. The fluid pressure under static equilibrium ($P_{0\ell}$ and P_{0r}) can also be related to the static load in the following manner:

$$P_{0l} = \frac{w_\ell}{A_{2\ell}} + P_a \quad ; \; P_{0r} = \frac{w_r}{A_{2r}} + P_a \tag{2.8}$$

Assuming a polytropic gas process, the gas pressure and volume corresponding to static equilibrium can be related to the initial charge pressure, $P_{c\ell}$ and P_{cr}:

$$P_{0\ell} V_{0\ell}^n = P_{c\ell} V_{c\ell}^n \quad ; \; P_{0r} V_{0r}^n = P_{cr} V_{cr}^n \tag{2.9}$$

where $V_{c\ell}$ and V_{cr} are the initial charge volumes of gas in the left and right struts, $V_{0\ell}$ and V_{0r} are the static volumes of gas in the left and right suspensions, respectively, and n is the polytropic exponent.

Fluid Flow Equations

Assuming incompressible fluid flows, the rate of change of fluid volume in chamber 2 can be expressed in terms of the suspension relative velocity (liu, 1994).

$$Q_{2\ell} = A_{2\ell} \dot{x}_\ell \; ; \; Q_{2r} = A_{2r} \dot{x}_r \tag{2.10}$$

where $Q_{2\ell}$ and Q_{2r} are the rate of change of fluid volume in chamber 2 of the left and right suspension struts; and $\dot{x}_\ell$ and $\dot{x}_r$ are the relative velocities across the left and right struts, respectively, given by:

$$\dot{x}_\ell = \dot{x}_s - \dot{x}_u - (\dot{\theta}_s - \dot{\theta}_u) l_\ell \; ; \; \dot{x}_r = \dot{x}_s - \dot{x}_u + (\dot{\theta}_s - \dot{\theta}_u) l_r \tag{2.11}$$

During compression or rebound strokes, the fluid flow through the damping restriction, (the flow rate from chamber 2 to chamber 3), $Q_{23\ell}$ and Q_{23r} can be expressed as (Liu, 1994):

$$Q_{23\ell} = C_d a_\ell \sqrt{\frac{2|P_{23\ell}|}{\rho}} \operatorname{sgn}(P_{23\ell}) \; ; \; Q_{23r} = C_d a_r \sqrt{\frac{2|P_{23r}|}{\rho}} \operatorname{sgn}(P_{23r}) \tag{2.12}$$

where a_ℓ and a_r represent the effective orifice areas of left- and right-struts, ρ is the fluid mass density and C_d is the discharge coefficient. The sgn function describes the direction of fluid flow:

$$\operatorname{sgn}(P_i) = \begin{cases} 1; \; P_i > 0 \\ 0; \; P_i = 0 \\ -1; P_i < 0 \end{cases} \qquad (i = 23\ell, 23r) \tag{2.13}$$

For incompressible fluid flows, the rates of change of fluid volume caused by piston movements, $Q_{2\ell}$ and Q_{2r}, are related to the orifice flow rate, $Q_{23\ell}$ and Q_{23r}, and conform to the conservation of mass, such that:

$$Q_{23\ell} = -Q_{2\ell} \; ; \; Q_{23r} = -Q_{2r} \tag{2.14}$$

Pressure Equations

The pressure differential, $P_{23\ell}$ and P_{23r}, can be derived from the Equations (2.10), (2.12), and (2.14):

$$P_{23\ell} = \frac{\rho}{2}\left(\frac{A_{2\ell}}{C_d a_\ell}\right)^2 \dot{x}_\ell^2 \operatorname{sgn}(\dot{x}_\ell) \; ; \; P_{23r} = \frac{\rho}{2}\left(\frac{A_{2r}}{C_d a_r}\right)^2 \dot{x}_r^2 \operatorname{sgn}(\dot{x}_r) \tag{2.15}$$

The instantaneous gas pressure in chamber 3 ($P_{3\ell}$ and P_{3r}) can be related to the initial charge pressure ($P_{0\ell}$ and P_{0r}), given by:

$$P_{3\ell} = P_{0\ell}(\frac{V_{0\ell}}{V_{0\ell} + A_{2\ell}x_\ell})^n;\ P_{3r} = P_{0r}(\frac{V_{cr}}{V_{0r} + A_{2r}x_r})^n \tag{2.16}$$

Dynamic Forces of Unconnected Suspension (Type I)

The dynamic forces, F_ℓ and F_r, generated by the suspension struts on each side are established from forces acting upon the piston:

$$F_\ell = N_u(P_{2\ell} - P_{0\ell})A_{2\ell}\ ;\ F_r = N_u(P_{2r} - P_{0r})A_{2r} \tag{2.17}$$

Where $P_{2\ell} = P_{23\ell} + P_{3\ell}$ and $P_{2r} = P_{23r} + P_{3r}$, are the instantaneous fluid pressures in chamber 2 of the left and right struts, respectively.

Equations (2.15) to (2.17), yield dynamic force developed by the struts as:

$$\begin{cases} F_\ell = P_{0\ell}A_{2\ell}N_u\left[\left(\dfrac{V_{0\ell}}{V_{0\ell} + A_{2\ell}x_\ell}\right)^n - 1\right] - \dfrac{\rho A_{2\ell}^3 N_u}{2C_d^2 a_\ell^2}\dot{x}_\ell^2\,\mathrm{sgn}(\dot{x}_\ell) \\ F_r = P_{0r}A_{2r}N_u\left[\left(\dfrac{V_{0r}}{V_{0r} + A_{2r}x_r}\right)^n - 1\right] - \dfrac{\rho A_{2r}^3 N_u}{2C_d^2 a_r^2}\dot{x}_r^2\,\mathrm{sgn}(\dot{x}_r) \end{cases} \tag{2.18}$$

In the above equations, the second term, $\frac{\rho A_2^3 N_u}{2C_d^2 a_j^2}\dot{x}_j^2\,\mathrm{sgn}(\dot{x}_j)\ (j = \ell, r)$, describes the non-linear damping force component related to the square of the relative velocities across the suspension unit developed due to turbulent flow through the orifice restrictions. The first term describes the nonlinear restoring force due to the gas in the accumulators.

2.3.3 Unconnected hydro-pneumatic suspension forces (Type II)

Figure 2.6 illustrates the roll plane model of the vehicle comprising Type II strut, which were described earlier (in section 2.2). This alternate design of the strut consists of four chambers, as shown in Figure 2.2. The chamber 1, 2 and 3

are filled with hydraulic fluid, while chamber 4 contains nitrogen gas. A floating piston separates the oil and the gas in chambers 2 and 4. Because the rod area on the main piston is larger than the former Type I strut, it requires relatively lower pressures to support the same sprung mass. The equations of motion for the vehicle model are identical to those expressed in Equation (2.1) to (2.4), while the forces developed by the struts differ considerably.

Assuming negligible mass due to floating piston, incompressible fluid flows and turbulent flows through the damping orifices, the dynamic force developed by the strut is derived in a manner similar to that presented in the previous section for Type I struts.

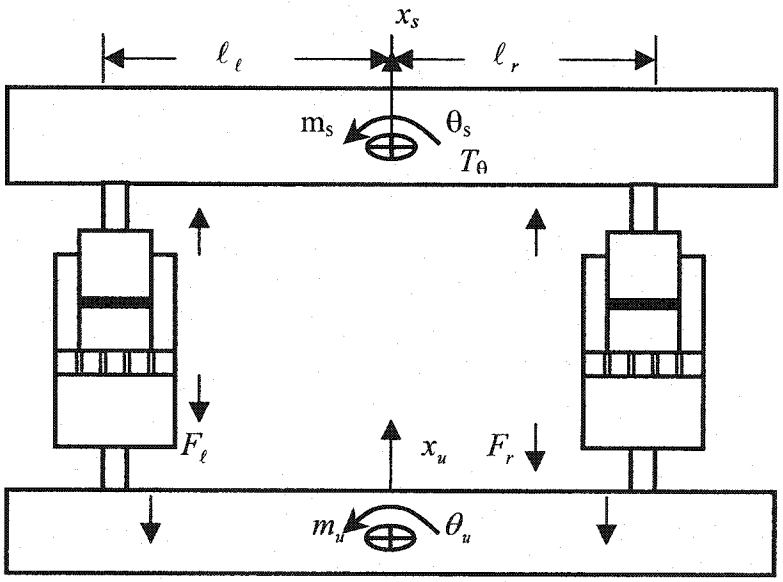

Figure 2.6: Type II unconnected strut in half vehicle roll plane model

The Static Equilibrium Equation

The pressure of the fluid within each strut under static equilibrium is related to the static load acting on the strut (refer to Figure 2.2):

$$w_\ell = (P_{1\ell 0} - P_a)A_{1\ell} - (P_{3\ell 0} - P_a)A_{3\ell};\ w_r = (P_{1r0} - P_a)A_{1r} - (P_{3r0} - P_a)A_{3r} \qquad (2.19)$$

Where P_{1j0} $(j = \ell, r)$ are the absolute internal pressures of fluid in chamber 1 on the left and right suspension struts under static equilibrium. P_{3j0} and P_{4j0} are the respective pressures of fluid chambers 3 and 4 corresponding to static equilibrium. p_a is atmospheric pressure; A_{1_j} is the piston head areas on the chamber 1 sides of the left and right struts; A_{3_j} is the piston head areas on the chamber 3 side of the left and right struts; A_{2_j} is the piston head area on the chamber 2. Under static equilibrium condition, the fluid pressures within each strut follow the relation: assume identical suspension, $P_{1\ell 0} = P_{2\ell 0} = P_{3\ell 0} = P_{4\ell 0} = P_{40}$, and $P_{1r0} = P_{2r0} = P_{3r0} = P_{4r0} = P_{40}$. Furthermore, the right and left struts are assumed to possess identical geometry, such that $A_{1\ell} = A_{1r} = A_1$, $A_{3\ell} = A_{3r} = A_3$, and $A_{2\ell} = A_{2r} = A_2$. Equation (2.19) can thus be rewritten as:

$$w_\ell = (P_{40} - P_a)A_2 \ ; \ w_r = (P_{40} - P_a)A_2 \qquad (2.20)$$

Comparing Equation (2.20) with Equation (2.6) for Type I struts, it is evident that the working area of Type I strut could be relatively smaller than that Type II struts, when identical fluid pressure and static loads are considered. The working area of strut Type II is the differential area of the piston, represented by A_2, while that of the Type I strut is the piston area A_2. The working area of Type I strut, however, would be considerably small when interconnections are introduced (rod area).

Fluid Flow Equations

The rate of change of fluid flow in chamber 1 can be expressed in terms of the relative velocity across the strut:

$$Q_{1\ell} = A_{1\ell}\dot{x}_\ell \; ; \; Q_{1r} = A_{1r}\dot{x}_r \tag{2.21}$$

Similarly, the rate of change of fluid flow between chambers 1 and 3 can be expressed as:

$$Q_{13\ell} = -A_{3\ell}\dot{x}_\ell \; ; \; Q_{13r} = -A_{3r}\dot{x}_r \tag{2.22}$$

Assuming turbulent flows through the damping orifices within the piston, the rates of fluid flows from chambers 1 to 2 and 1 to 3 can be expressed as (Liu, 1994):

$$Q_{12\ell} = C_d u a_{12\ell}\sqrt{\frac{2\,|\,P_{12\ell}\,|}{\rho}}\,\mathrm{sgn}(P_{12\ell}) \; ; \; Q_{12r} = C_d u a_{12r}\sqrt{\frac{2\,|\,P_{12r}\,|}{\rho}}\,\mathrm{sgn}(P_{12r}) \tag{2.23}$$

$$Q_{13\ell} = C_d v a_{13\ell}\sqrt{\frac{2\,|\,P_{13\ell}\,|}{\rho}}\,\mathrm{sgn}(P_{13\ell}) \; ; Q_{13r} = C_d v a_{13r}\sqrt{\frac{2\,|\,P_{13r}\,|}{\rho}}\,\mathrm{sgn}(P_{13r}) \tag{2.24}$$

where Q_{12_j} $(j = \ell, r)$ represents the rates of fluid flows between chambers 1 and 2 of the left- and right-struts, and Q_{13_j} represents the respective flow rates between chambers 1 and 3, P_{12_j} and P_{13_j} $(j = \ell, r)$ are the pressure differentials of fluids in chambers 1 and 2, and 1 and 3, respectively. u and v are the number of damping orifices that permit the flows between chambers 1 and 2, and chambers 1 and 3, respectively. The areas of orifices between chambers 1 and 2, and 1 and 3, are represented by a_{12_j} and a_{13_j} $(j = \ell, r)$. The principle of mass conservation yields:

$$Q_{1\ell} + Q_{12\ell} + Q_{13\ell} = 0 \; ; \; Q_{1r} + Q_{12r} + Q_{13r} = 0 \tag{2.25}$$

where the rates of change of fluid volumes in chamber 2 of the left and right struts can be derived by substituting Equation (2.21) and (2.22) in Equation (2.25), which yields.

$$Q_{12\ell} = -A_{2\ell}\dot{x}_\ell \; ; \; Q_{12r} = -A_{2r}\dot{x}_r \tag{2.26}$$

Pressure Equations

Equations (2.21) to (2.26) can be solved to derive expressions for the pressure differentials of fluids across the damping plate (piston):

$$P_{12\ell} = -\frac{\rho}{2}\left(\frac{A_{2\ell}}{C_d u a_{12\ell}}\right)^2 \dot{x}_\ell^2 \operatorname{sgn}(\dot{x}_\ell) \; ; \; P_{12r} = -\frac{\rho}{2}\left(\frac{A_{2r}}{C_d u a_{12r}}\right)^2 \dot{x}_r^2 \operatorname{sgn}(\dot{x}_r) \tag{2.27}$$

$$P_{13\ell} = \frac{\rho}{2}\left(\frac{A_{3\ell}}{C_d v a_{13\ell}}\right)^2 \dot{x}_\ell^2 \operatorname{sgn}(\dot{x}_\ell) \; ; \; P_{13r} = \frac{\rho}{2}\left(\frac{A_{3r}}{C_d v a_{13r}}\right)^2 \dot{x}_r^2 \operatorname{sgn}(\dot{x}_r) \tag{2.28}$$

Assuming that the gas in chamber 4 follows a polytropic process, the gas pressure and volume in chamber 4 demonstrate the following relationships:

$$P_{4\ell} V_{4\ell}^n = P_{4\ell 0} V_{4\ell 0}^n \; ; \; P_{4r} V_{4r}^n = P_{4r0} V_{4r0}^n \tag{2.29}$$

where P_{4j} and V_{4j} $(j = \ell, r)$ are the instantaneous pressures and volumes, gas in chamber 4 in strut j. Assuming identical left and right struts, $P_{4l0} = P_{4r0} = P_{40}$, $V_{4l0} = V_{4r0} = V_{40}$, the pressure and volume, P_{40} and V_{40}, can be expressed as:

$$P_{4\ell} = P_{40}\left(\frac{V_{40}}{V_{40} + A_2 x_\ell}\right)^n \; ; \; P_{4r} = P_{40}\left(\frac{V_{40}}{V_{40} + A_2 x_r}\right)^n \tag{2.30}$$

The pressure of fluid in chamber 1 can be expressed as a function of fluid pressure in chamber 2, ($P_{2\ell}$ and P_{2r}), and the pressure drop between chambers 1 and 2, ($P_{12\ell}$ and P_{12r}):

$$P_{1\ell} = P_{2\ell} + P_{12\ell} \; ; \; P_{1r} = P_{2r} + P_{12r} \tag{2.31}$$

In a similar manner, the fluid pressure in chamber 3, ($P_{3\ell}$ and P_{3r}) may be expressed as:

$$P_{3\ell} = P_{1\ell} - P_{13\ell} \; ; \; P_{3r} = P_{1r} - P_{13r} \tag{2.32}$$

The fluid in chambers 2 and 4 is separated by a floating piston area equals to A_2. Assuming the negligible friction force, due to floating piston seal and negligible mass, the force balance yield:

$$P_{2\ell}A_{2\ell} = P_{4\ell}A_{2\ell}\,;\; P_{2r}A_{2r} = P_{4r}A_{2r} \tag{2.33}$$

Dynamic Forces of Unconnected Suspension (Type II)

The dynamic forces generated by the left- and right-struts Type II are established from forces acting upon the piston:

$$F_\ell = N_u\left[(P_{1\ell} - P_{0\ell})A_{1\ell} - (P_{3\ell} - P_{0\ell})A_{3\ell}\right]$$

$$F_r = N_u\left[(P_{1r} - P_{0r})A_{1r} - (P_{3r} - P_{0r})A_{3r}\right] \tag{2.34}$$

Equations (2.27) to (2.34) yield following expressions for the total force developed by the left- and right-struts:

$$\begin{cases} F_\ell = N_u P_{0\ell}A_{2\ell}\left\{\left[\dfrac{V_{4\ell}}{V_{4\ell} + A_{2\ell}x_\ell}\right]^n - 1\right\} - \dfrac{N_u\rho}{2}A_{2\ell}^3\left(\dfrac{\dot{x}_\ell}{C_d u a_{12\ell}}\right)^2 \operatorname{sgn}(\dot{x}_\ell) - \dfrac{N_u\rho}{2}A_{3\ell}^3\left(\dfrac{\dot{x}_\ell}{C_d v a_{13\ell}}\right)^2 \operatorname{sgn}(\dot{x}_\ell) \\ F_r = N_u P_{0r}A_{2r}\left\{\left[\dfrac{V_{4r}}{V_{4r} + A_{2r}x_r}\right]^n - 1\right\} - \dfrac{N_u\rho}{2}A_{2r}^3\left(\dfrac{\dot{x}_r}{C_d u a_{12r}}\right)^2 \operatorname{sgn}(\dot{x}_r) - \dfrac{N_u\rho}{2}A_{3r}^3\left(\dfrac{\dot{x}_r}{C_d v a_{13r}}\right)^2 \operatorname{sgn}(\dot{x}_r) \end{cases} \tag{2.35}$$

The first terms in the above equations describe the restoring force component of the Type II struts. A comparison with the forces developed by Type I struts, Equation (2.19), suggests that both types of struts yield identical restoring force for identical charge pressure and volume, and working area. In this case, the damping forces attributed to the second terms in Equation (2.35) is also identical to that for strut Type I, provided $a_{12_j} = a_j$ $(j = \ell, r)$. The final terms in Equation (2.35), which represent damping forces associated with pressure drop due to

flows between chambers 1 and 3, however, are different from those of Type I struts.

2.3.4 Roll moment due to an anti-roll bar

Road vehicle suspensions, in general, are designed with an auxiliary roll stiffness mechanism to enhance the roll dynamics and directional control performance, and reduce the vehicle sensitivity to cross winds. Anti-roll bars are commonly used in road vehicles to achieve enhanced effective roll stiffness, which permit the use of relative soft suspension in the vertical mode. An anti-roll bar is normally fitted across the chassis with its ends linking the two road wheels on opposite sides, as shown in Figure 2.7 (Liu, 1994).

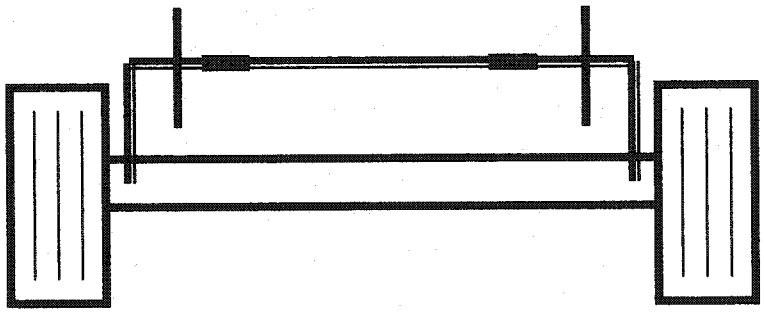

Figure 2.7: A schematic of the anti-roll bar.

It is bent near the ends to form trailing levers, while the center section is anchored to the sprung mass through bushings so that it is free to rotate. The trailing levers arc up and down with wheel deflections. The relative roll motion of sprung mass with respect to the unsprung mass, encountered under a single wheel bump or directional maneuver, causes the bar to twist, and thus provides resistance to bounce travel and body roll. Under pure vertical motions, the two

ends of the anti-roll bar only simply turn without twisting, and thus do not affect the vertical properties of the suspension.

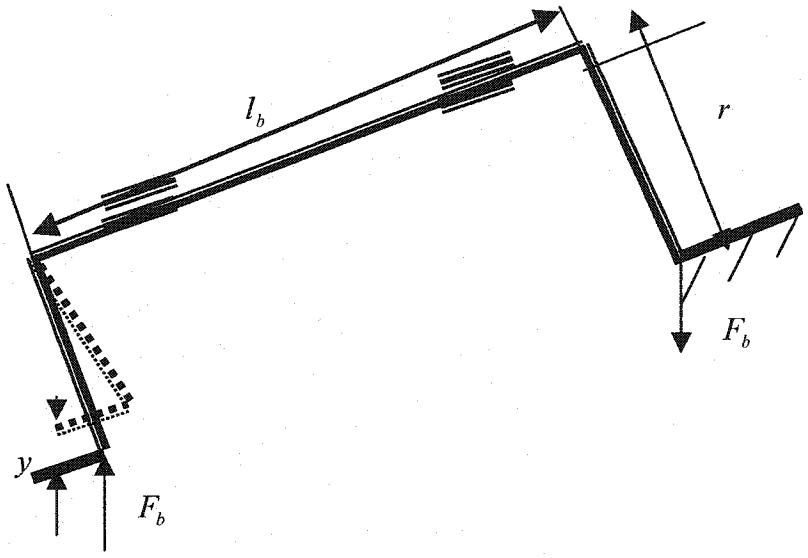

Figure 2.8: A model of the anti-roll bar.

As illustrated in Figure 2.8, roll motion of the sprung mass with respect to the unsprung mass ($\theta_s - \theta_u$) causes relative deflections of anti-roll bar, $y = \ell_b(\theta_s - \theta_u)$ and thus the restoring force F_b . The restoring force yields restoring roll moment, given by (Liu, 1994):

$$T_R = k_b \ell_b^2 (\theta_s - \theta_u) \tag{2.36}$$

where $k_b \ell_b^2$ is the effective roll stiffness of the anti-roll bar and is related to its geometry and material properties in the following manner (Liu, 1994):

$$k_\theta = k_b l_b^2 = \frac{\pi G d^4 l_b}{32 r^2} \tag{2.37}$$

where k_b is the spring constant, G is the shear modulus of the anti-roll bar; d is the diameter of the bar; r is the length of the trailing lever and l_b is the distance between the two ends of the anti-roll bar.

2.4 ROLL PLANE MODEL OF INTERCONNECTED HYDRO-PNEUMATIC STRUTS (TYPE I)

As shown in the Figure 2.9, the interconnected suspension system consists of double acting struts, external accumulators, damping restrictions and interconnecting pipes. The upper chamber of the left strut is connected to the lower chamber of the right strut, and the lower chamber of the left strut is connected to the upper chamber of the right strut. This type of interconnection has been analyzed by Liu (1994), and is referred to as 'Inc1'. The equations of motion for the vehicle model are derived in a manner similar to that described in section 2.3.1, where the dynamic forces due to interconnected struts alone differ from those derived for the unconnected struts in Equation (2.19). The dynamic forces developed by the interconnected struts are strongly influenced by the fluid flows through the interconnected pipes as described in the following subsections.

2.4.1 Dynamic forces of interconnected suspension (Type I)

As illustrated in Figure 2.9, the left and right chambers of the struts are interlinked in a cross formation. During turns or interactions of a single track with a bump induces a roll moment and deflection of the sprung mass. Considering a counter-clockwise roll deflection, the left suspension strut undergoes compression causing the flow of highly pressure fluid from chamber 2ℓ to $1r$ of

the right strut, which experiences extension. The fluid flow thus limits the motion of the right strut, and yield load equalization.

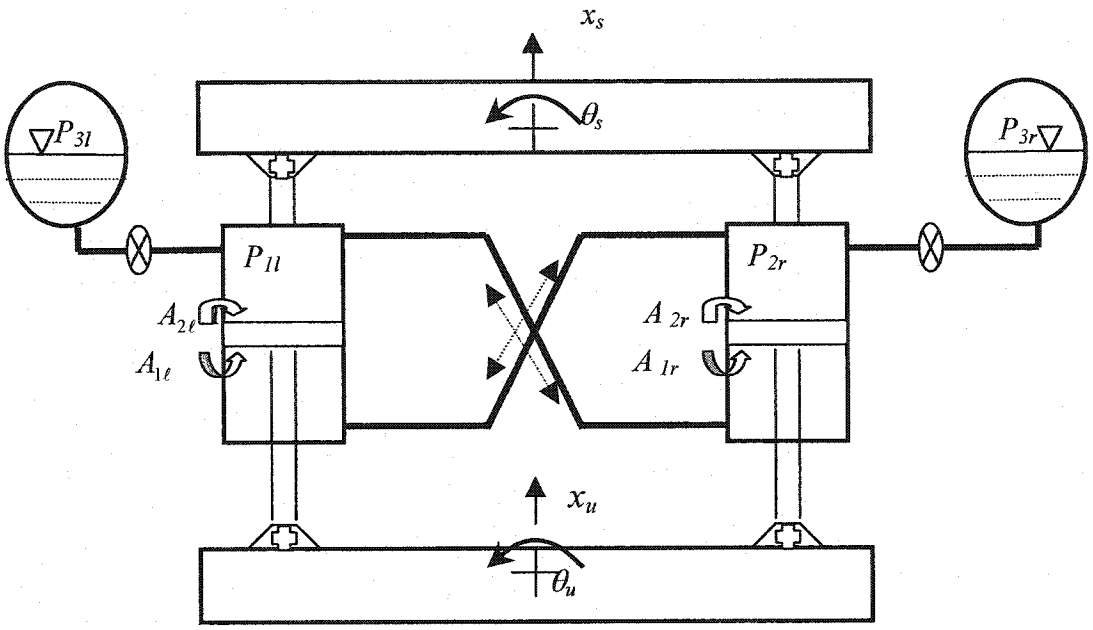

Figure 2.9: Roll plane representation of the Interconnected struts (Type I, Inc1)

The Static Equilibrium Equation

The static ride height, static deflection and operating pressure of the suspension struts are related to the static loads and the charge pressures. When the system reaches static equilibrium, the pressure of the different chambers must follow the relationships: $P_{3\ell 0} = P_{2\ell 0} = P_{1r0}$ and $P_{3r0} = P_{2r0} = P_{1\ell 0}$.

The static loads supported by the struts, w_ℓ and w_r, are related to the fluid pressure and the working area, in this case, which is the rod area ($A_{2\ell} - A_{1\ell}$ and $A_{2r} - A_{1r}$):

$$w_\ell = (P_{2\ell 0} - P_a)A_{2\ell} - (P_{1\ell 0} - P_a)A_{1\ell} \;;\; w_r = (P_{2r0} - P_a)A_{2r} - (P_{1r0} - P_a)A_{1r} \qquad (2.38)$$

The static pressure of the fluid in chamber 3 of the two interconnected struts can be derived, assuming a polytropic process of the confined gas:

$$P_{3\ell 0}V_{3\ell 0}^{n} = P_{3c\ell}V_{3c\ell}^{n};\ P_{3r0}V_{3r0}^{n} = P_{3cr}V_{3cr}^{n} \tag{2.39}$$

where P_{3j0} and P_{3cj} are the static and initial charge pressures of strut $j(j=\ell,r)$, and V_{3j0} and V_{3cj} are the corresponding volumes of gas in chamber 3.

The static deflections of the suspension struts, $x_{\ell 0}$ and x_{r0}, can be derived from the continuity equations under static equilibrium:

$$A_{2\ell}x_{\ell 0} = V_{\ell c} - V_{3\ell 0} + A_{1r}x_{r0};\ A_{2r}x_{r0} = V_{rc} - V_{3r0} + A_{1\ell}x_{\ell 0} \tag{2.40}$$

The above equations suggest that the static deflections of the right and left suspension struts are coupled due to interconnections.

Equations of fluid flow

Assuming turbulent flows through the orifice restrictions between chambers 2 and 3, the pressure differentials across the orifices relate to the volume flow change rate, as (Liu, 1994):

$$Q_{23\ell} = C_d a_\ell \sqrt{\frac{2|P_{23\ell}|}{\rho}}\,\mathrm{sgn}(P_{23\ell});\ Q_{23r} = C_d a_r \sqrt{\frac{2|P_{23r}|}{\rho}}\,\mathrm{sgn}(P_{23r}) \tag{2.41}$$

Assuming laminar fluid flow through the interconnecting pipes, and negligible entrance and exit losses, the volume flow rates across the interconnected chambers are expressed as:

$$Q_{2\ell 1r} = kP_{2\ell 1r};\ Q_{2r1\ell} = kP_{2r1\ell} \tag{2.42}$$

where the coefficient k could be represented as (Liu, 1994):

$$k = \frac{\pi D^4}{128\mu L} \tag{2.43}$$

$P_{2l1r} = P_{2l} - P_{1r}$, $P_{2r1l} = P_{2r} - P_{1l}$, and $Q_{2\ell 1r}$ and $Q_{2r1\ell}$ are the flow rates from chambers 2ℓ to $1r$, and $2r$ to 1ℓ, respectively. μ is the absolute viscosity of fluid, L is the length of the pipe and D is the diameter of the pipe.

The rates of change of fluid volumes in chambers 1 and 2 of the struts relate to the relative velocities of the struts; $\dot{x}_l$ and $\dot{x}_r$, in the following manner:

$$Q_{1\ell} = A_{1\ell}\dot{x}_\ell \; ; Q_{1r} = A_{1r}\dot{x}_r \text{ and } Q_{2\ell} = A_{2\ell}\dot{x}_\ell \; ; \; Q_{2r} = A_{2r}\dot{x}_r \tag{2.44}$$

Assuming incompressible fluid flow, the rates of change of volume in chambers 1 are related to the fluid flows through the interconnecting pipes:

$$Q_{1\ell} = -Q_{2r1\ell} \; ; \; Q_{1r} = -Q_{2\ell 1r} \tag{2.45}$$

The fluid flows will conform to the conservation of mass, such that:

$$Q_{23\ell} + Q_{2\ell} + Q_{2\ell 1r} = 0 \; ; Q_{23r} + Q_{2r} + Q_{2r1\ell} = 0 \tag{2.46}$$

Upon substituting the Equations (2.44) and (2.45) in (2.46), the fluid flow rates through damping restriction can be related to the relative velocity of the left and right struts:

$$Q_{23\ell} = A_{1r}\dot{x}_r - A_{2\ell}\dot{x}_\ell \; ; \; Q_{23r} = A_{1\ell}\dot{x}_\ell - A_{2r}\dot{x}_r \tag{2.47}$$

Pressure Equations

Rearranging Equation (2.47) yields following expressions for the pressure drops across the damping orifices, $P_{23\ell}$ and P_{23r}:

$$P_{23\ell} = \frac{\rho}{2}\left(\frac{Q_{23\ell}}{C_d a_\ell}\right)^2 \text{sgn}(Q_{23\ell}) \; ; \; P_{23r} = \frac{\rho}{2}\left(\frac{Q_{23r}}{C_d a_r}\right)^2 \text{sgn}(Q_{23r}) \tag{2.48}$$

Substituting for Q_{23l} and Q_{23r} from Equation (2.47) in (2.48), yield:

$$\begin{cases} P_{23\ell} = \dfrac{\rho}{2}\left(\dfrac{A_{1r}\dot{x}_r - A_{2\ell}\dot{x}_\ell}{C_d a_\ell}\right)^2 \operatorname{sgn}(A_{1r}\dot{x}_r - A_{2\ell}\dot{x}_\ell) \\ P_{23r} = \dfrac{\rho}{2}\left(\dfrac{A_{1\ell}\dot{x}_\ell - A_{2r}\dot{x}_r}{C_d a_r}\right)^2 \operatorname{sgn}(A_{1\ell}\dot{x}_\ell - A_{2r}\dot{x}_r) \end{cases} \tag{2.49}$$

The instantaneous fluid pressure in chambers 3 of the two interconnected struts are derived assuming a polytropic process of the confined gas:

$$P_{3\ell} = P_{3\ell 0}\left[\frac{V_{3\ell 0}}{V_{3\ell 0} - V_{23\ell}}\right]^n \; ; \; P_{3r} = P_{3r0}\left[\frac{V_{3r0}}{V_{3r0} - V_{23r}}\right]^n \tag{2.50}$$

$$V_{23\ell} = A_{1r}x_r - A_{2\ell}x_\ell \; ; \; V_{23r} = A_{1\ell}x_\ell - A_{2r}x_r \tag{2.51}$$

where $V_{23\ell}$ and V_{23r} represent the changes in gas volume chambers 3, which relate to relative deflections of the struts, x_ℓ and x_r. These relative deflections are derived from the generalized displacement coordinate of the roll plane vehicle model shown in Figure 2.12, such that $x_\ell = x_s - x_u - (\theta_s - \theta_u)\ell$ and $x_r = x_s - x_u + (\theta_s - \theta_u)\ell$. The instantaneous gas pressure and volume in the accumulator is further derived from:

$$P_{3\ell}V_{3\ell}^n = P_{3\ell 0}V_{3\ell 0}^n \; ; \; P_{3r}V_{3r}^n = P_{3r0}V_{3r0}^n \tag{2.52}$$

The pressure drops across the interconnecting pipes is computed from Equation (2.42) and (2.46):

$$P_{2\ell 1r} = \frac{-A_{1r}\dot{x}_r}{k} \; ; \; P_{2r1\ell} = \frac{-A_{1\ell}\dot{x}_\ell}{k} \tag{2.53}$$

The pressures of fluid in chambers 1 and 2 of each strut can be expressed as:

$$\begin{cases} P_{2l} = P_{23\ell} + P_{3\ell} \\ P_{2r} = P_{23r} + P_{3r} \end{cases} \text{ and } \begin{cases} P_{1\ell} = P_{2r} - P_{2r1\ell} \\ P_{1r} = P_{2\ell} - P_{2\ell 1r} \end{cases} \tag{2.54}$$

Equations (2.48) to (2.54) yield following expressions for fluid pressures in different chambers of the struts, as functions of the relative deflections and velocities.

$$\begin{cases} P_{1\ell} = P_{3r0}\left(\dfrac{V_{3r0}}{V_{3r0} - A_{1\ell}x_\ell + A_{2r}x_r}\right)^n + \dfrac{\rho}{2}\left(\dfrac{A_{1\ell}\dot{x}_\ell - A_{2r}\dot{x}_r}{C_d a_r}\right)^2 \operatorname{sgn}(A_{1\ell}\dot{x}_\ell - A_{2r}\dot{x}_\ell) + \dfrac{A_{1\ell}\dot{x}_\ell}{k} \\ P_{1r} = P_{3\ell 0}\left(\dfrac{V_{3\ell 0}}{V_{3\ell 0} - A_{1r}x_r + A_{2\ell}x_\ell}\right)^n + \dfrac{\rho}{2}\left(\dfrac{A_{1r}\dot{x}_r - A_{2\ell}\dot{x}_\ell}{C_d a_\ell}\right)^2 \operatorname{sgn}(A_{1r}\dot{x}_r - A_{2\ell}\dot{x}_\ell) + \dfrac{A_{1r}\dot{x}_r}{k} \end{cases} \tag{2.55}$$

$$\begin{cases} P_{2\ell} = P_{3\ell 0}\left(\dfrac{V_{3\ell 0}}{V_{3\ell 0} - A_{1r}x_r + A_{2\ell}x_\ell}\right)^n + \dfrac{\rho}{2}\left(\dfrac{A_{1r}\dot{x}_r - A_{2\ell}\dot{x}_\ell}{C_d a_\ell}\right)^2 \operatorname{sgn}(A_{1r}\dot{x}_r - A_{2\ell}\dot{x}_\ell) \\ P_{2r} = P_{3r0}\left(\dfrac{V_{3r0}}{V_{3r0} - A_{1\ell}x_\ell + A_{2r}x_r}\right)^n + \dfrac{\rho}{2}\left(\dfrac{A_{1\ell}\dot{x}_\ell - A_{2r}\dot{x}_r}{C_d a_r}\right)^2 \operatorname{sgn}(A_{1\ell}\dot{x}_\ell - A_{2r}\dot{x}_r) \end{cases} \tag{2.56}$$

The above equations clearly show that the fluid pressures in a given strut are related to relative motion responses of both the struts in a complex manner.

Dynamic Forces of Interconnected Suspension (Type I)

The total forces developed by the left and right interconnected strut, F_ℓ and F_r, derived from the forces acting on the pistons:

$$\begin{cases} F_\ell = N_u\left[(P_{2\ell} - P_{2\ell 0})A_{2\ell} - (P_{1\ell} - P_{1\ell 0})A_{1\ell}\right] \\ F_r = N_u\left[(P_{2r} - P_{2r0})A_{2r} - (P_{1r} - P_{1r0})A_{1r}\right] \end{cases} \tag{2.57}$$

The above equations can be rearranged as:

$$\begin{cases} F_\ell = N_u\left[(P_{3\ell} - P_{3\ell 0} + P_{23\ell})A_{2\ell} - (P_{3r} - P_{3\ell 0} + P_{23r} - P_{2r1\ell})A_{1\ell}\right] \\ F_r = N_u\left[(P_{3r} - P_{3r0} + P_{23r})A_{2r} - (P_{3\ell} - P_{3r0} + P_{23\ell} - P_{2\ell 1r})A_{1r}\right] \end{cases} \tag{2.58}$$

In the above equations, the fluid pressures P_{3l} and P_{3r} are described in Equations (2.52), while the pressure drops, P_{23l} and P_{23r}, are expressed in (2.49). The

pressure drops across the connecting pipes ($P_{2\ell 1r}$ and $P_{2r1\ell}$), are also described in Equation (2.53). The substitution for the pressures in terms of relative deflections and velocities would yield two components of the strut forces: a restoring force F_{sj} and a damping force F_{dj} ($j = \ell, r$), such that:

$$F_\ell = F_{c\ell} + F_{s\ell} \text{ and } F_r = F_{cr} + F_{sr}$$

The force components are derived as:

$$\begin{cases} F_{s\ell} = P_{\ell 0} A_2 N_u \left[\left(\dfrac{V_{\ell 0}}{V_{\ell 0} - A_1 x_r + A_2 x_\ell} \right)^n - 1 \right] - P_{\ell 0} A_1 N_u \left[\left(\dfrac{V_{\ell 0}}{V_{\ell 0} - A_1 x_\ell + A_2 x_r} \right)^n - 1 \right] \\ F_{sr} = P_{r0} A_2 N_u \left[\left(\dfrac{V_{r0}}{V_{r0} - A_1 x_\ell + A_2 x_r} \right)^n - 1 \right] - P_{r0} A_1 N_u \left[\left(\dfrac{V_{r0}}{V_{r0} - A_1 x_r + A_2 x_\ell} \right)^n - 1 \right] \end{cases} \quad (2.59)$$

The equations of damping forces can be expressed as:

$$\begin{cases} F_{d\ell} = N_u \left\{ \dfrac{\rho}{2} \left[\dfrac{A_{1r}\dot{x}_r - A_{2\ell}\dot{x}_\ell}{C_d a_\ell} \right]^2 \operatorname{sgn}\left(A_{1r}\dot{x}_r - A_{2\ell}\dot{x}_\ell\right) - \dfrac{\rho}{2} \left[\dfrac{A_{1\ell}\dot{x}_\ell - A_{2r}\dot{x}_r}{C_d a_r} \right]^2 \operatorname{sgn}\left(A_{1\ell}\dot{x}_\ell - A_{2r}\dot{x}_r\right) - \dfrac{128\mu L A_1^2}{\pi D^4} \dot{x}_\ell \right\} \\ F_{dr} = N_u \left\{ \dfrac{\rho}{2} \left[\dfrac{A_{1\ell}\dot{x}_\ell - A_{2r}\dot{x}_r}{C_d a_r} \right]^2 \operatorname{sgn}\left(A_{1\ell}\dot{x}_\ell - A_{2r}\dot{x}_r\right) - \dfrac{\rho}{2} \left[\dfrac{A_{1r}\dot{x}_r - A_{2\ell}\dot{x}_\ell}{C_d a_\ell} \right]^2 \operatorname{sgn}\left(A_{1r}\dot{x}_r - A_{2\ell}\dot{x}_\ell\right) - \dfrac{128\mu L A_1^2}{\pi D^4} \dot{x}_r \right\} \end{cases} \quad (2.60)$$

The restoring forces are influenced not only by the relative displacement of the same side struts but also by those of opposite side struts. The damping forces are through influenced by the coupling effect of the two struts. The flows through the interconnected pipes yield dissipative forces for a given strut as a function of its velocity response.

2.5 ROLL PLANE INTERCONNECTED HYDRO-PNEUMATIC STRUT (TYPE II)

The Type II hydro-pneumatic suspension strut consists of four different fluid chambers (Figure 2.2) and thus offers many options to realize

interconnections between the left and right struts. In this dissertation research, the static and dynamic properties of the suspension system are investigated for two interconnection: (1) interconnection of chambers 3ℓ and $1r$ and vice versa, referred to as 'Inc2'; and (2) interconnection of chambers $3r$ and 1ℓ, and vice versa, referred to as 'Inc3'. The dynamic forces developed by the two configurations are systematically derived in the following sub-section, while the equations of motion for the vehicle model are same as those presented in Equations (2.1) to (2.4).

2.5.1 Dynamic forces of interconnected suspension (Type II, Inc2)

Figure 2.10 illustrates the roll plane model of the vehicle that includes the interconnected struts for deriving the dynamic forces F_l and F_r. The struts are connected to permit flows between chambers 3ℓ and $1r$, and $3r$ and 1ℓ. In order to enhance the roll property of the suspension.

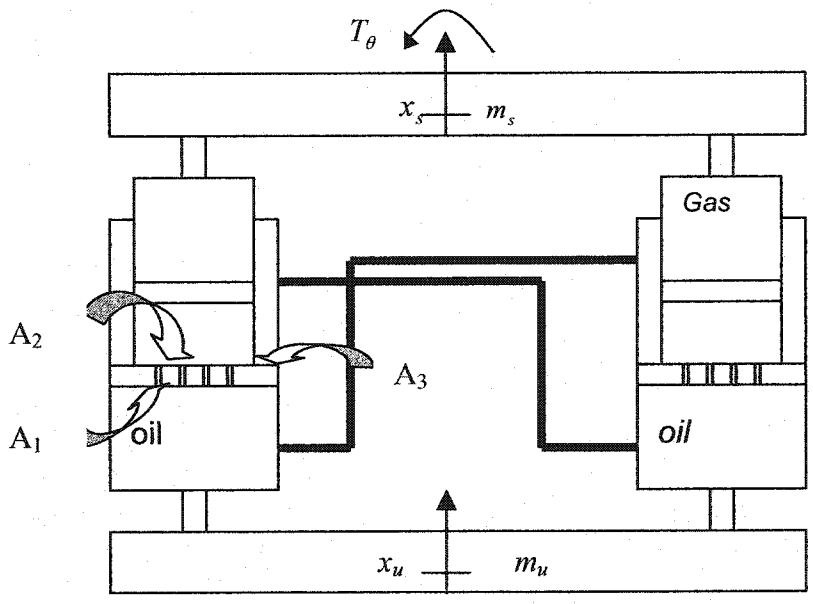

Figure 2.10: Roll plane representation of the interconnected struts (Type II, Inc2)

This configuration of interconnection is referred to as 'Inc2.' The damping orifices are introduced in the piston to permit chambers 1 and 2 of the same strut. The performance of roll motion of the sprung mass caused by either a turning maneuver or road induced excitation would cause compression of the left strut and the fluid in chamber 1ℓ. The high pressure fluid would flow from 1ℓ to $3r$, and thus limit the extension of the right strut. The proposed strut configuration and the interconnection would thus equalize the load distribution through enhanced roll stiffness and damping.

The Static Equilibrium Equation

The static loads supported by the struts, w_l and w_r, are related to the static equilibrium pressures ($P_{1j0} = P_{2j0} = P_{3j0} = P_{4j0}; j = \ell, r$) and effective working areas of the struts:

$$w_\ell = (P_{1\ell 0} - P_a)A_{1\ell} - (P_{3\ell 0} - P_a)A_{3\ell};\ w_r = (P_{1r0} - P_a)A_{1r} - (P_{3r0} - P_a)A_{3r} \tag{2.61}$$

The above expressions are identical to those derived for the unconnected suspension in Equation (2.19). Unlike the unconnected struts, the interconnection, tend to equalize the fluid pressures in both the struts. Considering this pressure equalization, Equation (2.61) may be simplified to yield:

$$w_\ell = (P_{4\ell 0} - P_a)A_{2\ell}\ ;\ w_r = (P_{4r0} - P_a)A_{2r} \tag{2.62}$$

Equations of Fluid Flow

Assuming turbulent flows through the damping orifices, the fluid flow rates from chambers 1 to 2 of left struts and right struts are derived as in the case of unconnected suspension:

$$Q_{12\ell} = C_d u a_{12\ell} \sqrt{\frac{2|P_{12\ell}|}{\rho}} \operatorname{sgn}(P_{12\ell}) \; ; \; Q_{12r} = C_d u a_{12r} \sqrt{\frac{2|P_{12r}|}{\rho}} \operatorname{sgn}(P_{12r}) \tag{2.63}$$

where u is the number of orifices that permit flows between chambers 1 and 2 of each strut.

Assuming laminar fluid flows through the interconnecting pipes, the fluid flow rates across the right and left struts ($Q_{1\ell 3r}$ and $Q_{1r3\ell}$) can be derived from:

$$Q_{1\ell 3r} = kP_{1\ell 3r} \; ; \; Q_{1r3\ell} = kP_{1r3\ell} \tag{2.64}$$

where $P_{1\ell 3r} = P_{1\ell} - P_{3r} \; ; \; P_{1r3\ell} = P_{1r} - P_{3\ell}$ (2.65)

The rate change of fluid volume in chambers 1 of strut is related to its relative velocity response, as in the case of unconnected struts:

$$Q_{1\ell} = A_{1\ell}\dot{x}_\ell \; ; \; Q_{1r} = A_{1r}\dot{x}_r \tag{2.66}$$

In accordance with mass conservation, the rates of fluid volumes are related in the following manner:

$$Q_{1\ell} + Q_{12\ell} + Q_{1\ell 3r} = 0 \; ; \; Q_{1r} + Q_{12r} + Q_{1r3\ell} = 0 \tag{2.67}$$

The rate of change of fluid volume can be further related to the fluid flows through the interconnecting pipes, and relative velocity responses of the struts:

$$Q_{3\ell} + Q_{1r3\ell} = 0 \; ; \; Q_{3r} + Q_{1\ell 3r} = 0 \tag{2.68}$$

The fluid flow rate in chamber 3 of the left and right suspension struts are related to the relative velocities of the suspension strut.

$$Q_{3\ell} = -A_{3\ell}\dot{x}_\ell \; ; \; Q_{3r} = -A_{3r}\dot{x}_r \tag{2.69}$$

Upon substituting for Q_{1j} and Q_{3j} from Equation (2.66) and (2.68) in (2.67) yields following expressions for the orifice flows in terms of coupled relative velocity responses of the two struts:

$$Q_{12\ell} = -A_{1\ell}\dot{x}_\ell + A_{3r}\dot{x}_r \; ; \; Q_{12r} = -A_{1r}\dot{x}_r + A_{3\ell}\dot{x}_\ell \tag{2.70}$$

Pressure Equations

The pressure differential associated with fluid flows across the damping orifices can also be expressed in terms of coupled relative velocity responses from Equation (2.63) and (2.70), and letting $a_{12\ell} = a_{12r} = a_{12}$:

$$\begin{cases} P_{12\ell} = \dfrac{\rho}{2}\left[\dfrac{A_{3r}\dot{x}_r - A_{1\ell}\dot{x}_\ell}{C_d u a_{12}}\right]^2 \operatorname{sgn}(A_{3r}\dot{x}_r - A_{1\ell}\dot{x}_\ell) \\ P_{12r} = \dfrac{\rho}{2}\left[\dfrac{A_{3\ell}\dot{x}_\ell - A_{1r}\dot{x}_r}{C_d u a_{12}}\right]^2 \operatorname{sgn}(A_{3\ell}\dot{x}_\ell - A_{1r}\dot{x}_r) \end{cases} \tag{2.71}$$

Equation (2.64) further yields the pressure drops across the connecting pipes ($P_{1\ell 3r}$ and $P_{1r3\ell}$) in terms of the relative velocity responses (Liu, 1994):

$$P_{1\ell 3r} = \frac{Q_{1\ell 3r}}{k} = \frac{(A_3\dot{x}_r)128\mu L}{\pi D^4} \; ; \; P_{1r3\ell} = \frac{Q_{1r3\ell}}{k} = \frac{(A_3\dot{x}_\ell)128\mu L}{\pi D^4} \tag{2.72}$$

The instantaneous pressure and volume of the gas in chamber 4 of each strut is related to the static equilibrium pressure and volumes:

$$P_{4\ell 0}V_{4\ell 0}^n = P_{4\ell}V_{4\ell}^n \; ; \; P_{4r0}V_{4r0}^n = P_{4r}V_{4r}^n \tag{2.73}$$

The change in the gas volume of a given strut is dependent upon the relative deflections of both the struts. The instantaneous gas pressures ($P_{4\ell}$ and P_{4r}) are thus derived as:

$$P_{4\ell} = P_{4\ell 0}\left(\frac{V_{4\ell 0}}{V_{4\ell 0} + A_{1\ell}x_\ell - A_{3r}x_r}\right)^n \; ; \; P_{4r} = P_{4r0}\left(\frac{V_{4r0}}{V_{4r0} + A_{1r}x_r - A_{3\ell}x_\ell}\right)^n \tag{2.74}$$

Considering that $P_{4j} = P_{2j}$ for negligible seal friction and inertia of the floating piston, fluid pressures in chamber 3ℓ and $3r$ can be expressed as:

$$P_{3\ell} = P_{4r} + P_{12r} - P_{1r3\ell};\ P_{3r} = P_{4\ell} + P_{12\ell} - P_{1\ell 3r} \tag{2.75}$$

In the above equations, the terms P_{4j} and P_{12j} $(j = \ell, r)$ have been described in Equation (2.74) and (2.71), respectively, in terms of relative position and velocity responses. The pressure differentials across the interconnections ($P_{1\ell 3r}$ and $P_{1r3\ell}$) have also been derived as functions of the position and velocity response in Equation (2.72). The above equations clearly illustrate that fluid pressures in a given strut are related to relative motion responses of both the strut due to the interconnection.

Dynamic Suspension Forces

The suspension forces developed by the left and right struts can be derived from:

$$\begin{cases} F_\ell = N_u\left[(P_{1\ell} - P_{0\ell})A_{1\ell} - (P_{3\ell} - P_{0\ell})A_{3\ell}\right] \\ F_r = N_u\left[(P_{1r} - P_{0r})A_{1r} - (P_{3r} - P_{0r})A_{3r}\right] \end{cases} \tag{2.76}$$

The above equation can be rearranged as:

$$\begin{cases} F_\ell = N_u\left[(P_{2\ell} + P_{12\ell} - P_{0\ell})A_{1\ell} - (P_{2r} + P_{12r} - P_{1r3\ell} - P_{0\ell})A_{3\ell}\right] \\ F_r = N_u\left[(P_{2r} + P_{12r} - P_{0r})A_{1r} - (P_{2\ell} + P_{12\ell} - P_{1\ell 3r} - P_{0r})A_{3r}\right] \end{cases} \tag{2.77}$$

Upon substituting for fluid pressures from Equations (2.71), (2.72) and (2.74), forces developed by the struts can be expressed by:

$$\begin{cases} F_{s\ell} = N_u P_{40} A_1 \left\{ \left[\dfrac{V_{40}}{V_{40} + A_1 x_\ell - A_3 x_r} \right]^n - 1 \right\} - N_u P_{40} A_3 \left\{ \left[\dfrac{V_{40}}{V_{40} + A_1 x_r - A_3 x_\ell} \right]^n - 1 \right\} \\ F_{sr} = N_u P_{40} A_1 \left\{ \left[\dfrac{V_{40}}{V_{40} + A_1 x_r - A_3 x_\ell} \right]^n - 1 \right\} - N_u P_{40} A_3 \left\{ \left[\dfrac{V_{40}}{V_{40} + A_1 x_\ell - A_3 x_r} \right]^n - 1 \right\} \end{cases} \tag{2.78}$$

$$\begin{cases} F_{d\ell} = \dfrac{\rho}{2} N_u A_1 \left[\dfrac{A_3\dot{x}_r - A_1\dot{x}_\ell}{C_d u a_{12}} \right]^2 \operatorname{sgn}(A_3\dot{x}_r - A_1\dot{x}_\ell) - \dfrac{\rho}{2} N_u A_3 \left[\dfrac{A_3\dot{x}_\ell - A_1\dot{x}_r}{C_d u a_{12}} \right]^2 \operatorname{sgn}(A_3\dot{x}_\ell - A_1\dot{x}_r) - \dfrac{(A_3^2\dot{x}_r)128\mu L N_u}{\pi D^4} \\ F_{dr} = \dfrac{\rho}{2} N_u A_1 \left[\dfrac{A_3\dot{x}_\ell - A_1\dot{x}_r}{C_d u a_{12}} \right]^2 \operatorname{sgn}(A_3\dot{x}_\ell - A_1\dot{x}_r) - \dfrac{\rho}{2} N_u A_3 \left[\dfrac{A_3\dot{x}_r - A_1\dot{x}_\ell}{C_d u a_{12}} \right]^2 \operatorname{sgn}(A_3\dot{x}_r - A_1\dot{x}_\ell) - \dfrac{(A_3^2\dot{x}_\ell)128\mu L N_u}{\pi D^4} \end{cases} \quad (2.79)$$

where F_{sj} and F_{dj} represent the restoring and damping force components of strut j ($j = \ell, r$), respectively. It is evident that the restoring and damping forces developed by a strut are dependent upon not only the relative motion response of the same strut, but also that of the strut on the other side of the track. The flows through the interconnecting pipes yield dissipative force component of a strut as a function of the relative velocity response of the other strut, which represents the feedback effect of the interconnected struts.

2.5.2 Dynamic forces of interconnected struts (Type II, Inc3)

Figure 2.11 illustrates the roll plane model of the vehicle that includes the interconnected struts for deriving the dynamic forces F_ℓ and F_r. The struts are interconnected to permit flows between chambers 1ℓ and $2r$, and 2ℓ and $1r$. This configuration of interconnection is referred to as 'Inc3.' The damping orifices are introduced in the piston to allow fluid flow between chambers 1 and 3 of each strut. Under roll motion of the sprung mass would cause the highly pressure fluid flow from chambers 1 of the left strut to chamber 2 of the right strut. This would equalize the loads on the two struts by enhancing the suspension roll properties. The fluid flows in chamber $2r$, however, may cause considerable compression of

the gas in chamber 4, which would most likely nullify the effect of the strut interconnection.

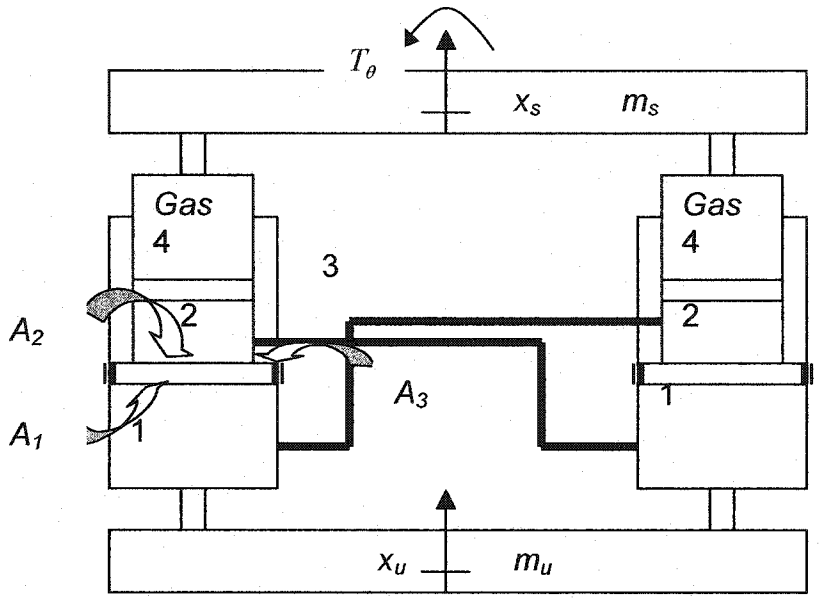

Figure 2.11: Roll plane representation of the Interconnected struts (Type II, Inc3)

The Static Equilibrium Equation

The static loads supported by the struts, w_l and w_r, are related to the static equilibrium pressures ($P_{1j0} = P_{2j0} = P_{3j0} = P_{4j0}; j = \ell, r$) and effective working areas of the struts:

$$w_\ell = (P_{1\ell 0} - P_a)A_{1\ell} - (P_{3\ell 0} - P_a)A_{3\ell};\ w_r = (P_{1r0} - P_a)A_{1r} - (P_{3r0} - P_a)A_{3r} \qquad (2.80)$$

The above expressions are identical to those derived for the unconnected suspension in Equation (2.19). Unlike the unconnected struts, the interconnection, tend to equalize the fluid pressures in both the struts. Considering this pressure equalization, Equation (2.80) may be simplified to yield:

$$w_\ell = (P_{4\ell 0} - P_a)A_{2\ell};\ w_r = (P_{4r0} - P_a)A_{2r} \tag{2.81}$$

Equations of Fluid Flow

Assuming turbulent flows through the damping orifices, the fluid flow rates from chambers 1 to 3 of left struts and right struts are derived as in the case of unconnected suspension:

$$Q_{13\ell} = C_d v a_{13\ell}\sqrt{\frac{2|P_{13\ell}|}{\rho}}\,\mathrm{sgn}(P_{13\ell});\ Q_{13r} = C_d v a_{13r}\sqrt{\frac{2|P_{13r}|}{\rho}}\,\mathrm{sgn}(P_{13r}) \tag{2.82}$$

where v is the number of orifices that permit flows between chambers 1 and 3 of each struts.

Assuming laminar fluid flows through the interconnecting pipes, the fluid flow rates across the right and left struts ($Q_{1\ell 2r}$ and $Q_{1r2\ell}$) can be derived from:

$$Q_{1\ell 2r} = kP_{1\ell 2r};Q_{1r2\ell} = kP_{1r2\ell} \tag{2.83}$$

where $P_{1\ell 2r} = P_{1\ell} - P_{2r};\ P_{1r2\ell} = P_{1r} - P_{2\ell}$ (2.84)

The rate change of fluid volume in chambers 1 of strut is related to its relative velocity response, as in the case of unconnected struts:

$$Q_{1\ell} = A_{1\ell}\dot{x}_\ell;\ Q_{1r} = A_{1r}\dot{x}_r \tag{2.85}$$

In accordance with mass conservation, the rates of fluid volumes are related in the following manner:

$$Q_{1\ell} + Q_{13\ell} + Q_{1\ell 2r} = 0;\ Q_{1r} + Q_{13r} + Q_{1r2\ell} = 0 \tag{2.86}$$

The rate of change of fluid volume can be further related to the fluid flows through the interconnecting pipes, and relative velocity responses of the struts:

$$Q_{2\ell} + Q_{1r2\ell} = 0;\ Q_{2r} + Q_{1\ell 2r} = 0 \tag{2.87}$$

The fluid flow rate in chamber 3 of the left and right suspension struts are related to the relative velocities of the suspension strut.

$$Q_{13\ell} = -A_{3\ell}\dot{x}_\ell \; ; \; Q_{13r} = -A_{3r}\dot{x}_r \tag{2.88}$$

Upon substituting for Q_{1j} and Q_{3j} from Equation (2.85) and (2.88) in (2.86) yields following expressions for the orifice flows in terms of coupled relative velocity responses of the two struts:

$$Q_{1\ell 2r} = -A_{2r}\dot{x}_r \; ; \; Q_{1r2\ell} = -A_{2\ell}\dot{x}_\ell \tag{2.89}$$

Pressure Equations

The pressure differential associated with fluid flows across the damping orifices can also be expressed in terms of coupled relative velocity responses from Equation (2.82) and (2.88), and letting $a_{13\ell} = a_{13r} = a_{13}$:

$$P_{13\ell} = \frac{\rho}{2}\left[\frac{A_{3\ell}\dot{x}_\ell}{C_d v a_{13}}\right]^2 sign(-\dot{x}_\ell) \; ; \; P_{13r} = \frac{\rho}{2}\left[\frac{A_{3r}\dot{x}_r}{C_d v a_{13}}\right]^2 sign(-\dot{x}_r) \tag{2.90}$$

Equation (2.91) further yields the pressure drops across the connecting pipes ($P_{1\ell 2r}$ and $P_{1r2\ell}$) in terms of the relative velocity responses:

$$P_{1\ell 2r} = \frac{Q_{1\ell 2r}}{K} = \frac{(-A_{2r}\dot{x}_r)128\mu L}{\pi D^4} \; ; \; P_{1r2\ell} = \frac{Q_{1r2\ell}}{K} = \frac{(-A_{2\ell}\dot{x}_\ell)128\mu L}{\pi D^4} \tag{2.91}$$

The change in the gas volume of a given strut is dependent upon the relative deflections of both the struts. The instantaneous gas pressures ($P_{4\ell}$ and P_{4r}) are thus derived as:

$$P_{4\ell} = P_{4\ell 0}\left(\frac{V_{4\ell 0}}{V_{4\ell 0} + A_{2r}x_r}\right)^n \; ; \; P_{4r} = P_{4r0}\left(\frac{V_{4r0}}{V_{4r0} + A_{2\ell}x_\ell}\right)^n \tag{2.92}$$

Considering that $P_{4j} = P_{2j}$ for negligible seal friction and inertia of the floating piston, fluid pressures in chambers $1j$ and $3j$ $(j = \ell, r)$ can be expressed as:

$$\begin{cases} P_{1\ell} = P_{2r} + P_{1\ell 2r} \\ P_{1r} = P_{2\ell} + P_{1r2\ell} \end{cases} \tag{2.93}$$

$$\begin{cases} P_{3\ell} = P_{1\ell} - P_{13\ell} = P_{2r} + P_{1\ell 2r} - P_{13\ell} \\ P_{3r} = P_{1r} - P_{13r} = P_{2\ell} + P_{1r2\ell} - P_{13r} \end{cases} \tag{2.94}$$

In the above equations, the terms P_{4j} and P_{13j} have been described in Equation (2.92) and (2.90), respectively, in terms of relative position and velocity responses. The pressure differentials across the interconnections ($P_{1\ell 3r}$ and $P_{1r3\ell}$) have also been derived as functions of the position and velocity response in Equation (2.91). The above equations clearly illustrate that fluid pressures in a given strut are related to relative motion responses of both the strut due to the interconnection.

The dynamic forces of the interconnected suspension

The suspension forces developed by the left and right struts can be derived from:

$$\begin{cases} F_\ell = N_u\left[(P_{1\ell} - P_{0\ell})A_{1\ell} - (P_{3\ell} - P_{0\ell})A_{3\ell}\right] \\ F_r = N_u\left[(P_{1r} - P_{0r})A_{1r} - (P_{3r} - P_{0r})A_{3r}\right] \end{cases} \tag{2.95}$$

The above equation can be rearranged as:

$$\begin{cases} F_\ell = N_u\left[P_{4r}A_{1\ell} - P_{0\ell}A_{1\ell} + P_{1\ell 2r}A_{1\ell} - P_{4r}A_{3\ell} - P_{1\ell 2r}A_{3\ell} + P_{0\ell}A_{3\ell} + P_{13\ell}A_{3\ell}\right] \\ F_r = N_u\left[P_{4r}A_{1r} - P_{0r}A_{1r} + P_{1\ell 2r}A_{1r} - P_{4\ell}A_{3r} - P_{1r2\ell}A_{3r} + P_{0r}A_{3r} + P_{13r}A_{3r}\right] \end{cases} \tag{2.96}$$

Upon substituting for fluid pressures from Equations (2.90), (2.91) and (2.92), forces developed by the struts can be expressed by their restoring and dissipative force components, as discussed in the previous section:

$$F_{s\ell} = N_u P_{40} A_2 \left\{ \left[\frac{V_{40}}{V_{40} + A_2 x_\ell} \right]^n - 1 \right\}; \; F_{sr} = N_u P_{40} A_2 \left\{ \left[\frac{V_{40}}{V_{40} + A_2 x_r} \right]^n - 1 \right\} \tag{2.97}$$

$$\begin{cases} F_{d\ell} = -N_u \dfrac{\rho}{2} A_3 \left[\dfrac{A_3 \dot{x}_\ell}{C_d v a_{13}} \right]^2 \operatorname{sgn}(\dot{x}_\ell) - N_u \dfrac{A_2^2 \dot{x}_r 128 \mu L}{\pi D^4} \\ F_{dr} = -N_u \dfrac{\rho}{2} A_3 \left[\dfrac{A_3 \dot{x}_r}{C_d v a_{13}} \right]^2 \operatorname{sgn}(\dot{x}_r) - N_u \dfrac{(A_2^2 \dot{x}_\ell) 128 \mu L}{\pi D^4} \end{cases} \tag{2.98}$$

where F_{sj} and F_{dj} represent the restoring and damping force components of strut j ($j = \ell, r$), respectively. It is evident that the restoring and damping forces developed by a strut are dependent upon not only the relative motion response of the same strut, but also related to that of the strut on the other side of the track. The flows through the interconnecting pipes yield dissipative force component of a strut as a function of the relative velocity response of the other strut, which represents the feedback effect of the interconnect struts.

2.5 SUMMARY

Two different designs of hydro-pneumatic suspension struts are presented and discussed to realize roll-plane interconnected suspension. A generalized four-DOF roll plane model of a heavy vehicle is developed to investigate the static and dynamic properties of different unconnected and interconnected suspension configurations involving Type I and Type II struts. A total of three interconnected suspension configurations are formulated. Those include: (1) Type I struts that has been reported in an earlier study; (2) Type II struts with interconnections between the lower chamber of left strut to the upper confined chamber of the right strut; and (3) Type II strut with lower chamber of the left strut to the upper chamber of the right strut adjacent to the gas chamber. The

equations of motion of the vehicle model are derived under excitations arising from the road and maneuver induced roll moment. The dynamic forces developed by the unconnected and interconnected struts are derived using the fluid flow and pressure equations. The resulting restoring and dissipative force components of different interconnected struts are discussed.

CHAPTER 3

PROPERTIES OF THE DIFFERENT HYDRO-PNEUMATIC SUSPENSION SYSTEMS

3.1 INTRODUCTION

The ride quality, handling and directional control performance of a vehicle is strongly related to the static and dynamic properties of its suspension. Ride and roll dynamic performance characteristics of a vehicle are directly influenced by the suspension properties, such as suspension vertical spring rate, roll stiffness, and damping characteristics. The analytical models of different unconnected and interconnected suspension systems developed in the previous chapter are thus analyzed to derive their vertical and roll properties. Sharp and Hassan (1986) have stated that the performance characteristics of competitive suspension should be compared on the basis of equal working space. The static and dynamic properties of the suspension systems are evaluate in terms of those related to ride and roll dynamic properties are described below: The relative properties of the suspension systems are evaluated in terms of their load-carrying capacities charge pressure requirement, vertical spring rates, roll stiffness, and vertical and roll mode damping characteristics. The parameters of various suspension systems are selected to achieve identical load carrying capacity and maximum travel, furthermore, the parameters are tuned to realize comparable ride related parameters, specifically, the vertical spring rate and damping.

3.2 DEFINITIONS OF STATIC AND DYNAMIC

Load-Carrying Capacity is the load supported by the suspension system at the design ride height, it is related to its static force-deflection characteristics, initial charge pressure and the working area. Relative evaluations of different suspension configurations should be carried out under identical load carrying capacity, which may be realized by varying the charge pressure and the working area. Relationships between the load carrying capacity, working area and charge pressure, for different suspension configurations have been described in Equation (2.6), (2.19), (2.29), (2.61), (2.80).

The Suspension Rate of a vehicle is its vertical spring rate at a specific operating point. The vertical spring rate due to a strut is derived from the change in the strut force with respect to a change in the relative deflection. The suspension rate of a hydro-pneumatic strut is derived from pressure-deflection relationships for the confined gas.

Suspension Roll Stiffness The rate of change in the restoring moment caused by the strut forces, F_ℓ and F_r, with respect to change in the relative roll deflection.

The Damping Forces Damping characteristics of suspension in the vertical mode are expressed in terms of vertical force-vertical velocity characteristics. The vertical damping due to a suspension configuration is derived from the total damping force produced by the right and left struts, as described in Equation (2.18), (2.35), with respect to the relative velocity response of the sprung and unsprung masses ($\dot{x}_s - \dot{x}_u$).

3.3 LOAD-CARRYING CAPACITY AND STRUT DESIGN PARAMETERS

The force developed by a hydro-pneumatic suspension strut comprises two components: a restoring force component attributed to the gas chambers; and the damping force attributed to flows through damping restriction. The load carrying capacity of the strut depends upon the gas charge pressure, gas volume and the effective working area. The load carrying capacity thus relates to the restoring force property of the strut. The strut design parameters are selected to achieve identical values of vertical spring rates, irrespective of the strut type and interconnection configuration. The fluid pressure corresponding to static equilibrium is also held constant for all suspension configurations. With the exception of interconnected Type I struts (Inc1), where the rod area serves as the effective working area. Assuming symmetric load distribution on left and right struts, the anti-roll bars have no effect on the vertical suspension rate, which relates to the pressure and volume of the confined gas, and the effective working area. The load-carrying capacity of an unconnected suspension with an anti-roll bar is thus the same as that of unconnected without anti-roll bar. The load carry capacity of the Type I strut can be expressed from Equation 2.5:

$$W = 2N_u(P_0 - P_a)A_2 \tag{3.1}$$

where W is the total load carrying capacity, A_2 is the effective working area of the strut, which is the piston head area in Type I strut, and the floating piston area in Type II struts. Assuming equal load distribution, the gas pressure is related to the static deflections, x_0:

$$P_0 = P_c\left(\frac{V_c}{V_c - A_2 x_0}\right)^n \tag{3.2}$$

where P_c and V_c are the initial charge pressure and volume of the gas, respectively.

Interconnected Type I Strut (Inc1)

The interconnection of type 1 struts yields the effective working area as $A_2 - A_1$, as described in section 2. This would require the use of either high charge pressure or larger rod area, in order to achieve the same load carrying capacity. By selecting the rod area equal to the effective working areas offered by Type I and Type II strut would yield relatively larger strut size or relatively small volume of chamber 1. The load carrying capacity of the Inc1 configuration could be derived from Equation (2.38), as:

$$W = 2N_u(P_0 - P_a)(A_2 - A_1) \tag{3.3}$$

Assume equal load distribution and static deflection, the static equilibrium may be expressed as:

$$P_0 = P_c\left(\frac{V_c}{V_c - A_r x_0}\right)^n \tag{3.4}$$

In an effort to achieve identical suspension rate, the fluid pressure P_0 is selected to be slightly higher that that used in the unconnected struts, which further yields slightly lower gas volume, as summarized in Table 3.3.

Interconnected Type II Struts (Inc 2 and Inc3)

The load-carrying capacities of Inc2 and Inc3 suspension configurations are described in a similar manner, as.

$$W = 2N_u(P_{40} - P_a)A_2 \tag{3.5}$$

where A_2 represent the floating piston area. For this configuration the same values of P_0 and V_0 yield identical suspension rate. The relationship between the static deflection and the static pressure is identical to that described in Equation (3.6)

3.4 SUSPENSION RATES OF DIFFERENT STRUT CONFIGURATIONS

Assuming identical geometry of struts used employed in the left-and-right-tracks, ($A_{1\ell} = A_{1r} = A_1$; $A_{3\ell} = A_{3r} = A_3$; and $A_{2\ell} = A_{2r} = A_2$), the restoring force F_s developed by an unconnected struts (Type I and Type II) is related to the vertical deflection x and the static equilibrium pressure, as described earlier in section (2.3.2):

$$F_s = \left[P_0 \left(\frac{V_0}{V_0 - A_2 x} \right)^n - P_a \right] A_2 \tag{3.6}$$

The vertical rate, k_v, of the suspension strut can be derived as:

$$k_v = -\frac{dF_s}{dx} = nP_0 V_0^n A_2^2 \frac{1}{(V_0 - A_2 x)^{n+1}} \tag{3.7}$$

The static stiffness (k_{vu}^0) corresponding to the static design height ($x = 0$) is thus computed from:

$$k_{vu}^0 = nA_2^2 \frac{P_0}{V_0} \tag{3.8}$$

The static stiffness is a proportional function of the static equilibrium pressure, and inversely proportional to the design gas volume. The resulting static deflection of the strut, x_0, is derived as:

$$x_0 = \frac{w}{k_{vu}^0} = \frac{wV_0}{nA_2^2 P_0} \tag{3.9}$$

where w is the load supported by one strut at the design ride height.

Interconnected Type I Strut (Inc1)

The restoring forces developed by the interconnected right- and left-struts relate to instantaneous deflection of both the struts, as described earlier in section 2.4.1. Equation (2.59):

$$\begin{cases} F_{s\ell} = P_0 V_0^n \left[\dfrac{A_2}{(V_0 + A_2 x_\ell - A_1 x_r)^n} - \dfrac{A_1}{(V_0 + A_2 x_r - A_1 x_\ell)^n} \right] - P_a (A_2 - A_1) \\ F_{sr} = P_0 V_0^n \left[\dfrac{A_2}{(V_0 + A_2 x_r - A_1 x_\ell)^n} - \dfrac{A_1}{(V_0 + A_2 x_\ell - A_1 x_r)^n} \right] - P_a (A_2 - A_1) \end{cases} \tag{3.10}$$

The suspension rate due to each interconnected strut is thus dependent upon the deflections of both the struts:

$$k_{v\ell} = nP_0 V_0^n \left\{ \frac{A_2^2 - A_1 A_2 \dfrac{dx_r}{dx_\ell}}{\left[V_0 + A_2 x_\ell - A_1 x_r\right]^{n+1}} + \frac{A_1^2 - A_1 A_2 \dfrac{dx_r}{dx_\ell}}{\left[V_0 + A_2 x_r - A_1 x_\ell\right]^{n+1}} \right\}$$

$$k_{vr} = nP_0 V_0^n \left\{ \frac{A_2^2 - A_1 A_2 \dfrac{dx_\ell}{dx_r}}{\left[V_0 + A_2 x_r - A_1 x_\ell\right]^{n+1}} + \frac{A_1^2 - A_1 A_2 \dfrac{dx_\ell}{dx_r}}{\left[V_0 + A_2 x_\ell - A_1 x_r\right]^{n+1}} \right\} \tag{3.11}$$

Considering that both the struts would encounter identical relative displacements, under a pure bounce motion ($x_\ell = x_r = x$). Equation (3.11) is simplified to yield following form of the suspension rate due to each strut:

$$k_{vi} = nP_0 V_0^n A_r^{\,2} \frac{1}{\left[V_0 + A_r x\right]^{n+1}} \quad (i = \ell, r) \tag{3.12}$$

where A_r is the piston rod area ($A_2 - A_1$).

Interconnected Type II Strut (Inc2)

The restoring forces developed by the interconnected right-and left-struts relate to instantaneous deflection of both the struts, as described earlier in section (2.5.1). Equation (2.78):

$$\begin{cases} F_{s\ell} = nP_{40}V_{40}\left[\dfrac{A_1}{(V_{40}+A_1x_\ell - A_3x_r)^n} - \dfrac{A_3}{(V_{40}+A_1x_r - A_3x_\ell)^n}\right] - P_a(A_1 - A_3) \\ F_{sr} = nP_{40}V_{40}\left[\dfrac{A_1}{(V_{40}+A_1x_r - A_3x_\ell)^n} - \dfrac{A_3}{(V_{40}+A_1x_\ell - A_3x_r)^n}\right] - P_a(A_1 - A_3) \end{cases} \tag{3.13}$$

The suspension rate due to each interconnected strut is thus dependent upon the deflections of both the struts:

$$k_{v\ell} = nP_{40}V_{40}^n\left\{\frac{A_1^2 - A_1A_3\dfrac{dx_r}{dx_\ell}}{[V_{40}+A_1x_\ell - A_3x_r]^{n+1}} + \frac{A_3^2 - A_1A_3\dfrac{dx_r}{dx_\ell}}{[V_{40}+A_1x_r - A_3x_\ell]^{n+1}}\right\}$$

$$k_{vr} = nP_{40}V_{40}^n\left\{\frac{A_1^2 - A_1A_3\dfrac{dx_\ell}{dx_r}}{[V_{40}+A_1x_r - A_3x_\ell]^{n+1}} + \frac{A_3^2 - A_1A_3\dfrac{dx_\ell}{dx_r}}{[V_{40}+A_1x_\ell - A_3x_r]^{n+1}}\right\} \tag{3.14}$$

Considering that both the struts would encounter identical relative displacements, under a pure bounce motion ($x_\ell = x_r = x$), Equation (3.14) is simplified to yield following form of the suspension rate due to each strut:

$$k_{vi} = nP_{40}V_{40}^nA_2^2\frac{1}{(V_{40}+A_2x)^{n+1}} \qquad (i = \ell, r) \tag{3.15}$$

Interconnected Type II Strut (Inc3)

An examination of this configuration of interconnected suspension system suggests that the chamber 2 and 4 remain uncoupled with chamber 1 and 3 of the same strut due to absence of orifice flows between chamber 1 and 2. The chambers 1 of the right strut, however is coupled to chamber 2 and 4 of the left strut. A deflection of the left strut would thus develop a restoring force in the right strut as a function of its relative deflection response, and vice-versa. Under pure bounce motion, the restoring force developed by each strut in the interconnected configuration and thus the suspensions are identical to that of the unconnected Type II strut.

3.5 SUSPENSION ROLL STIFFNESS OF DIFFERENT STRUTS

The vehicle sprung mass experiences a roll motion, θ, and a displacement with respect to unsprung mass, $x_s - x_u$, when subjected to a roll moment, as shown in Figure 2.3. The roll motion of the sprung mass caused by either a directional maneuver or a road bump is strongly dependent upon the effective roll stiffness of the suspension. The vehicle suspensions are mostly designed to yield low vertical suspension rate to achieve acceptable ride quality. The low vertical spring rates, however, yield lower roll stiffness and thus higher roll motion of the sprung mass. Auxiliary roll stiffness is thus frequently used to enhance the effective roll stiffness. Owing to the nonlinear force-deflection relationship, the hydro-pneumatic suspensions yield a relatively complex relationship between the restoring roll moment and roll deflection. The right and left struts (Type I and II) in the unconnected suspension configurations undergo relative deflections,

$x_\ell = x_s - x_u - \ell_\ell(\theta_s - \theta_u)$ and $x_r = x_s - x_u + \ell_r(\theta_s - \theta_u)$ respectively, where $x = x_s - x_u$ is the relative vertical deflection and $\theta = \theta_s - \theta_u$ is the relative roll deflection. The moment developed due to differential restoring forces can be derived from:

$$M = N_u(P_\ell - P_r)A_2\ell = N_u P_0 V_0^n A_2 \ell \left\{ \frac{1}{\left[V_0 + (x - \ell\theta)A_2\right]^n} - \frac{1}{\left[V_0 + (x + \ell\theta)A_2\right]^n} \right\} \tag{3.16}$$

The effective roll stiffness of the unconnected suspension, k_r, can be derived as:

$$k_r = \frac{dM}{d\theta} = nP_0V_0^n A_2^2 \ell^2 N_u \left\{ \frac{1 - \frac{dx}{d\theta}/\ell}{\left[V_0 + (x - \ell\theta)\right]^{n+1}} + \frac{1 + \frac{dx}{d\theta}/\ell}{\left[V_0 + (x + \ell\theta)\right]^{n+1}} \right\} \tag{3.17}$$

where $\frac{dx}{d\theta}$ can be computed from the static equilibrium equation, Equation (3.18):

$$(P_\ell - P_0)A_2 + (P_r - P_0)A_2 = 0 \tag{3.18}$$

where P_ℓ and P_r were expressed in Equation (3.16), the equation of static equilibrium can be obtained by combing the Equation (3.16) and (3.18):

$$g(x,\theta) = \frac{1}{\left[V_0 + (x - \ell\theta)A_2\right]^n} + \frac{1}{\left[V_0 + (x + \ell\theta)A_2\right]^n} - \frac{2}{V_0^n} = 0 \tag{3.19}$$

The above equation can be manipulated to yield:

$$\frac{dx}{d\theta} = -\frac{\partial g/\partial\theta}{\partial g/\partial\theta} = \ell \left\{ \frac{\left[V_0 + (x + \ell\theta)A_2\right]^{n+1} - \left[V_0 + (x - \ell\theta)A_2\right]^{n+1}}{\left[V_0 + (x + \ell\theta)A_2\right]^{n+1} + \left[V_0 + (x - \ell\theta)A_2\right]^{n+1}} \right\} \tag{3.20}$$

Equation (3.17) to (3.20) can be solved simultaneously to derive the restoring roll moment corresponding to a given relative roll deflection.

The total roll stiffness of an unconnected suspension with anti-roll bar is the sum of the auxiliary roll stiffness due to the anti-roll bar and the roll stiffness arising from the hydro-pneumatic struts described in Equation (3.17), such that:

$$k_r^{'} = k_r + k_\theta \tag{3.21}$$

where $k_r^{'}$ is the total roll stiffness of the unconnected suspension with anti-roll bar, and k_θ is the auxiliary roll stiffness due to anti-roll bar, as described in section 2.3.4.

Interconnected Type I Strut (Inc1)

Under the sprung mass roll motion, the gas pressures in the left and right struts ($P_{3\ell}$ and P_{3r}), as described earlier in Equation (2.50), yield a restoring roll moment, given by:

$$M = N_u (P_{3\ell} - P_{3r})(A_1 + A_2)\ell \tag{3.22}$$

Upon substituting for $P_{3\ell}$ and P_{3r} from Equation (3.22), the restoring roll moment can be expressed as a function of the roll deflection

$$M = P_0 V_0^n (A_1 + A_2) l N_u \left\{ \frac{1}{\left[V_0 + A_2 z_\ell - A_1 z_r\right]^n} - \frac{1}{\left[V_0 + A_2 z_r - A_1 z_\ell\right]^n} \right\} \tag{3.23}$$

The roll stiffness of the interconnected suspension is then derived in a manner similar to that described for the unconnected suspension:

where $\frac{dx}{d\theta}$ can be computed from the static equilibrium equation:

$$g(x,\theta) = \frac{1}{\left[V_0 + (x - \ell\theta)A_2 - A_1(x + \ell\theta)\right]^n} + \frac{1}{\left[V_0 + (x + \ell\theta)A_2 - A_1(x - \ell\theta)\right]^n} - \frac{2}{V_0^n} = 0 \tag{3.25}$$

which yields:

$$\frac{dx}{d\theta}=\frac{(A_2+A_1)\ell}{A_2-A_1}\left\{\frac{\left[V_0+(x+\ell\theta)A_2-A_1(x-\ell\theta)\right]^{n+1}-\left[V_0+(x-\ell\theta)A_2-A_1(x+\ell\theta)\right]^{n+1}}{\left[V_0+(x+\ell\theta)A_2-A_1(x-\ell\theta)\right]^{n+1}+\left[V_0+(x-\ell\theta)A_2-A_1(x+\ell\theta)\right]^{n+1}}\right\} \tag{3.26}$$

simultaneous solution of Equations (3.24) to (3.26) yields the roll stiffness as a function of relative roll deflection θ.

Interconnected Type II Strut (Inc2)

Under a roll motion, the interconnected suspension would yield a restoring roll moment attributed to instantaneous gas pressures in chambers 4ℓ and $4r$, such that:

$$M=N_u(P_{4\ell}-P_{4r})(A_1+A_3)\ell \tag{3.27}$$

Upon substituting for $P_{4\ell}$ and P_{4r} from Equation (2.74), the restoring roll moment due to Inc2 suspension can be expressed as:

$$M=P_{40}V_{40}^n(A_1+A_3)\ell N_u\left\{\frac{1}{\left[V_{40}+A_1z_\ell-A_3z_r\right]^n}-\frac{1}{\left[V_{40}+A_1z_r-A_3z_\ell\right]^n}\right\} \tag{3.28}$$

The roll stiffness of interconnected suspension (Inc2) can then be derived from:

$$k_r=nP_{40}V_{40}^n(A_1+A_3)\ell N_u\left\{\frac{(A_1+A_3)\ell-(A_1-A_3)\frac{dx}{d\theta}}{\left[V_{40}+A_1(x-\ell\theta)-A_3(x+\ell\theta)\right]^{n+1}}+\frac{(A_1+A_3)\ell+(A_1-A_3)\frac{dx}{d\theta}}{\left[V_{40}+A_1(x+\ell\theta)-A_3(x-\ell\theta)\right]^{n+1}}\right\} \tag{3.29}$$

where $\frac{dx}{d\theta}$ is computed from the static equilibrium equation:

$$g(x,\theta)=\frac{1}{\left[V_{40}+A_1(x-\ell\theta)-A_3(x+\ell\theta)\right]^n}+\frac{1}{\left[V_{40}+A_1(x+\ell\theta)-A_3(x-\ell\theta)\right]^n}-\frac{2}{V_{40}^n}=0 \tag{3.30}$$

which yield:

$$\frac{dx}{d\theta} = \frac{A_1 + A_3}{A_1 - A_3} \ell \left\{ \frac{\left[V_{40} + A_1(x + \ell\theta) - A_3(x - \ell\theta)\right]^{n+1} - \left[V_{40} + A_1(x - \ell\theta) - A_3(x + \ell\theta)\right]^{n+1}}{\left[V_{40} + A_1(x + \ell\theta) - A_3(x - \ell\theta)\right]^{n+1} + \left[V_{40} + A_1(x - \ell\theta) - A_3(x + \ell\theta)\right]^{n+1}} \right\}$$

(3.31)

simultaneous solution of Equations (3.29) to (3.31) yields the roll stiffness as a function of relative roll deflection θ.

Interconnected Type II struts (Inc3)

Owing to the nature of interconnection and the strut configuration, the Inc3 suspension would yield roll stiffness identical to that of the unconnected (Type II strut) suspension, as described in the previous section. Equation (3.29) to (3.31) can thus be used to derive the roll stiffness of the Inc3 suspension.

3.6 DAMPING PROPERTIES OF SUSPENSION CONFIGURATIONS

The damping properties of different suspension configurations are derived from the formulations presented in Chapter 2. The damping forces developed by left- and right-struts of unconnected Type I and Type II struts have been expressed in Equation (2.18), and (2.35), respectively. The damping forces developed by the unconnected struts under pure roll motion could be derived by letting $\dot{x}_\ell = -\dot{x}_r$.

The expression for damping forces due to Inc1, Inc2 and Inc3 struts have been presented in Equation (2.60), (2.79) and (2.98), respectively. The expressions for the damping forces are further analyzed to derive the bounce as well as roll mode damping force. For the Inc1 suspension, the damping forces due to the interconnected struts may be rewritten as:

$$\begin{cases} F_{d\ell} = \dfrac{N_u \rho A_1^3}{2C_d^2 a^2}\left[\left(\dot{x}_\ell - \dfrac{A_2}{A_1}\dot{x}_r\right)^2 \operatorname{sgn}\left(\dot{x}_\ell - \dfrac{A_2}{A_1}\dot{x}_r\right) - \dfrac{A_2}{A_1}\left(\dot{x}_r - \dfrac{A_2}{A_1}\dot{x}_\ell\right)^2 \operatorname{sgn}\left(\dot{x}_r - \dfrac{A_2}{A_1}\dot{x}_\ell\right)\right] + \dfrac{128 N_u \mu L A_1^2}{\pi D^4}\dot{x}_\ell \\ F_{dr} = \dfrac{N_u \rho A_1^3}{2C_d^2 a^2}\left[\left(\dot{x}_r - \dfrac{A_2}{A_1}\dot{x}_\ell\right)^2 \operatorname{sgn}\left(\dot{x}_r - \dfrac{A_2}{A_1}\dot{x}_\ell\right) - \dfrac{A_2}{A_1}\left(\dot{x}_\ell - \dfrac{A_2}{A_1}\dot{x}_r\right)^2 \operatorname{sgn}\left(\dot{x}_\ell - \dfrac{A_2}{A_1}\dot{x}_r\right)\right] + \dfrac{128 N_u \mu L A_1^2}{\pi D^4}\dot{x}_r \end{cases} \tag{3.32}$$

Under a pure vertical motion, the relative velocities across the right- and left-struts would be identical, such that $\dot{x}_\ell = \dot{x}_r = \dot{x}_i$. The terms involving coupling between $\dot{x}_\ell$ and $\dot{x}_r$ could be simplified as:

$$\left(\dot{x}_\ell - \frac{A_2}{A_1}\dot{x}_r\right)^2 = \left(\dot{x}_r - \frac{A_2}{A_1}\dot{x}_\ell\right)^2 = \left(1 - \frac{A_2}{A_1}\right)^2 \dot{x}_i^2 \tag{3.33}$$

Considering that $A_2 / A_1 > 1$, the terms containing the sgn function in Equation (3.32) could be simplified as:

$$\operatorname{sgn}\left(\dot{x}_\ell - \frac{A_2}{A_1}\dot{x}_r\right) = \operatorname{sgn}\left(\dot{x}_r - \frac{A_2}{A_1}\dot{x}_\ell\right) = -\operatorname{sgn}(\dot{x}_i) \tag{3.34}$$

The damping force in the pure bounce mode is thus simplified as:

$$F_{dv} = \frac{\rho A_1^3}{2C_d^2 a^2}\left(\frac{A_2}{A_1} - 1\right)^3 \dot{x}_i^2 \operatorname{sgn}(\dot{x}_i) + \frac{128 \mu L A_1^2}{\pi D^4}\dot{x}_i \tag{3.35}$$

The damping force in the pure roll mode could be simplified as:

$$F_{dr} = \frac{\rho A_1^3}{2C_d^2 a^2}\left(\frac{A_2}{A_1} + 1\right)^3 \dot{x}_i^2 \operatorname{sgn}(\dot{x}_i) + \frac{128 \mu L A_1^2}{\pi D^4}\dot{x}_i \tag{3.36}$$

The bounce and roll mode damping forces due to Inc2 and Inc3 suspensions are further derived in a similar manner.

Inc2 Suspension

$$F_{vd} = \frac{N_u \rho A_3^3}{2C_d^2 a^2}\left(\frac{A_1}{A_3} - 1\right)^3 \dot{x}^2 \operatorname{sgn}(\dot{x}) + \frac{128 N_u \mu L A_3^2}{\pi D^4}\dot{x} \tag{3.37}$$

$$F_{rd} = \frac{N_u \rho A_3^3}{2C_d^2 a^2}\left(\frac{A_1}{A_3}+1\right)^3 \dot{x}^2 \operatorname{sgn}(\dot{x}) + \frac{128 N_u \mu L A_3^2}{\pi D^4}\dot{x} \tag{3.38}$$

Inc3 Suspension

$$\begin{cases} F_{d\ell} = \dfrac{\rho A_3 N_u \left(A_3 \dot{x}_\ell\right)^2}{2\left(C_d u a_{12}\right)^2}\operatorname{sgn}\left(\dot{x}_\ell\right) + \dfrac{128\mu L A_2^2 N_u}{\pi D^4}\dot{x}_r \\ F_{dr} = \dfrac{\rho A_3 N_u \left(A_3 \dot{x}_r\right)^2}{2\left(C_d u a_{12}\right)^2}\operatorname{sgn}\left(\dot{x}_r\right) + \dfrac{128\mu L A_2^2 N_u}{\pi D^4}\dot{x}_\ell \end{cases} \tag{3.39}$$

3.7 SIMULATION PARAMETERS

The geometry parameters of the Type I and Type II struts are selected to achieve identical load carrying capacity and suspension rates of different suspension configurations. Furthermore, the auxiliary roll stiffness due to anti-roll bar and the interconnected (Inc1) suspension. The stiffness and damping properties of two unconnected and three interconnected suspension configurations, termed as Unc1, Unc2, Inc1, Inc2 and Inc3, are evaluated using the formulations presented in section (3.4) to (3.6). The design parameters of the struts are summarized in Table 3.1. The static and dynamic properties of suspension configurations are evaluated through solution of equation of motion for the roll plane vehicle model, described in section (2.3). Table 3.2 summaries the simulation parameters used for the vehicle model. The load carrying capacities and static deflection of different suspension configurations are evaluated using Equation (3.1), (3.3), and (3.5), and the results are summarized in Table 3.3. The results show identical load carrying capacity and static deflections of all the suspension configurations. The static equilibrium pressure is also identical for all configurations, with the exception of Inc1 struts, which tends to be slightly higher.

The suspension rate and bounce mode damping properties are evaluated through solutions of equations of motion of the vehicle model subject to in-phase vertical excitations at the left- and right-tires of peak amplitude of 0.125 *m*. The roll stiffness and roll mode damping forces are evaluated under identical but out-of-phase excitations. Table 3.3 further summarizes the static suspension rate and roll stiffness of different suspension. The results clearly show that all the suspension configurations are selected to yield identical suspension rate, while the roll stiffness of Inc1 suspension is identical to that of the unconnected suspension with anti-roll bar. Furthermore the static roll stiffness of the Inc2 suspension involving Type II strut is considerably larger than the Inc1 suspension, while the Inc3 suspension yields roll stiffness identical to that of the unconnected suspension.

Table 3.1: Simulation parameters of different hydro-pneumatic struts

Parameters	A_1	A_2	A_3	P_0	V_0
Unconnected (Type I)		0.01194		3×10^6	0.001885
Unconnected (Type II)	0.01433	0.01194	0.0024	3×10^6	0.001885
Interconnected Inc1	0.00119	0.01199	0.0108	3296634.8	0.002072
Interconnected Inc2	0.01433	0.01194	0.0024	3×10^6	0.001885
Interconnected Inc3	0.01433	0.01194	0.0024	3×10^6	0.001885

Table 3.2: Simulation parameters of the vehicle model

Symbols	Description	Parameter values
m_s	Sprung mass	14110 kg
m_u	Unsprung mass	3616 kg
I_s	Moment of inertia of sprung mass	19300 kgm^2
I_u	Moment of inertia of unsprung mass	3819.9 kgm^2
$k_{t\ell}, k_{tr}$	Stiffness coefficients of left and right tires	3574800 N/m
$c_{t\ell}, c_{tr}$	Damping coefficients of left and right tires	9500 Ns/m
ℓ_ℓ, ℓ_r	Lateral distances from left and right struts to sprung mass c.g.	0.7 m
$\ell_{t\ell}$, ℓ_{tr}	Lateral distances from left and right tires to unsprung mass c.g.	1.03 m
h_2	Vertical distance between sprung mass c.g. and its roll center	0.62 m
h_1	Vertical distance between unsprung mass c.g. and its roll center	0 m
C_d	Discharge coefficient	0.7
n	Polytropic coefficient	1.38
N_u	Number of struts used on each side	2
P_a	Atmospheric pressure	101300 Pa
μ	Dynamic viscosity of fluid	0.6 Ns/m^2
ρ	Mass density of fluid	797 kg/m^3

Table 3.3 Static properties of different struts

Property	Unc1 & Unc2	Unc1 with anti-roll bar	Inc1	Inc2	Inc3
Load-carrying capacity (kg)	14110	14110	14110	14110	14110
Suspension rate (kN/m)	313.017	313.017	313.017	313.017	313.017
Roll stiffness (kNm)	613.6	882.328	882.328	1204.64	613.6
Static deflection (m)	0.1105	0.1105	0.1105	0.1105	0.1105

3.9 COMPARISON OF STIFFNESS AND DAMPING PROPERTIES OF STRUTS

The stiffness and damping properties of the five suspension systems are evaluated from the suspension forces and moment responses, as described in sections 3.6 and 3.7, as functions of the vertical and roll displacements and velocity responses of the sprung and unsprung masses. An in-plane excitation at the right- and left-tires yields vertical forces as function of the relative vertical deflections and velocities across the strut. The resulting forces are analyzed to derive the suspension rate as a function of the vertical deflections. Figure 3.1 illustrates the vertical suspension rates of the five suspension configurations as a function of the relative displacement across the struts. As can be seen, all the suspensions exhibit identical suspension rates near design height. Furthermore, all the suspension configurations yield very similar suspension rates in extension and compression up to 0.125 m. The suspension rates exhibit progressively hardening effect in compression and softening effect in extension, which is

attributed to the compressible medium. The Inc1 suspension yields slightly lower spring rate in compression due to its larger gas volume. All other suspensions exhibit identical spring rate.

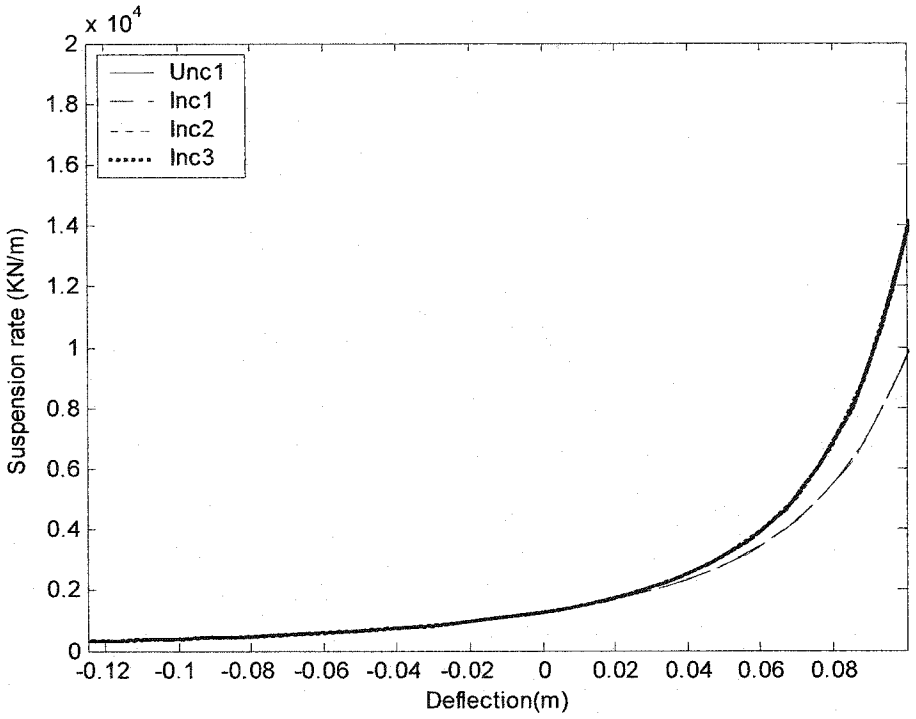

Figure 3.1: The vertical suspension rate of different suspensions.

Figure 3.2 illustrates a comparison of total vertical damping force developed by the suspension configurations as a function of the vertical relative velocity response under in-phase vertical excitation. The Inc3 suspension yields nearly linear damping characteristics due to relatively large orifice areas. The damping force is thus dominantly contributed by the viscous effect associated with flows through the interconnecting pipes. All the other suspension configurations yield very similar vertical mode damping characteristics. These results suggest only little contributions due to flows through the interconnecting pipes in Inc1 and Inc2 suspension.

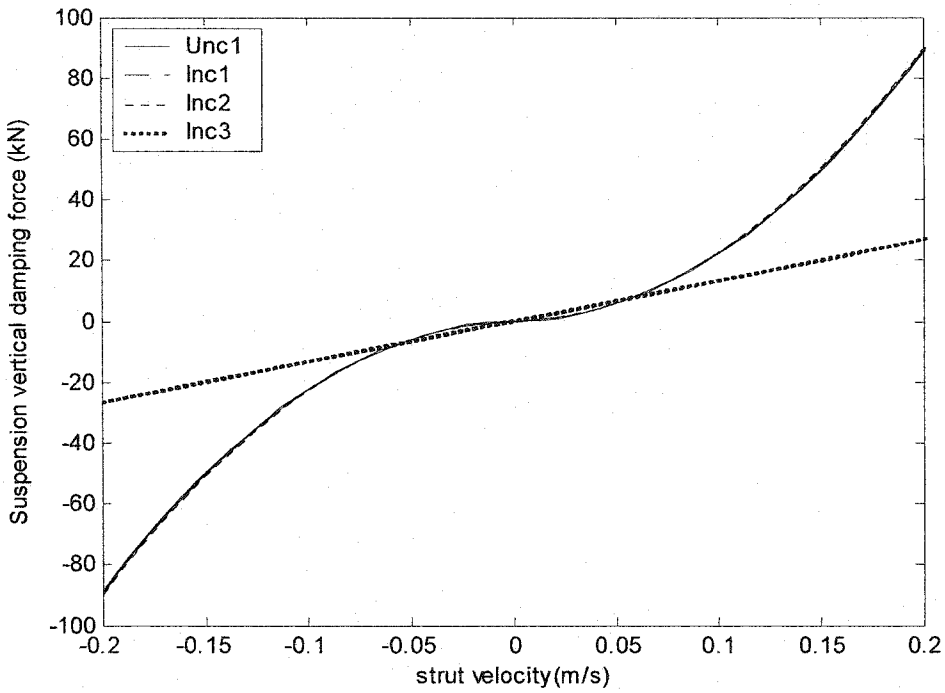

Figure 3.2: Comparison of vertical mode damping force characteristics of different suspension systems.

Figure 3.3 illustrates a comparison of the roll stiffness properties of different suspension systems, derived from restoring moment under out-of-phase excitation. The static roll stiffness of different suspension configurations is a function of the relative roll angle response of the sprung mass with respect to the unsprung mass. The roll stiffness of the interconnected suspensions (Inc1) is similar to that of the unconnected suspension with anti-roll bar. The Unc1, Unc2 and Inc3 suspensions yield identical roll stiffness over the entire range of roll deflection response, as expected from the analytical formulations presented in sections (3.5). The addition of anti-roll bar of constant roll stiffness tends to shift the roll stiffness response of the unconnected suspension upwards. The high roll stiffness due to Inc1 suspension is attributed to the coupling effect of the left-and-

right struts. The Inc2 suspension configuration yields considerably high roll stiffness corresponding to low magnitude roll deflection, due to larger effective area. The roll stiffness, however, decreases at a higher rate with the roll deflection response, which is attributed to the softening and hardening effect of the gas spring. The results also suggest that the static roll stiffness of the suspension employing unconnected struts is almost 70% of the Inc1 suspension and nearly 50% of the Inc2 suspension. All the suspension configurations yield roll mode damping force, which increases nearly quadratically with the velocity. While Inc3 yields nearly linear roll mode damping force varieties, the Inc2 suspension yields highest damping forces in the roll mode.

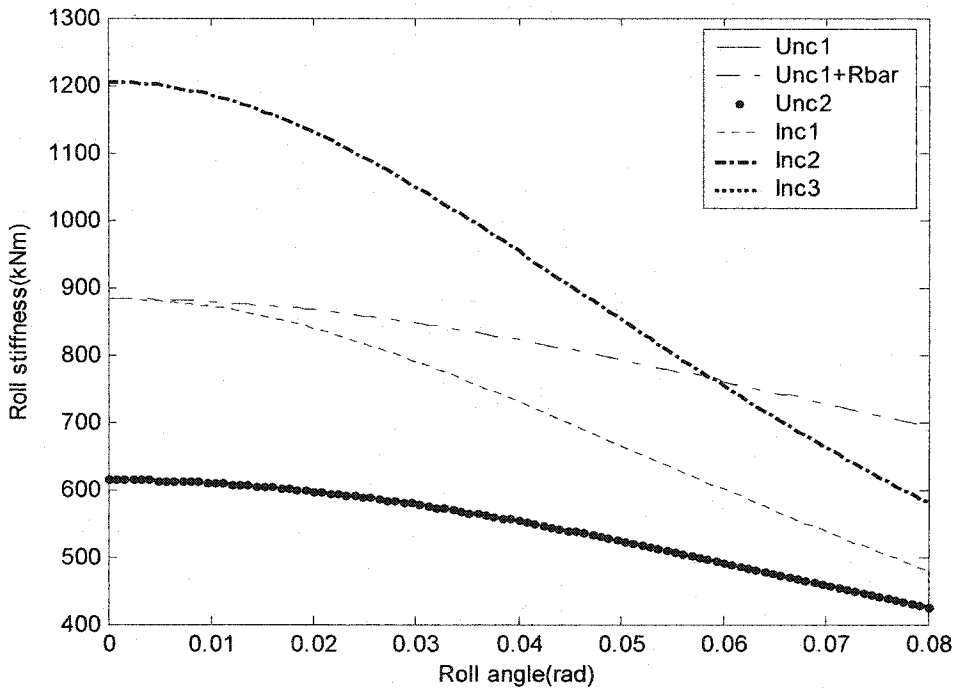

Figure 3.3: Comparison of roll stiffness of different suspension configurations

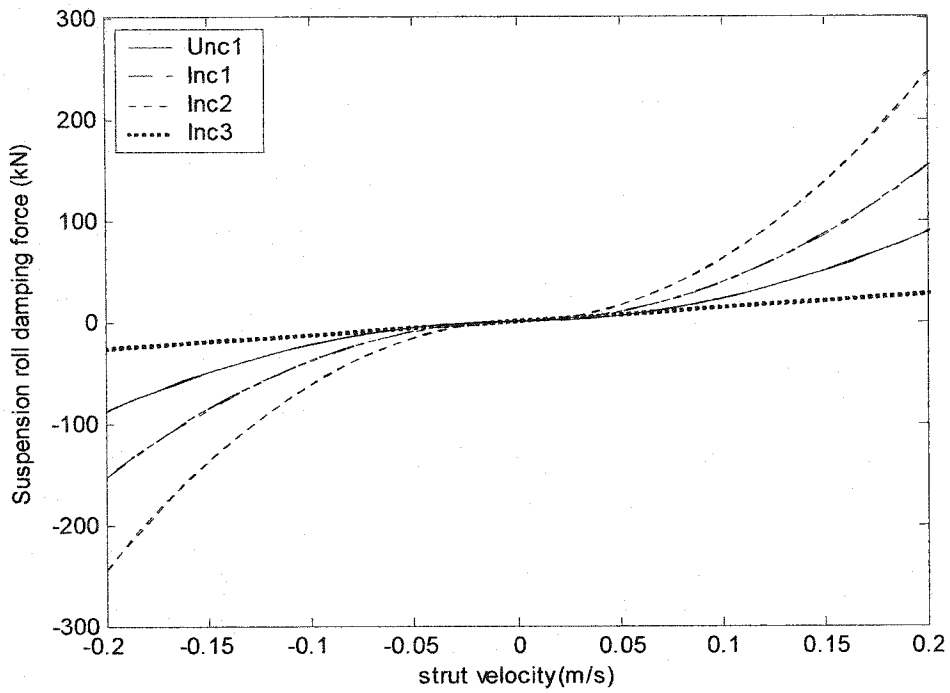

Figure 3.4: Roll mode damping force characteristics of different suspension systems.

Figure 3.4 illustrates a comparison of total roll damping force developed by the suspension configurations as a function of the relative velocity response under out-of-phase roll excitation. The roll mode damping forces due to the interconnected struts (Type I and Type II), however, increase considerably due to feedback effects, as described in Equations (3.32), (3.37), (3.38) and (3.39). The roll mode damping forces of Inc1 and Inc2 struts are much larger than those in the bounce mode. The roll mode damping force of the Inc III suspension strut is mainly obtained from the laminar pipe flow, while the turbulent flow from the orifice is insignificant due to very small working area in chamber 3.

3.10 INFLUENCE OF INTERCONNECTING PIPE SIZES

Equations (2.60), (2.79), and (2.98) describing the relationship between suspension damping force and velocity for the three interconnected suspension, respectively, suggest that the effective damping forces could be influenced by the size of the interconnecting tubes. The influence of variations in the pipe length (*L*) and diameter (*D*) on the vertical and roll mode damping properties of the suspensions is thus investigated. Two values of pipe length (1.5 and 2.0 m) and three different values of the diameter (0.015, 0.02 and 0.25 m) are considered for the analysis. An examination of the damping force expressions derived for the three interconnected suspensions suggests that the damping force associated with feedback effect if generally related to $\frac{A_i^2 \dot{x}_i 128 \mu L}{\pi D^4}$. The contribution due to the pipe size to the damping force is a proportional function of the pipe length, and inversely proportional function of diameter raise to power 4. The diameter of pipes is thus expected to reveal most significant influence. Apart from the pipe size, the contribution due to coupling effect is directly related to working area for the feedback effect A_i.

The feedback damping effect of the Inc1 and Inc2 suspension relies and rod side piston area (A_1=0.00119 m^2 for Inc1, and A_3=0.00119 m^2 for Inc2), while that for the Inc3 depends on the rod area (A_2=0.0119 m^2), which is considerably larger. The contributions due to the feedback effect and the influences of pipe sizes are thus expected be most significant for Inc3 suspension. Figures 3.5 to 3.7 illustrate the influence of variations in L and D on the vertical mode damping properties of the Inc1, Inc2 and Inc3, suspension configurations, respectively.

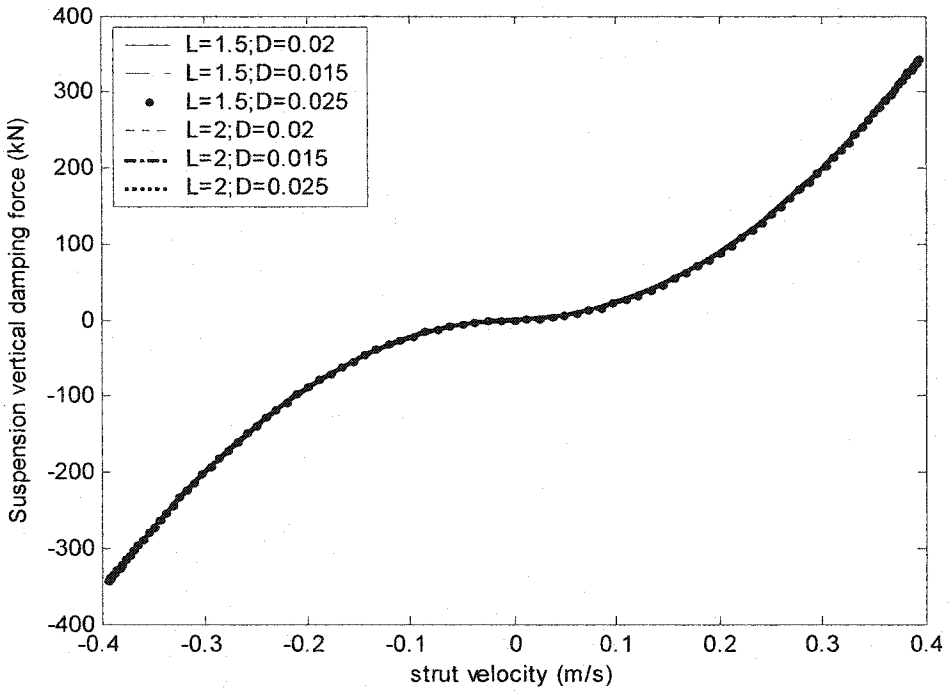

Figure 3.5: Comparison of vertical mode damping force characteristics of interconnected suspension (Inc1) with different connecting pipe geometry.

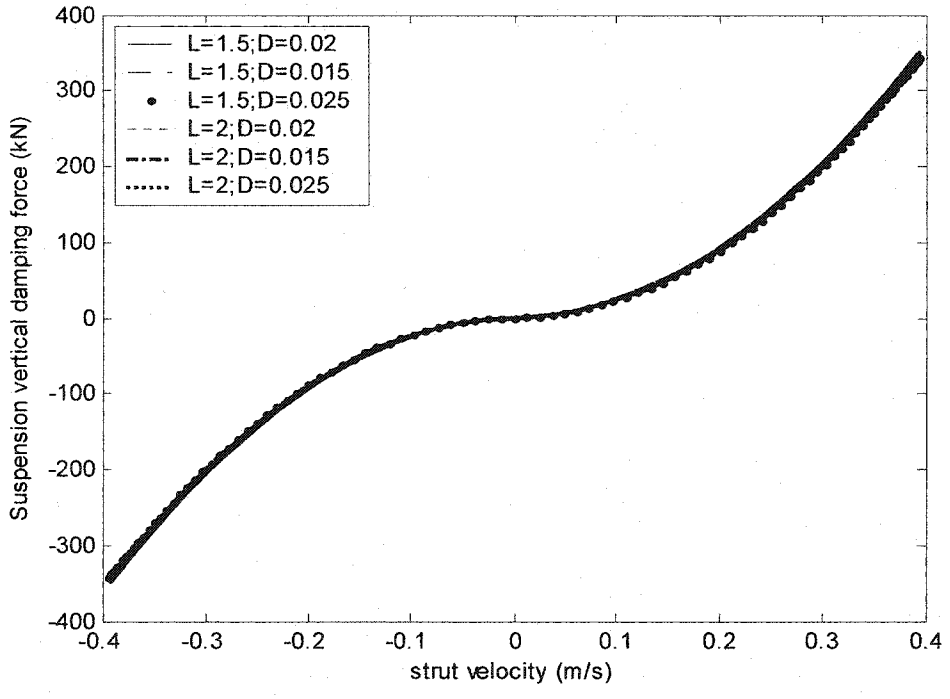

Figure 3.6: Comparison of vertical mode damping force characteristics of interconnected suspension (Inc2) with different connecting pipe geometry.

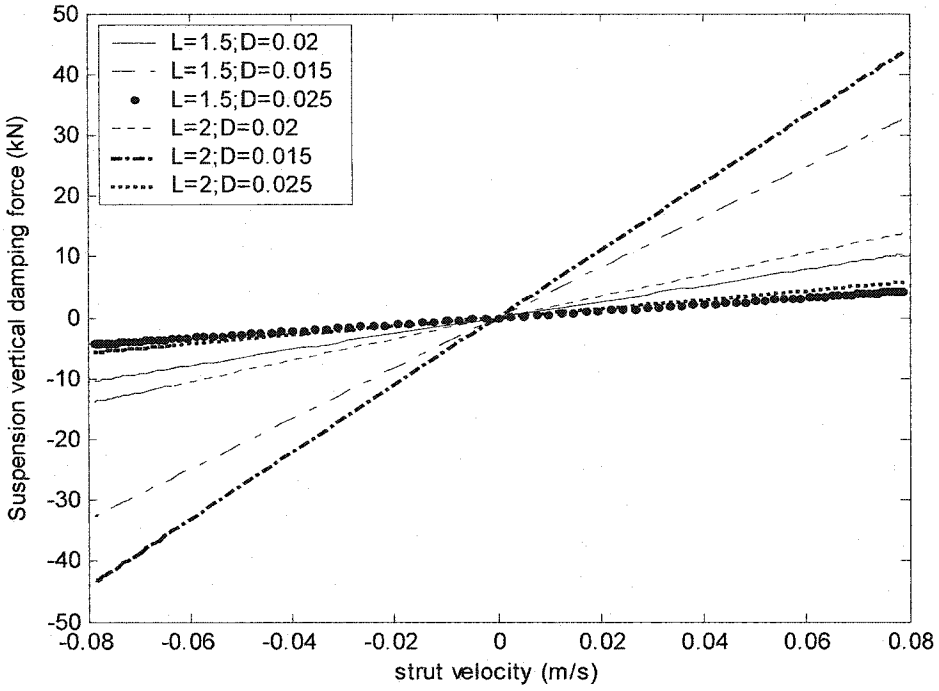

Figure 3.7: Comparison of vertical mode damping force characteristics of interconnected suspension (Inc3) with different connecting pipe geometry.

The influence of L and D on the vertical mode damping properties of Inc1 and Inc2 suspensions is very small due to extremely small working area associated with the feedback effect, as descried above. The larger working area of Inc3 suspension, however, yields significant effects of variations in both L and D of the interconnecting pipes, where the effect of pipe diameter is far more significant. An increase in pipe length for a given diameter yields relatively small increase in the damping force, while a decrease in diameter from 0.02 m to 0.015 m yields significantly larger damping force. Figures 3.8, 3.9 and 3.10 illustrate that the influence of variations in pipe length and diameter on the roll mode damping properties of Inc3 suspensions, respectively. The results show similar effect of pipe length and diameter, as observed for the vertical mode damping.

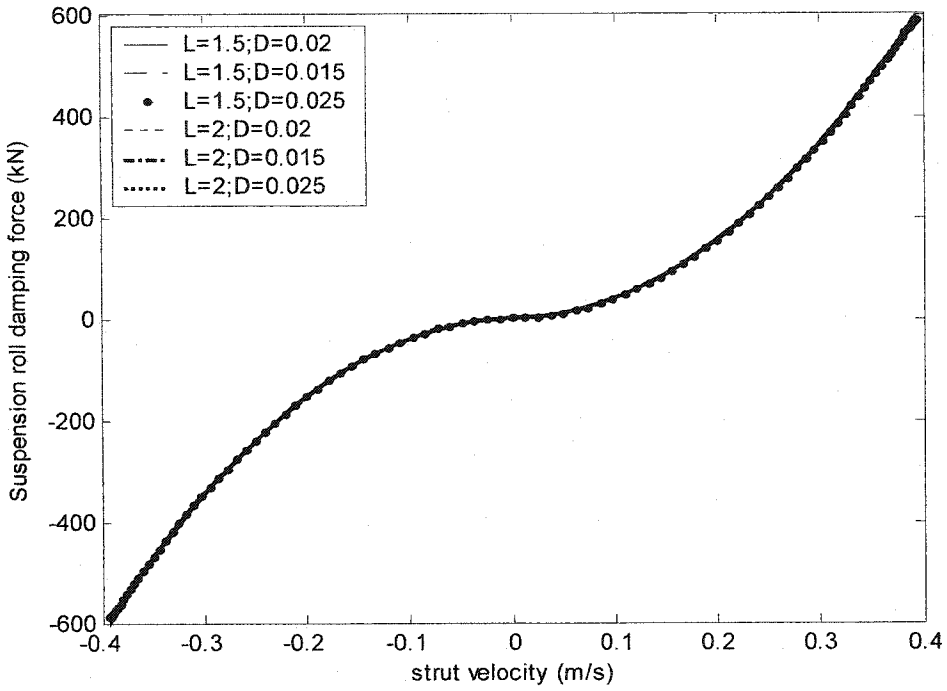

Figure 3.8: Comparison of roll mode damping force characteristics of interconnected suspension (Inc1) with different connecting pipe geometry.

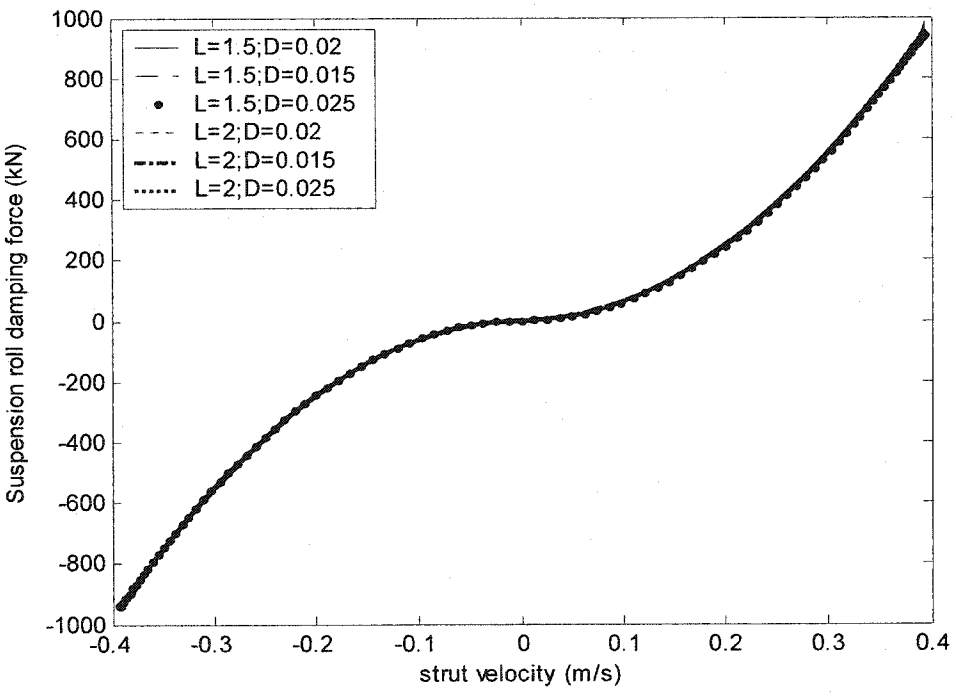

Figure 3.9: Comparison of roll mode damping force characteristics of interconnected suspension (Inc2) with different connecting pipe geometry.

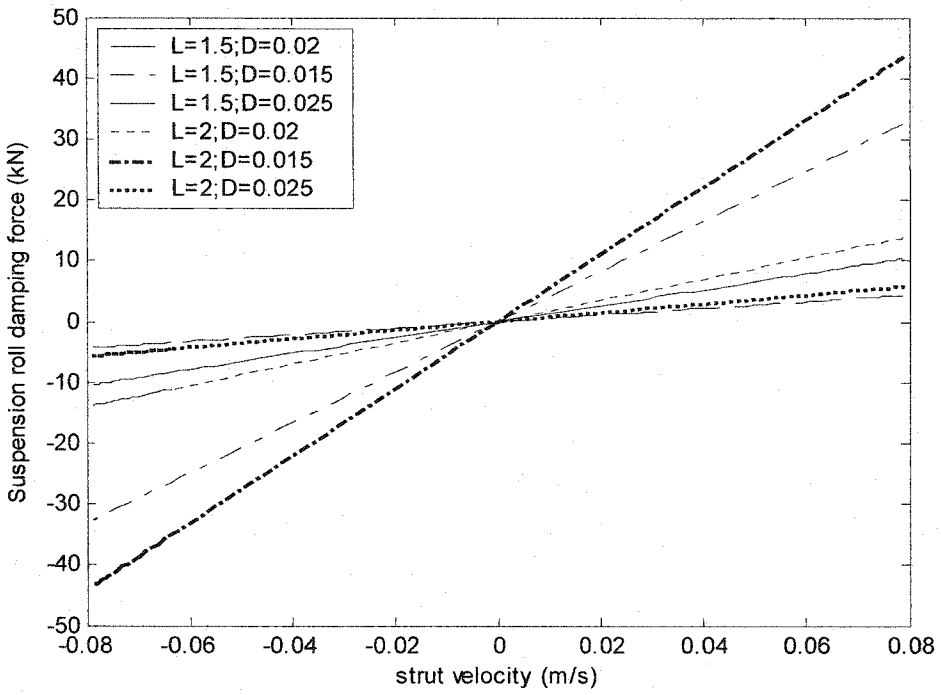

Figure 3.10: Comparison of roll mode damping force characteristics of interconnected suspension (Inc3) with different connecting pipe geometry.

3.11 SUMMARY

The design parameters of the two unconnected and three different interconnecting suspension configurations are selected to achieve identical load carrying capacity, static deflection and suspension rate. The dynamic forces developed by the struts are analyzed to derive expressions for suspension rates, roll stiffness, vertical and roll modes damping forces. Simulations are performed to derive the suspension rates, roll stiffness and damping properties of all the suspension configurations. A comparison of the properties suggests that all the suspension configurations yield identical load-carrying capacity, suspension rate and static roll stiffness. The interconnected suspensions (Inc1 and Inc2) exhibit an inherent anti-roll property and thus yield high roll stiffness. All of the

suspension configurations exhibit progressively hardening suspension rates, while their roll stiffness rates tend to decrease with an increase in the sprung mass roll angle. The interconnected suspensions (Inc1 and Inc2) yield considerably large damping in the roll mode due to the coupling effects.

CHAPTER 4

DYNAMIC RESPONSES TO DETERMINISTIC EXCITATION

4.1 INTRODUCTION

Vehicle ride and handling is influenced by two main sets of disturbances: the road roughness, and the forces and moments that originate due to various inertial and aerodynamic loadings, as caused by braking, turning and wind gusts (Hrovat, 1997). The ride quality of a vehicle may be assessed in terms of the acceleration perceived by the passenger/driver or the acceleration response of the sprung mass to road excitations. The handling response of the vehicle is related to the roll and lateral response of the sprung and unsprung masses when the vehicle is subjected to a directional maneuver. In this chapter, the roll plane model of a high-way bus equipped with different configurations of unconnected and interconnected suspensions, described in Chapters 2 and 3, is analyzed to determine the relative vertical and roll responses of the vehicle subject to road irregularities and centrifugal forces arising from a directional maneuver. The nature of excitations arising from tire-terrain interactions and steering inputs are described. The roll performance characteristics of the suspension systems are evaluated in terms of the steady state and transient roll responses of sprung and unsprung masses during under steady turning and transient lateral accelerations. The dynamic ride performance is established in terms of both heave and roll shock and vibration isolation characteristics of the suspensions subjected to road excitations. Vibration transmissibility characteristics of different suspensions are

also investigated by using harmonic in-phase and out-of-phase excitations arising from the tire-terrain interactions.

4.2 DESCRIPTION OF EXCITATIONS

The analysis of ride quality and handling performance characteristics of vehicle models requires identification of excitations that are representative of those arising from the steering maneuvers and the tire-terrain interactions. The input data due to steering maneuvers can be expressed in terms of steady steering and transient lateral acceleration experienced by the sprung and unsprung masses (Campos,1998; Cooperrider, 1990). The excitations arising from tire-terrain interactions are characterized as half-sine displacement bumps and a rounded step displacement excitation.

4.2.1 Lateral acceleration excitations

The directional performance of a vehicle is related to its ease of handling and directional response. Although vehicles spend around 80% of their travel time during straight driving, their anti-roll capabilities are very important for road safety during cornering and emergency high-way maneuvers. The sprung and unsprung masses of a vehicle are subjected to centrifugal acceleration during a directional maneuver, which causes an overturning roll moment and roll motions of the sprung and unsprung masses. The handling quality of a vehicle is primarily related to vehicle's ability to counteract the overturning moment. Various studies have concluded that rollover threshold of heavy vehicles (Thomas, 1992; Kelly, 2000), which is the maximum value of lateral acceleration that a vehicle can withstand during a steady turn, directly relates to the overturning moment and its

value lies in the range of 0.3 g to 0.5 g. The rounded step displacement excitation is a transient excitation encountered due to a sudden change in roadway elevation, such as a small curb, or crossing from an old to new section of paved road surface. The lateral acceleration encountered during a steady turn maneuver is approximated as in Figure 4.1 (Rakheja, 1985). The peak amplitude of lateral acceleration is considered as 2.5 m/s^2.

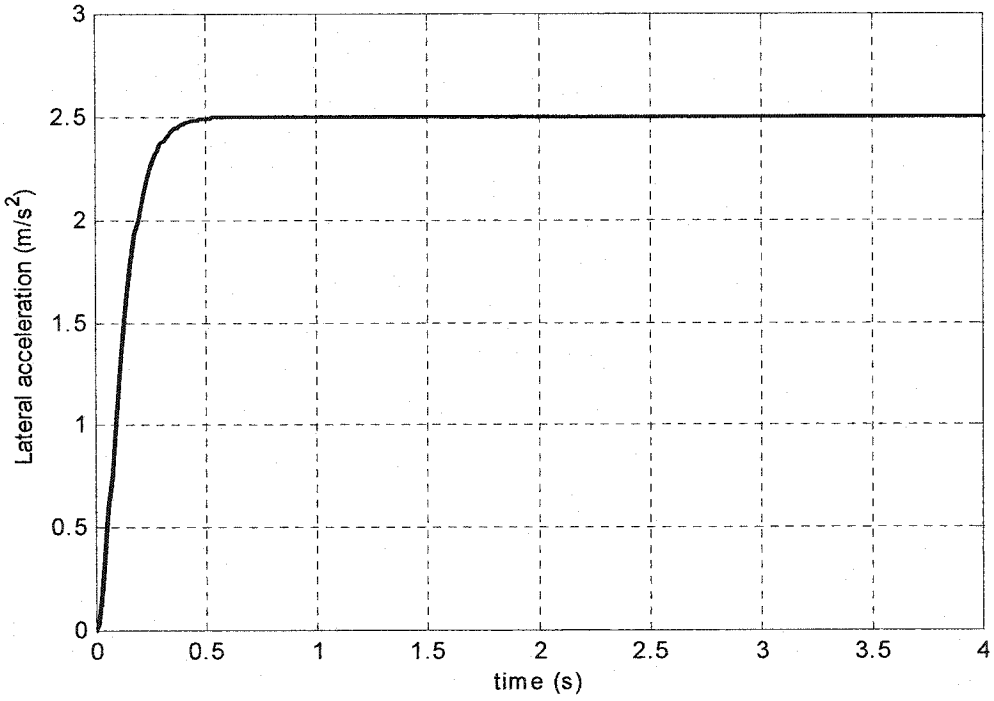

Figure 4.1: A rounded step steady turning lateral acceleration excitation.

Rounded step steady steering lateral acceleration may be described as a fast rising continuous time function, which achieves a steady state value after a finite time. The acceleration excitation due to the rounded step can be expressed as:

$$x_0(t) = X_{\max}[1 - e^{-\gamma\omega_0 t}(1 + \gamma\omega_0 t)] \qquad (4.1)$$

where $e = 2.71828$, and γ is the pulse severity parameter, defined by:

$\gamma = \frac{\pi}{\omega_0 \tau_s}$, and τ_s is the duration of pulse.

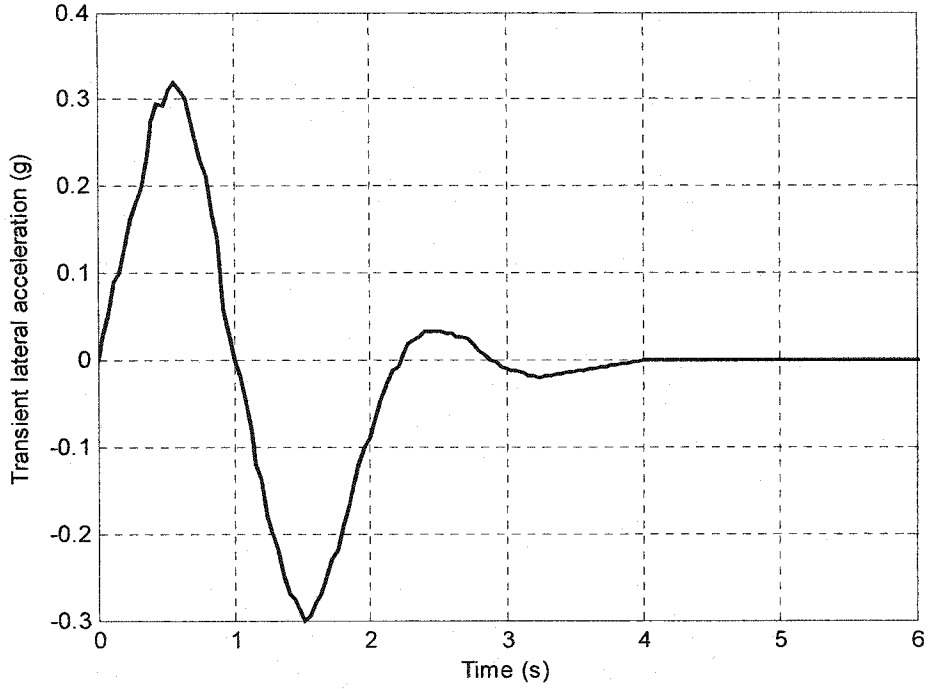

Figure 4.2: A transient lateral acceleration excitation of an inter-city bus during lane change (Dulac, 1992).

Field tests performed on a highway bus concluded that although a lateral acceleration as high as 0.5 *g* can be achieved on a skid-pad, the maximum level of lateral acceleration measured during a continuous lane change maneuver at maximum permissible speed is in the order of 0.3 *g*. Figure 4.2 shows the transient lateral acceleration measured during a lane change maneuver at a forward speed of 30 *m/s*. (Dulac, 1992). The magnitude of lateral acceleration excitation, however, decreases when the maneuvers are preformed at reduced speeds. This lateral acceleration excitation may thus be considered to be realistic under severe maneuvers.

4.2.2 Excitations due to tire terrain interactions

Apart from the centrifugal force excitation, the vehicle encounters disturbances due to tire's interactions with the road elevation of either deterministic or random in nature. A sinusoidal road profile represents an idealized input description to study the frequency response characteristic of the vehicle suspension model. Assuming sinusoidal road profile of wavelength λ and amplitude A, the displacement excitation at the tire-road interface may be expresses a function of forward speed v:

$$x_{ij} = A\sin(\frac{2\pi v}{\lambda}t);\ (j = \ell, r) \tag{4.2}$$

Frequency response characteristics of the vehicle employing different hydro-pneumatic suspension configurations are considered using two types of harmonic excitations to evaluate relative vibration transmissibility. (1) In-phase harmonic excitation, right and left tires subjected to identical vertical sinusoidal excitations of 0.01 m amplitude; and (2) Out-of-phase excitation, right and left tires subjected to vertical sinusoidal excitations of identical amplitude but 180 degrees out-of-phase. The response to in-phase excitation will yield the vertical vibration transmission characteristics of the suspension systems, whereas the response to out-of-phase excitation will primarily provide roll vibration transmission characteristics of the suspension systems. The road roughness, however, is more accurately described by the elevation of the road profile along the wheel tracks over which the vehicle passes. The road profiles fit the general category of "wide-band random signals", which can be described either by the profile or by the statistical properties (Wong, 1978). The road roughness is

typically specified as a random process of a given displacement power spectral density (PSD). The response characteristics of vehicle models subject to such excitation are presented in the following chapter.

The relative transient ride responses of vehicle suspension can be further evaluated using deterministic excitations representing the tire-terrain interactions, such as a bump excitation characterized by a half sine pulse displacement, as shown in Figure 4.3 (Jacobsen, 1958). Vertical shock attenuation performance characteristics can be evaluated using in-phase bump excitations at both wheels, while the out-of-phase excitations at the two wheels can provide the coupled vertical and roll response characteristics. The roll responses of the vehicle-suspension models were further evaluated under a rounded step displacement input applied at only one track, as illustrated in Figure 4.4.

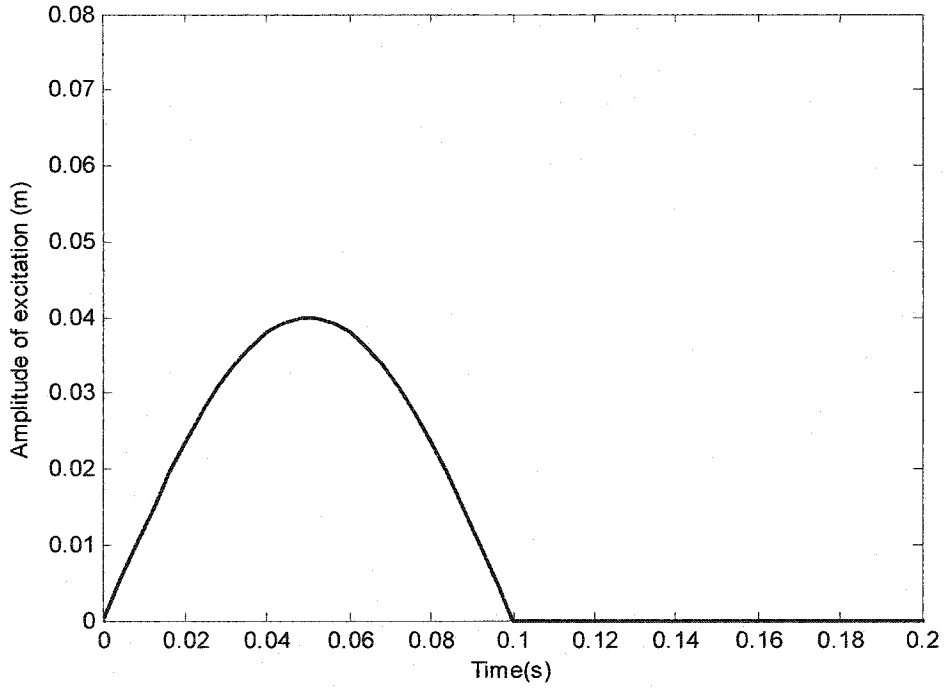

Figure 4.3: A half sine bump excitation occurring at tire-terrain interface.

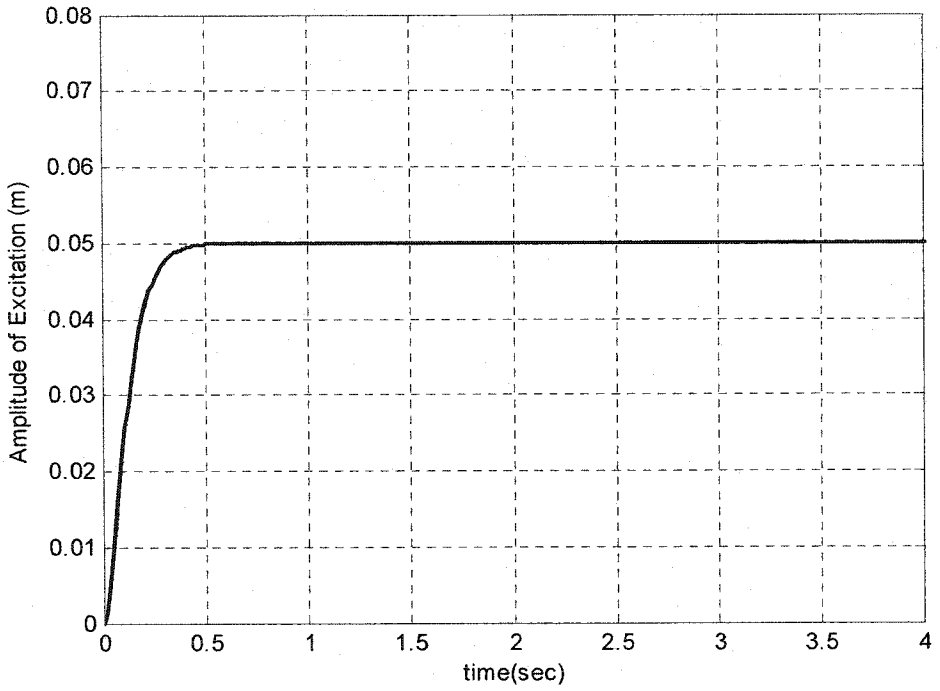

Figure 4.4: A rounded step displacement input only on right tire.

4.3 RESPONSE TO LATERAL ACCLERATION EXCITATIONS

The response characteristics of the roll-plane vehicle model comprises different hydro-pneumatic suspension configurations, are evaluated to assess the relative effectiveness of the interconnected suspensions. The equations of motion for the vehicle roll models are solved under steady turning and transient lateral accelerations shown in Figures 4.1 and 4.2. The responses of the vehicle models are presented and discussed in terms of the roll displacement and velocity of the sprung and unsprung masses.

4.3.1 Responses to a rounded step lateral acceleration

Figure 4.5 illustrates a comparison of the roll angle response characteristics of the sprung mass of the vehicle employing different suspension

systems and subject to a rounded step lateral acceleration. The results show that the sprung mass experiences relatively larger roll angle when unconnected hydro-pneumatic suspensions (Unc1 and Unc2) are used, irrespective of the strut type. The identical roll responses of both the unconnected suspension are attributed to their identical design parameters. The interconnected suspension, Inc3, owing to its interconnection configuration and lower roll stiffness yields higher roll response. This interconnected suspension, however, yields rapid decay of the roll response due to its higher damping caused by the viscous flows through the interconnected pipes. The peak magnitudes of roll responses of the unconnected and Inc3 suspensions approach 0.057 and 0.061 radians, respectively. All the three suspension, however, yield identical steady state roll response, which can be attributed to their moment-deflection properties.

The roll responses of the sprung mass of the vehicle with the unconnected and Inc3 suspension reveal oscillation frequency of approximately 0.7 Hz, which would correspond to the roll mode resonant frequency of the vehicle model. The addition of the anti-roll bar yields high roll stiffness and thus considerably lower sprung mass roll angle response. The frequency of oscillations tends to be higher (in the order of 0.9 Hz). The magnitude of oscillations tends to be relatively large with lower rate of decay due to its lower roll mode damping characteristics, as illustrated in Figure 3.4. The interconnected (Inc1) strut suspension yields roll angle response similar to that of the unconnected suspension with anti-roll bar. This is attributed to their identical static roll stiffness property. The high roll-mode damping of the Inc1 suspension, however, results in relatively lower roll angle

and faster response decay. Both the unconnected suspension with roll bar and Inc1 suspension approach identical steady state roll response of 0.032 rad. The Inc1 suspension also yields identical oscillation frequency in the order of 0.9 Hz.

The Inc2 suspension with Type II struts yields the lowest magnitude of the roll angle response due to its relatively higher roll stiffness. This is also evident from the relative higher frequency of oscillation (near 1 Hz). Furthermore, the oscillations in the roll response decay at a considerably faster rate due to its high roll mode damping. The roll angle response of the sprung mass with Inc2 suspension approaches a steady state value of 0.023 rad, which is 28% lower than that attained with Inc1 and unconnected suspension with anti-roll bar. This steady state response is also nearly 52% lower than those attained with unconnected and Inc3 suspension. The Inc3 suspension with its high damping also yields high rise time, when compared to that of the other configurations.

The results clearly suggest that the roll response of the vehicle subject to a steady lateral acceleration could be considerably lowered by the interconnected suspension, specifically the Inc2. Figure 4.6 illustrates a comparison of the corresponding roll velocity responses of the sprung mass with different suspensions. The results suggest that the Inc2 suspension yields lowest peak response and rapid decay as observed in Figure 4.5. The unconnected and Inc3 suspensions yield highest peak response, while the addition of anti-roll bar suppresses the peak response to some extent but the rate of decay of oscillations is considerably lower. Lower settling time of Inc3 suspension may be

attributed to its high roll mode damping in the low velocity range, as can be seen in Figure 3.4.

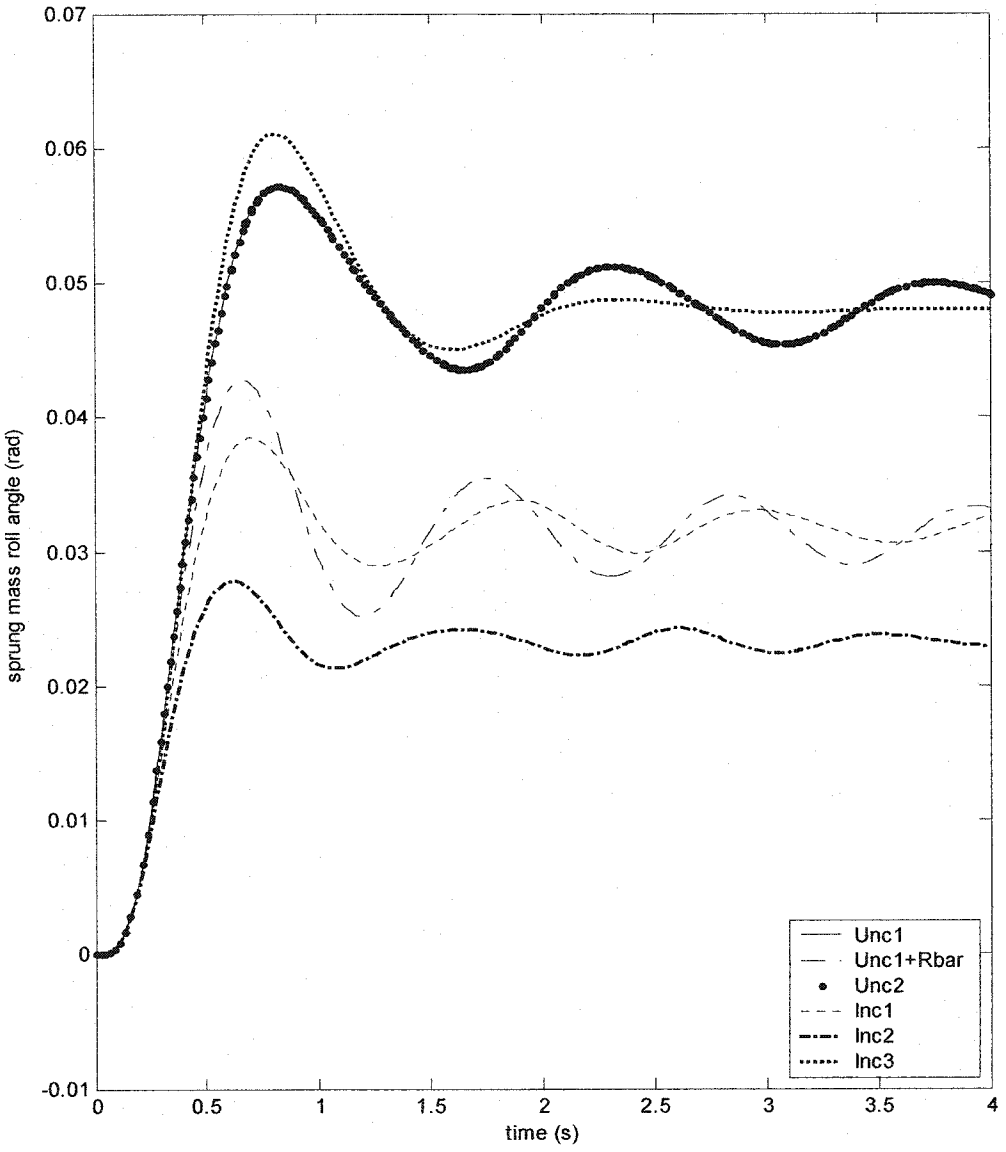

Figure 4.5: Comparison of sprung mass roll angle response of the vehicle model employing different suspension configurations (rounded step lateral acceleration).

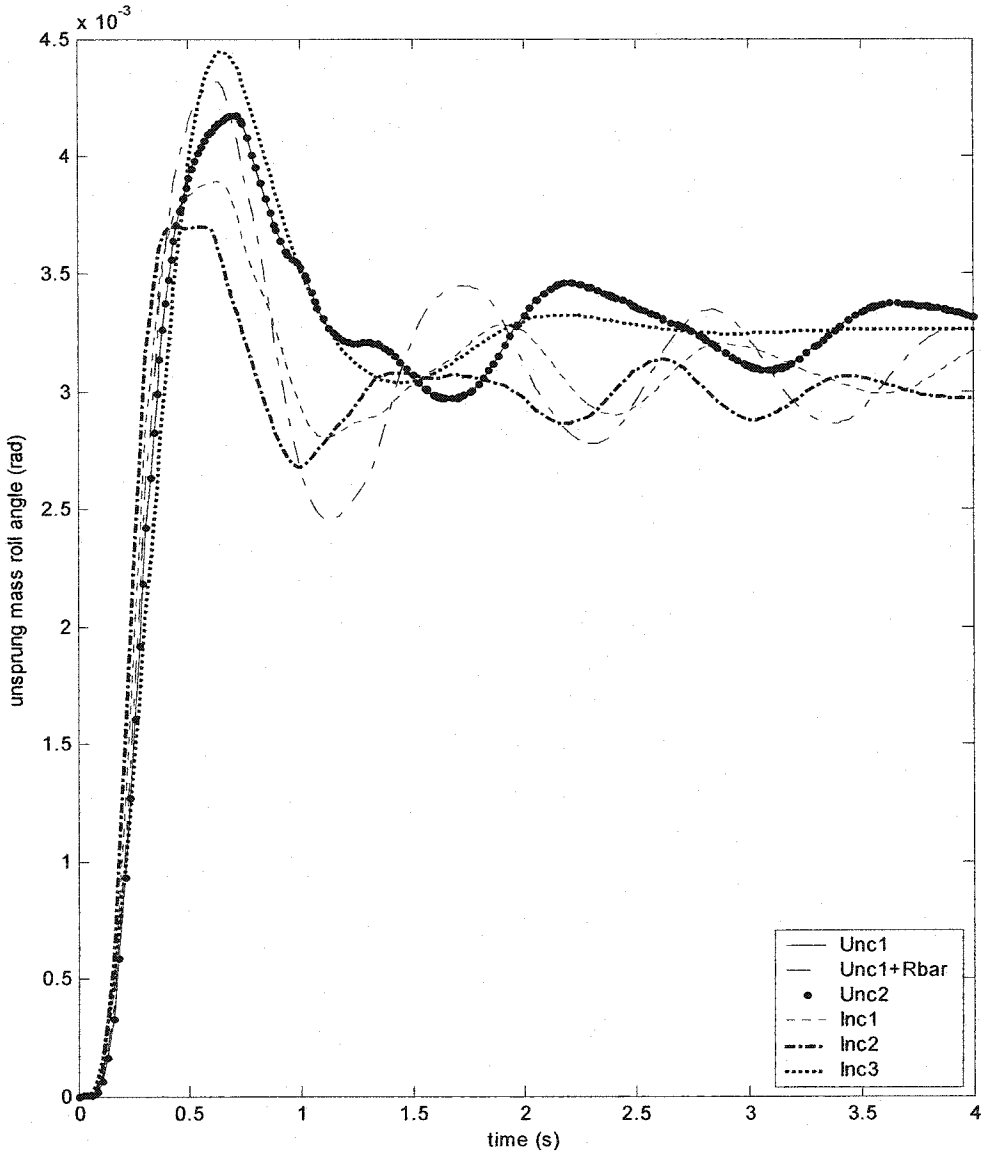

Figure 4.6: Comparison of unsprung mass roll angle response of the vehicle model employing different suspension configurations (rounded step lateral acceleration).

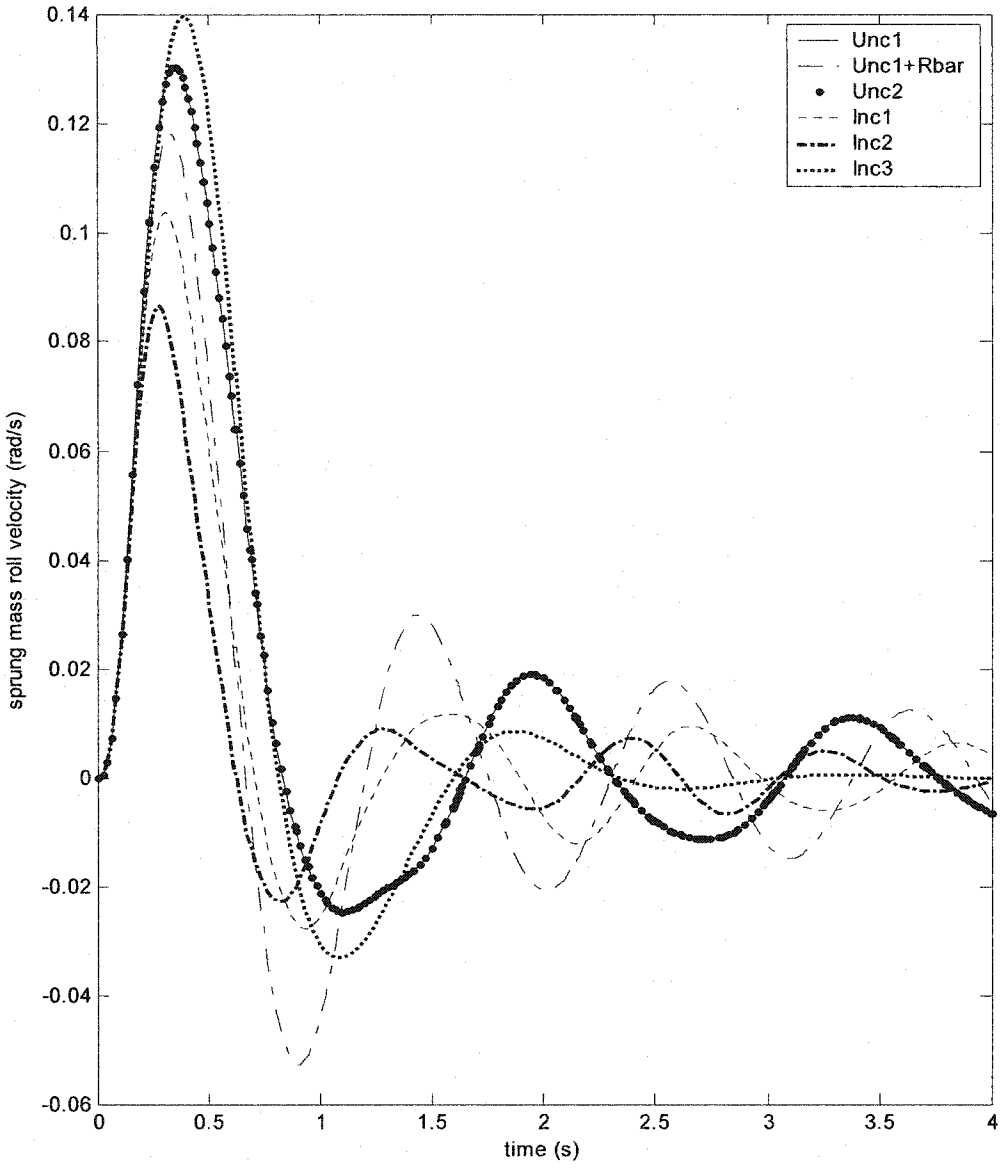

Figure 4.7: Comparison of sprung mass roll velocity response of the vehicle model employing different suspension configurations (rounded step lateral acceleration).

The lateral acceleration excitation imposed on the vehicle also causes roll motion of the unsprung mass, which could lead to considerable load transfer from the inboard track to the outboard track. The dynamic load shift encountered under a directional maneuver often serves as an indicator of potential loss of contact between a tire and the road (Aleksander, 2002), and is directly related to the roll angle response of the unsprung mass. The use of high roll stiffness interconnected suspension could effectively reduce the magnitude of unsprung mass roll angle and thus the dynamic load transfer, as evident in Figure 4.7. As observed from the sprung mass roll angle response, the Inc2 suspension yields lowest unsprung mass roll response, while the unconnected suspensions yield highest values of the peak response. The unconnected suspension with anti-roll bar causes high magnitude oscillations of the roll response due to its light damping property.

4.3.2 Response to a transient lateral acceleration

Figure 4.8 illustrates a comparison of the roll angle response characteristics of the sprung mass of the vehicle employing different suspension systems and subject to a transient lateral acceleration, shown in figure 4.2. The results show that the sprung mass experiences relatively larger roll angle when supported on unconnected hydro-pneumatic suspensions (Unc1 and Unc2). Owing to its properties, the Inc3 suspension also yields high roll angle response of the sprung mass. The identical roll responses of both the unconnected suspensions are attributed to their identical properties and design parameters, The addition of the anti-roll bar yields high roll stiffness and thus considerably

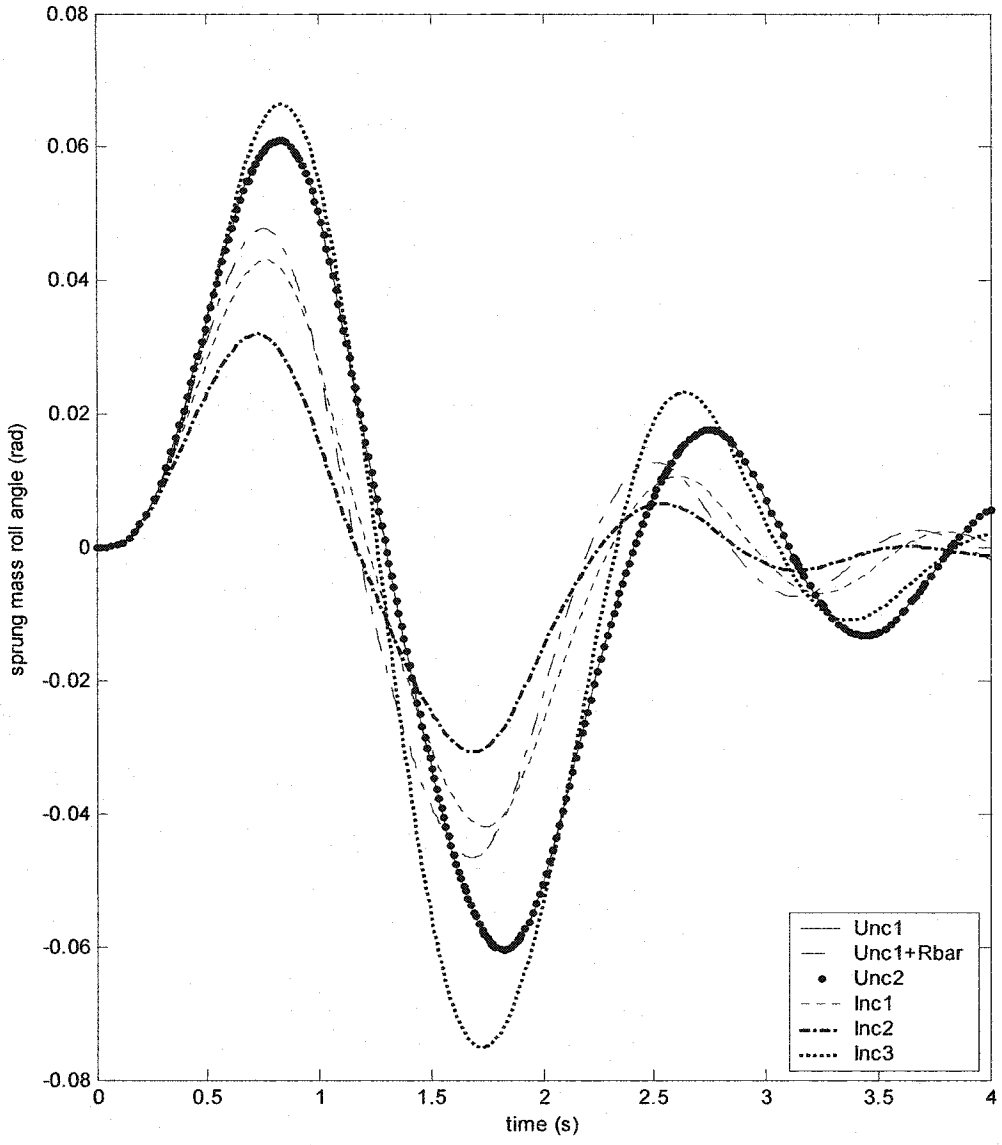

Figure 4.8: Comparison of sprung mass roll angle response of the vehicle model employ different suspension configurations (transient lateral acceleration).

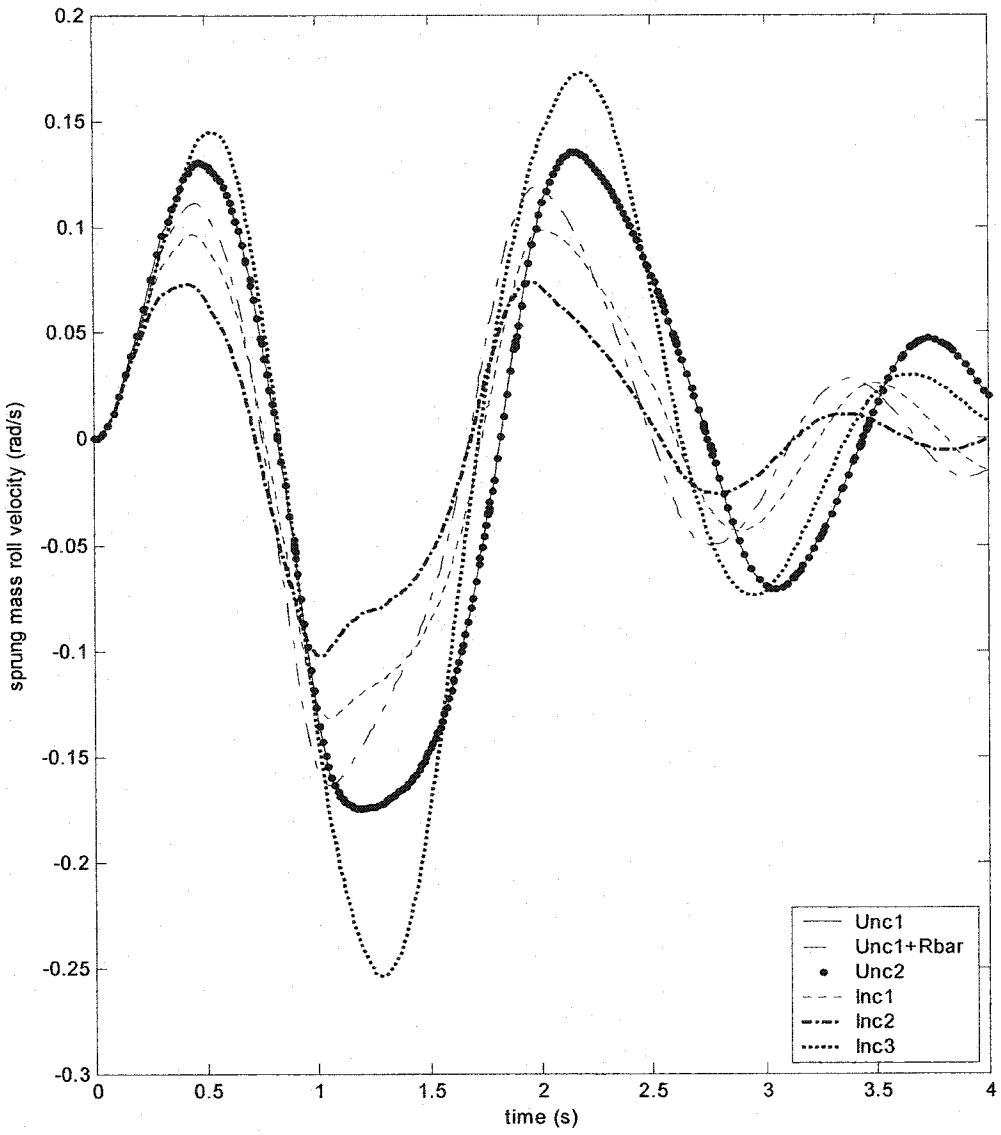

Figure 4.9: Comparison of sprung mass roll velocity response of the vehicle model employ different suspension configurations (transient lateral acceleration).

lower sprung mass roll angle response. The interconnected Type I strut suspension (Inc1) yields roll angle response slightly lower than that of the unconnected suspension with anti-roll bar. The Inc2 suspension with Type II struts yields the lowest magnitude of the roll angle response due to its relatively higher roll stiffness. The results clearly suggest that the roll response of the vehicle subject to a transient lateral acceleration could be considerably lowered by the roll plane interconnected suspension, specifically the Inc2. Figure 4.9 illustrates a comparison of the corresponding roll velocity responses of the sprung mass with different suspensions. The results suggest that the Inc2 suspension yields lowest peak response and rapid decay as observed in Figure 4.8. The unconnected and Inc3 suspensions yield highest peak velocity response, while the addition of anti-roll bar suppresses the peak response to some extent but the rate of decay of oscillations is considerably lower.

4.4 VEHICLE RESPONSE TO DETERMINISTIC ROAD EXCITATIONS

Dynamic ride characteristics of the vehicle employing different suspension configurations are analyzed in terms of transient vertical and roll responses of the sprung mass when subjected to the deterministic tire-terrain excitations. The vertical shock attenuation characteristics are evaluated for an in-phase half-sine displacement excitation as shown in Figure 4.3, while the roll response characteristics are evaluated for an out-of-phase half-sine displacement excitation. A rounded step displacement excitation occurring only at the right tire-terrain interface is further used to evaluate the combined bounce and roll response characteristics of different suspension configurations.

The vertical displacement and acceleration response characteristics of the sprung mass of the vehicle employing different suspensions, subjected to an in-phase half-sine bump, are presented in Figures 4.10 and 4.11, respectively. The displacement responses of the sprung mass employing unconnected, and Inc1 and Inc2 suspensions are identical due to their identical bounce mode damping and suspension rate. The response curves corresponds to three suspensions thus overlap in Figure 4.10 and 4.11. The high bounce-mode damping property of the Inc3 suspension configuration yields considerably lower peak responses and rapid decay, as shown in the figures.

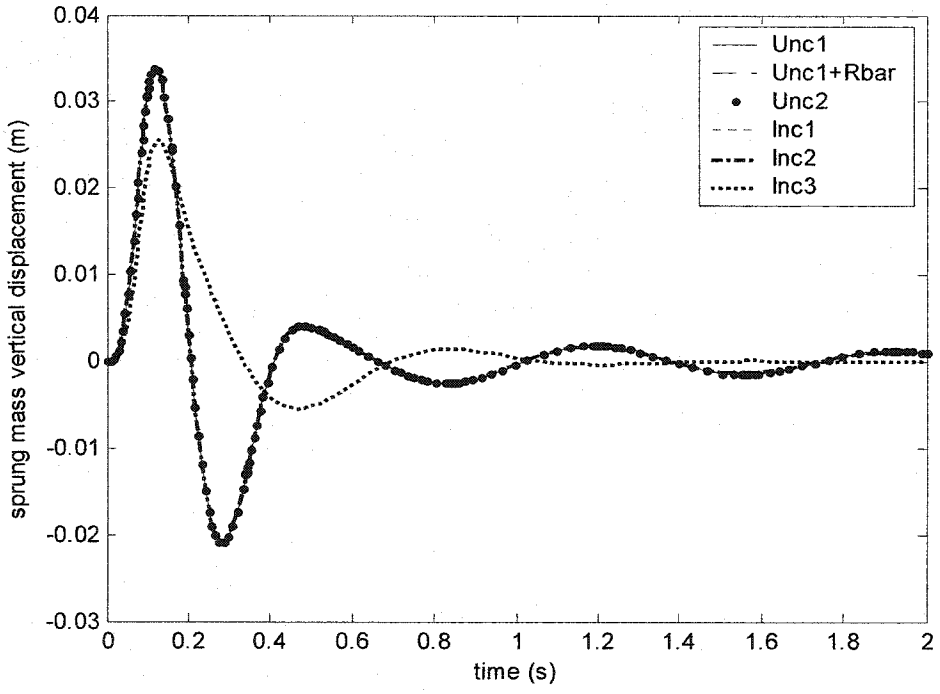

Figure 4.10: Comparison of sprung mass vertical displacement response of the vehicle model employing different suspension configurations (in-phase half sine displacement).

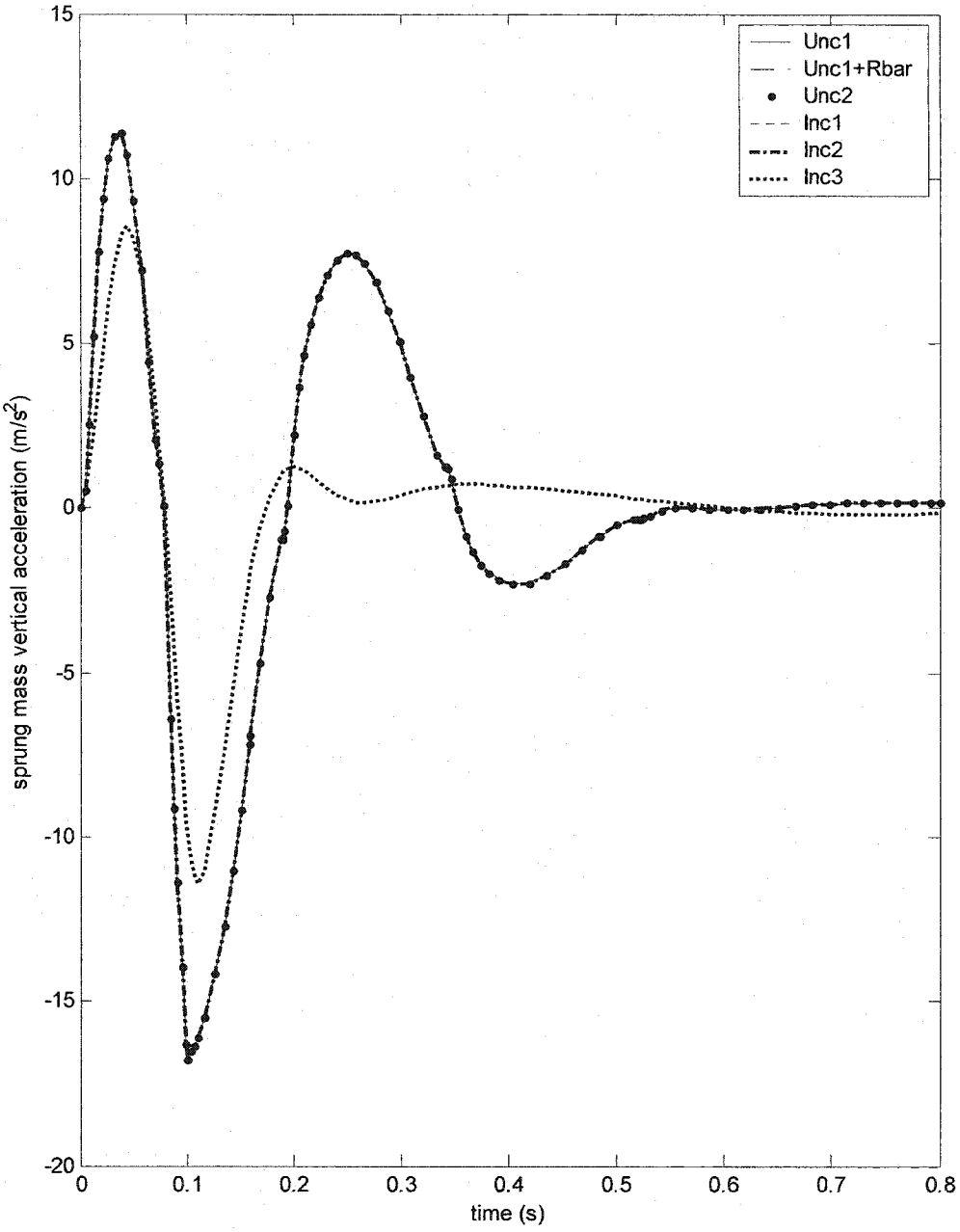

Figure 4.11: Comparison of sprung mass vertical acceleration response of the vehicle model employing different suspension configurations (in-phase half sine displacement).

The peak vertical acceleration response of the Inc3 suspension is observed to be nearly 33% lower than the peak acceleration response with other suspension configurations, as shown in Figure 4.11. The roll angle and acceleration response characteristics of the sprung mass of the vehicle employing different suspensions, subjected to an out-of-phase bump, are compared in Figures 4.12 and 4.13, respectively. The unconnected suspensions yield relatively large roll angle response occurring mostly in the vicinity of the roll resonant frequency. The addition of anti-roll bar tends does not affect the peak roll displacement magnitude corresponding to the first oscillation but yields lower decay of the response oscillations. The Inc1 and Inc2 suspensions yield higher roll response corresponding to the first peak but yield rapid decay of the roll response. The Inc3 suspension yields the lowest peak roll displacement and acceleration response, as evident in Figure 4.12 and 4.13. It should be noted that the relative damping properties of Inc3 suspension are strongly dependent upon the relative velocity response of the struts. The response behaviour of the Inc3 suspension is thus strongly dependent upon the nature of excitations, such as magnitude and frequency. Furthermore, the half-sine pulse considered for the simulation would yield a fundamental frequency component near 10 Hz and near 5 Hz, if a full cycle is considered. Such as excitation could excite the unsprung mass modes. The relative response characteristics of different suspension configurations are further investigated under out-of-phase half-sine displacement excitation of duration of 0.8s (Frequency=0.67Hz). The results are shown in Figure 4.14.

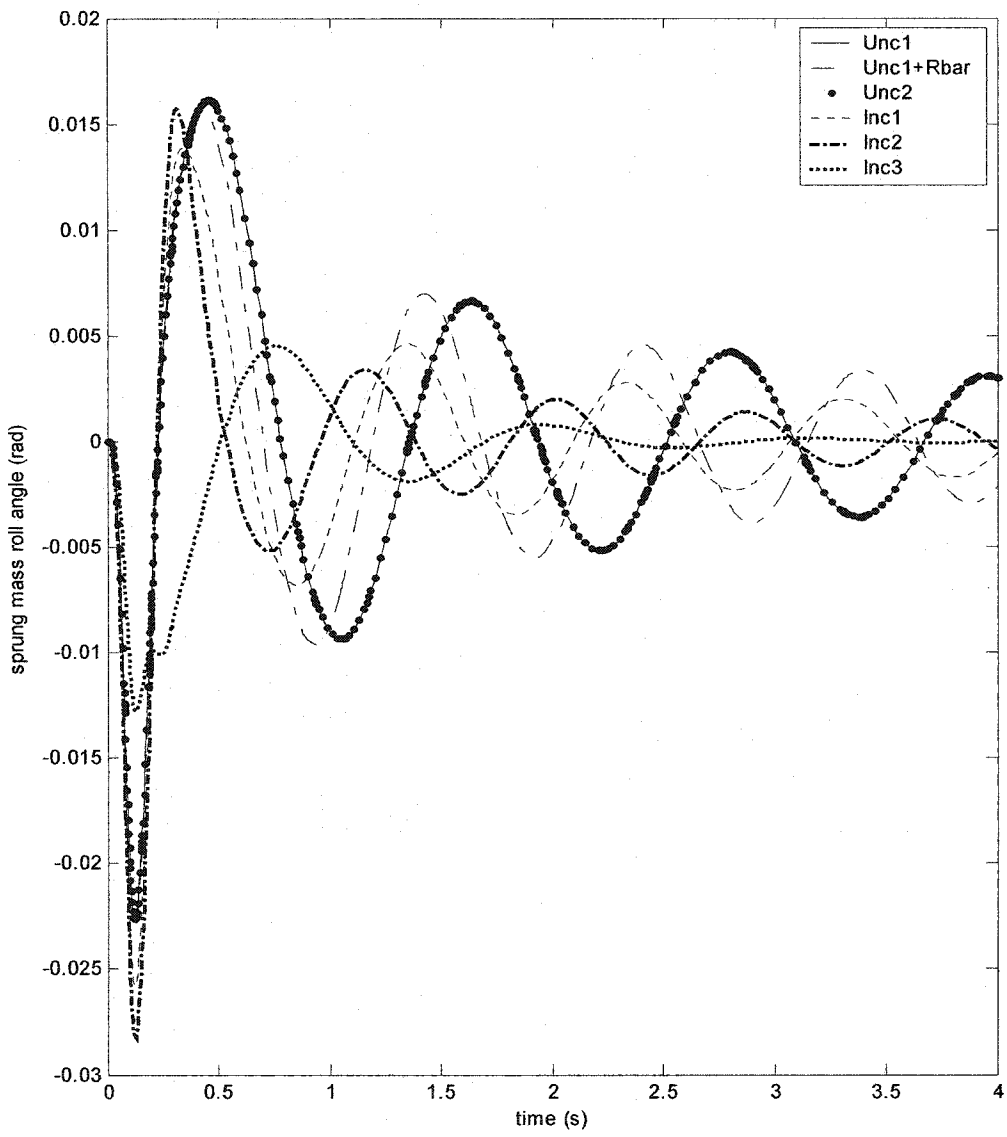

Figure 4.12: Comparison of sprung mass roll angle response of the vehicle model employing different suspension configurations (out-of-phase half sine displacement).

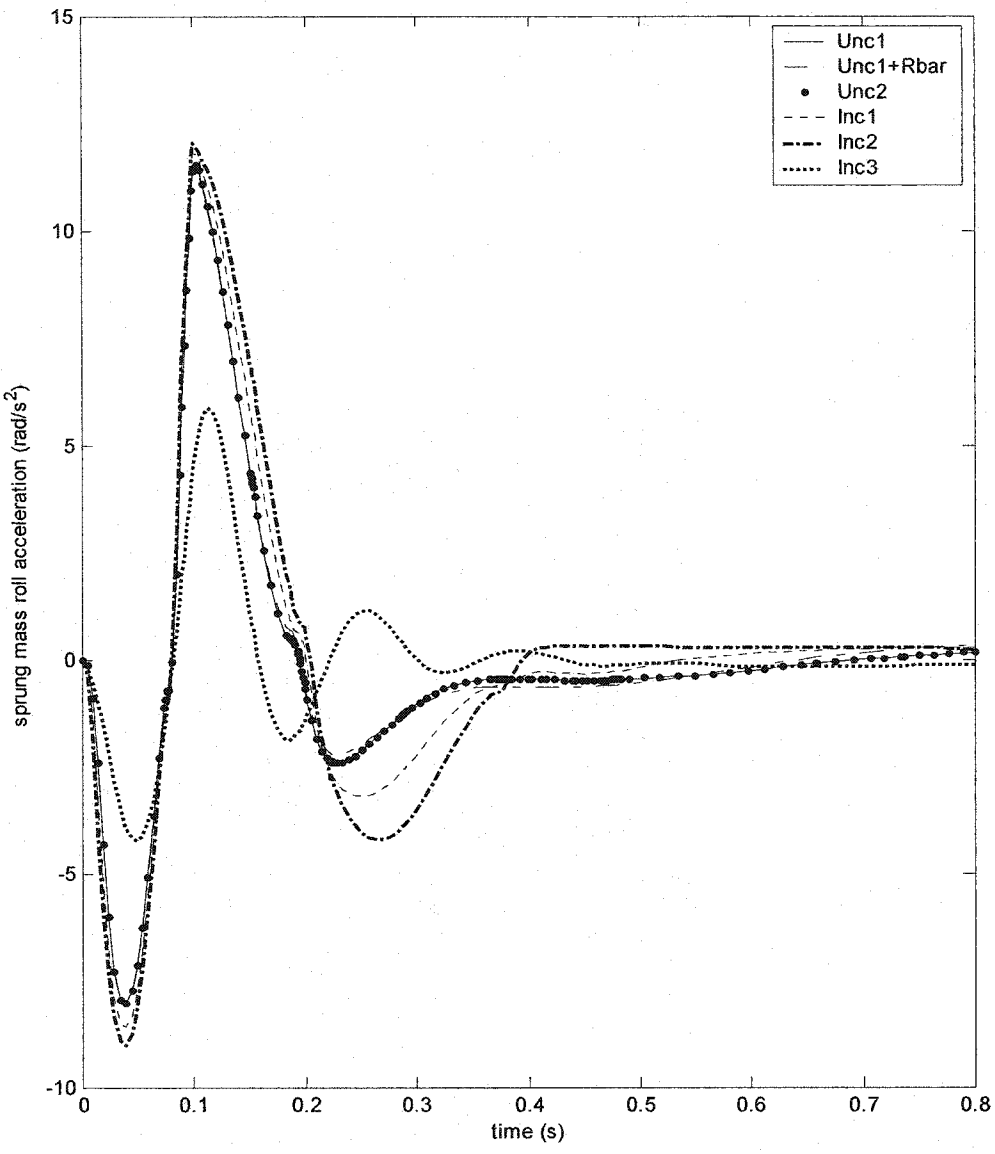

Figure 4.13: Comparison of sprung mass roll acceleration response of the vehicle model employing different suspension configurations (out-of-phase half sine displacement).

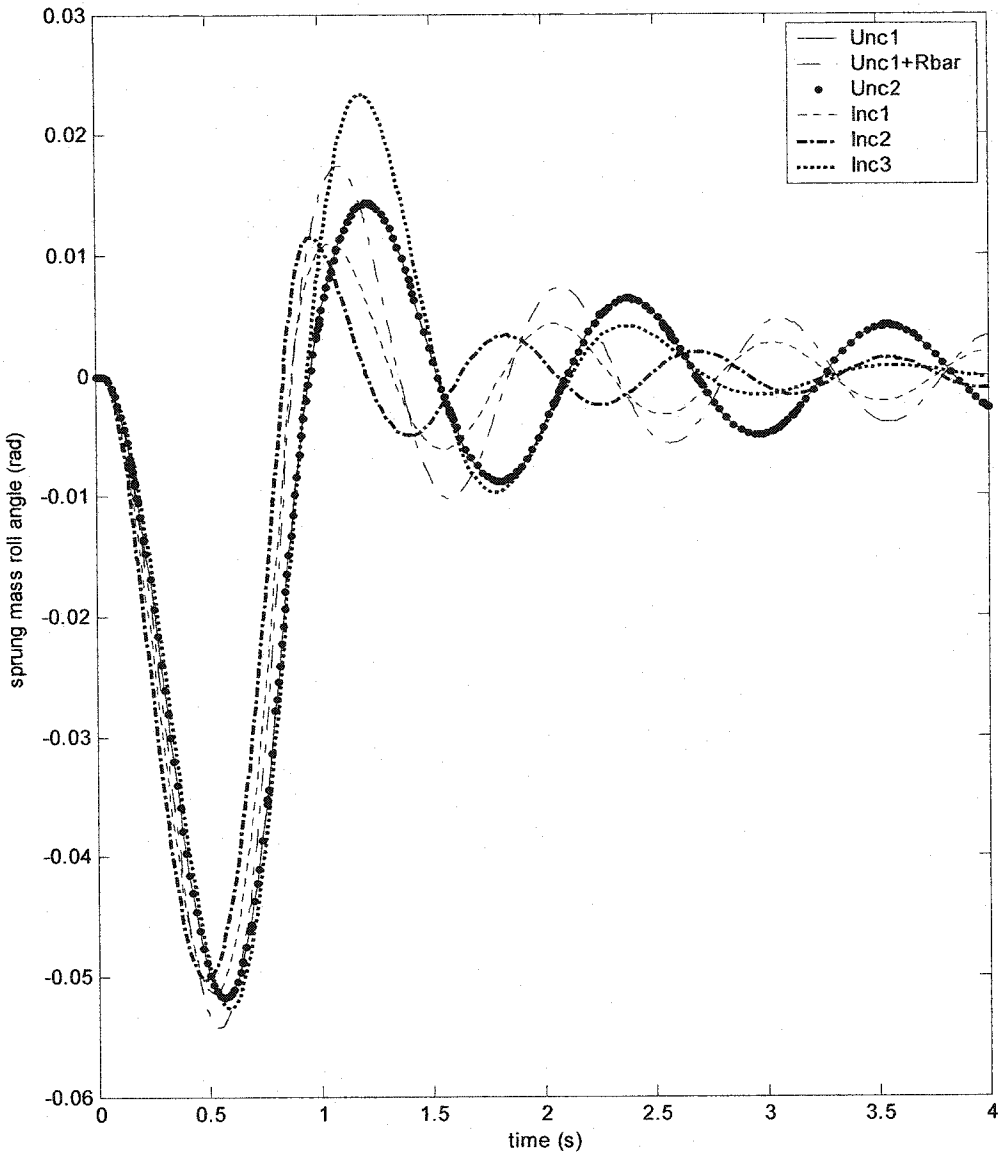

Figure 4.14: Comparison of sprung mass roll angle response of the vehicle model employing different suspension configurations (out-of-phase half sine displacement).

The shock attenuation performance characteristics of the different suspension configurations are further evaluated under a rounded step displacement excitation applied only to the right tire track. Such an excitation is expected to excite both the bounce and roll mode of the vehicle model. The vertical and roll acceleration response characteristics of the sprung mass of the vehicle equipped with different suspensions are illustrated in Figures 4.15 and 4.16, respectively. Similar to the results presented earlier, all the suspension configurations with the exception of Inc3 yield similar magnitudes of peak vertical acceleration response. The Inc3 suspension, however, yields lower peak vertical acceleration response, which may be attributed to its relatively lower damping properties. It should be noted that all the suspension configurations provide constant orifice damping; damping force varying with square of the relative velocity. Conventional automotive suspension dampers also yield similar damping phenomenon, while the damping force is limited at higher velocities through the use of valves. The high vertical mode damping properties of interconnected suspension would necessitate the damping force saturation at some higher velocity through the use of damping valves. The variable damping properties of the struts are expected to yield improved vehicle response in the roll as well as bounce modes.

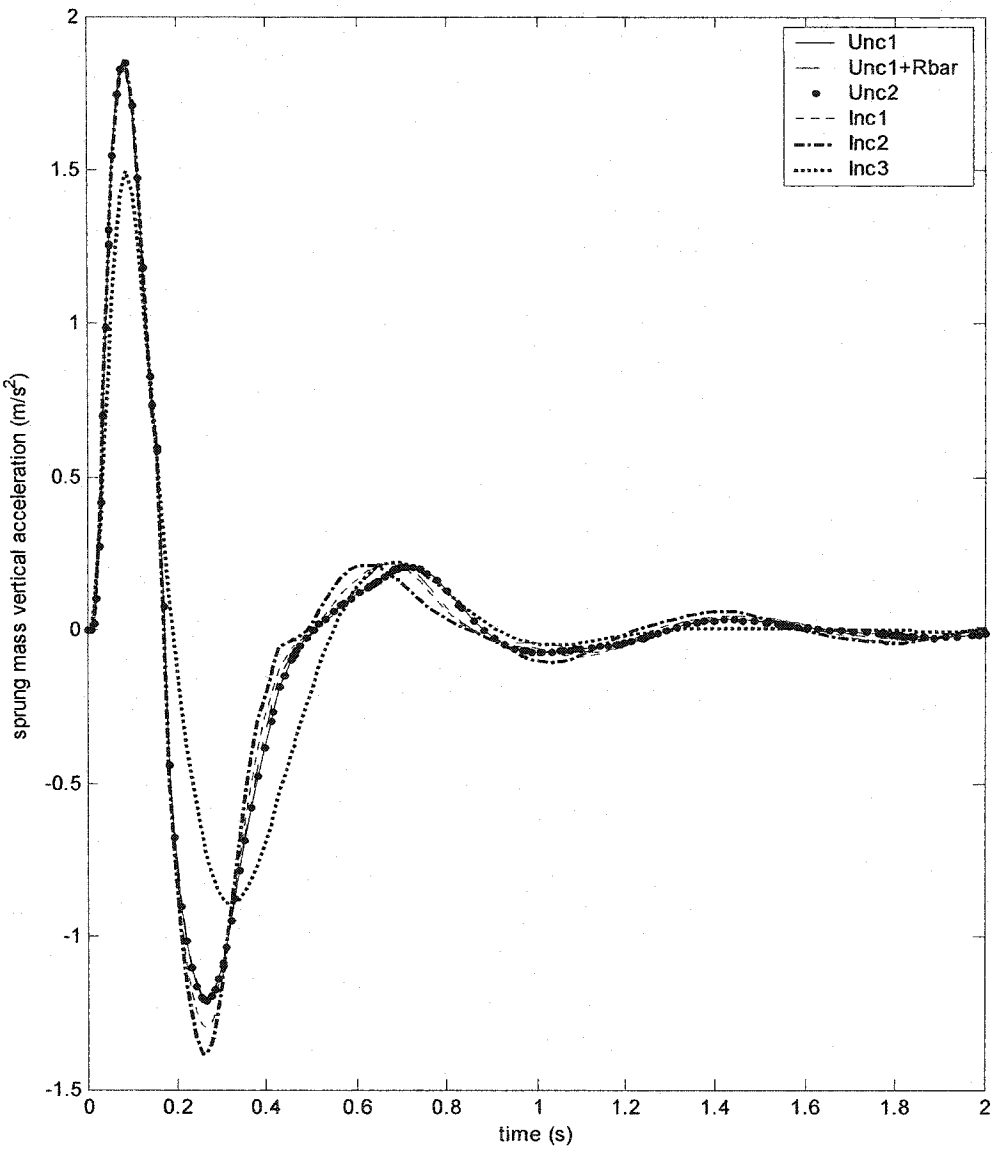

Figure 4.15: Comparison of sprung mass vertical acceleration response of the vehicle model employing different suspension configurations (rounded step displacement excitation only at right tire-terrain interface)

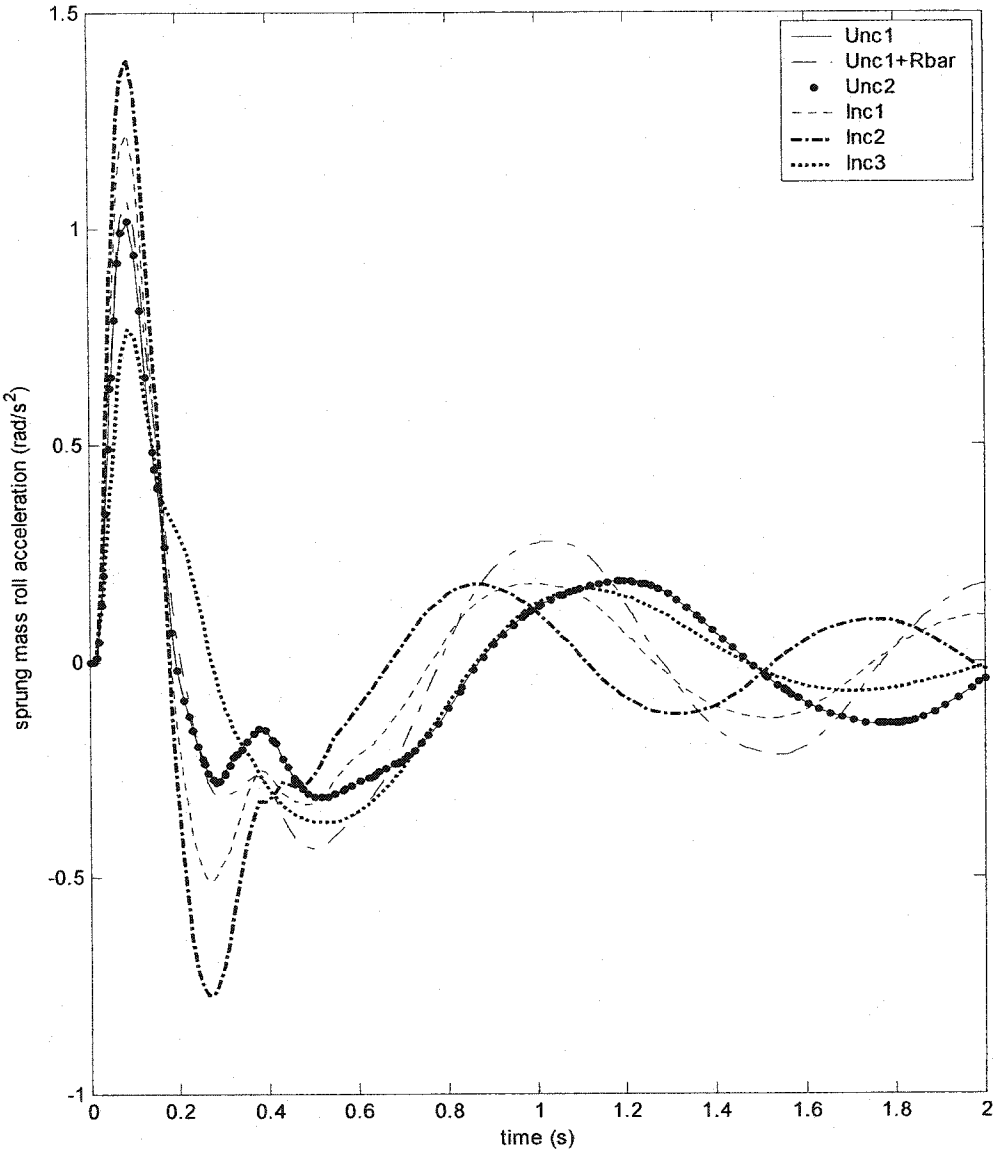

Figure 4.16: Comparison of sprung mass roll acceleration response of the vehicle model employing different suspension configurations (rounded step displacement excitation only at right tire-terrain interface)

4.5 FREQUENCY RESPONSE CHARACTERISTICS

Frequency response characteristics of the vehicle model employing different hydro-pneumatic suspension configurations are evaluated in terms of vertical displacement and roll displacement transmissibility characteristics of the sprung and unsprung masses. The vertical displacement transmissibility characteristics are evaluated for a 0.01m amplitude in-phase sinusoidal excitations at the right and left tire-terrain interfaces. The roll transmissibility characteristics are evaluated for the 0.01m amplitude out-of-phase sinusoidal excitations ($x_{il} = x_{ir} = X_e \sin(\omega t)$, $X_e = 0.01$ m). The frequency response characteristics are obtained by computing the ratio of steady state response amplitude to the excitation amplitude in time-domain over the entire frequency range. The vibration transmission characteristics of different suspension systems are expressed by the following transmissibility ratios:

Vertical displacement transmissibility of sprung mass, $T_{xs} = \dfrac{X_s}{X_e}$

Vertical displacement transmissibility of unsprung mass, $T_{xu} = \dfrac{X_u}{X_e}$

Roll displacement transmissibility of sprung mass, $T_{\theta s} = \dfrac{T\theta_s}{X_e}$

Roll displacement transmissibility of unsprung mass, $T_{\theta u} = \dfrac{T\theta_u}{X_e}$

Where X_s and X_u are the steady state amplitudes of displacement response of the sprung and unsprung masses, respectively; X_e is the amplitude of harmonic

excitation; θ_s and θ_u are the amplitude of roll angle response of the sprung and unsprung masses, respectively; and T is the suspension track.

Vertical displacement transmissibility characteristics of the sprung and unsprung masses of the vehicle with different suspensions are present in Figure 4.17 and 4.18. The frequency response characteristics of the sprung and unsprung masses exhibit their respective resonant frequencies corresponding to peak magnitudes. The bounce frequencies of the sprung and unsprung masses, as identical from the frequency response, under 0.01 m in-phase harmonic excitation, are illustrated in Table 4.1. The vertical mode sprung mass frequency is observed to be near 1.1 Hz, when used with unconnected and Inc1 and Inc2 suspension. The displacement response characteristics of both the unsprung and sprung masses are identical when these suspensions are used. This is attributed to their nearly identical suspension rate and bounce mode damping properties. The relatively high and monotonically increasing damping properties yield the second peak response at a considerably lower frequency near 3.2 Hz. A reduction or limiting of their bounce mode damping would most likely shift this peak to a higher frequency. The Inc3 suspension, with its lighter damping yields peak response near 1.4 Hz, for the sprung mass and near 5.2 Hz for the unsprung mass. A reduction in the suspension damping, as realized by increase in the orifice size from 0.00005 m^2 to 0.0005 m^2, resulted in relatively higher bounce mode frequencies of the sprung as well as unsprung mass, as evident from Table 4.1. An exception to this trend was observed for Inc3 suspension, which showed insignificant influence on the sprung mass frequency and relatively

small effect on the unsprung mass frequency. This is attributed to the fact that the damping properties of Inc3 suspension are mostly attributed to flows through the interconnecting pipes.

Table 4.1: Bounce mode frequencies of the sprung and unsprung masses of the vehicle with different suspensions

Suspension configurations		Frequency (Hz)			
		Unc1 &Unc2	Inc1	Inc2	Inc3
sprung mass	Nominal	1.1	1.1	1.1	1.4
	Light damping	1.3	1.3	1.3	1.3
unsprung mass	Nominal	3.2	3.2	3.2	5.2
	Light damping	7.6	7.6	7.6	7.6

Table 4.2: Roll mode frequencies of sprung and unsprung masses of the vehicle with different suspensions

Suspension configurations		Frequency (Hz)				
		Unc1 & Unc2	Unc1+Rbar	Inc1	Inc2	Inc3
Sprung mass	Nominal	0.8	0.9	0.9	1.0	0.8
	Light damping	0.8	0.9	0.9	1.1	0.8
Unsprung mass	Nominal	4.0	4.0	3.1	3.0	6.8
	Light damping	7.0	7.1	7.1	7.2	7.0

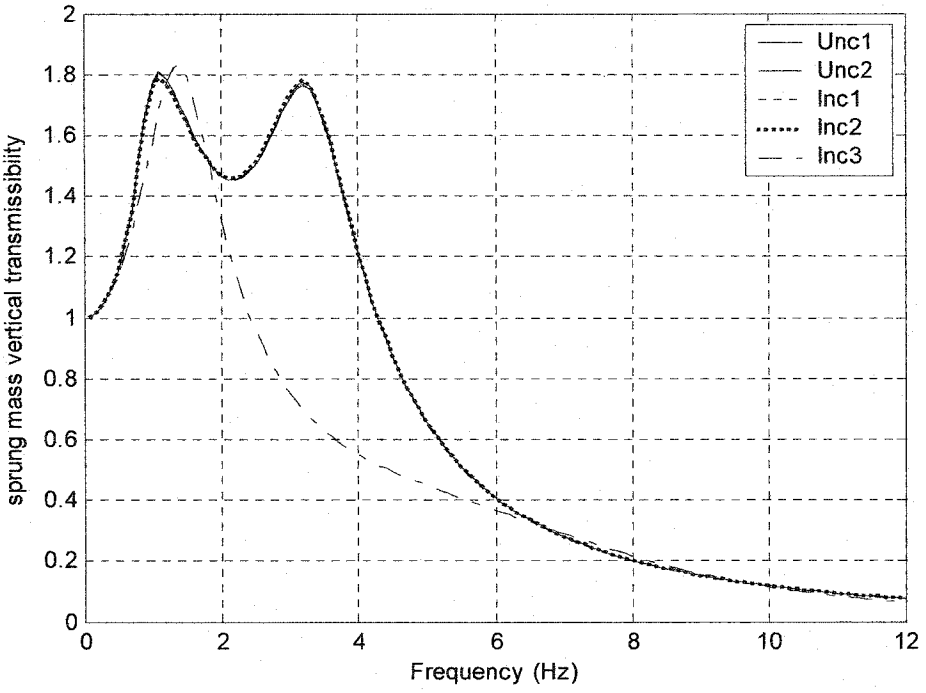

Figure 4.17: Comparison of sprung mass vertical transmissibility of the vehicle model employing different suspension configurations.

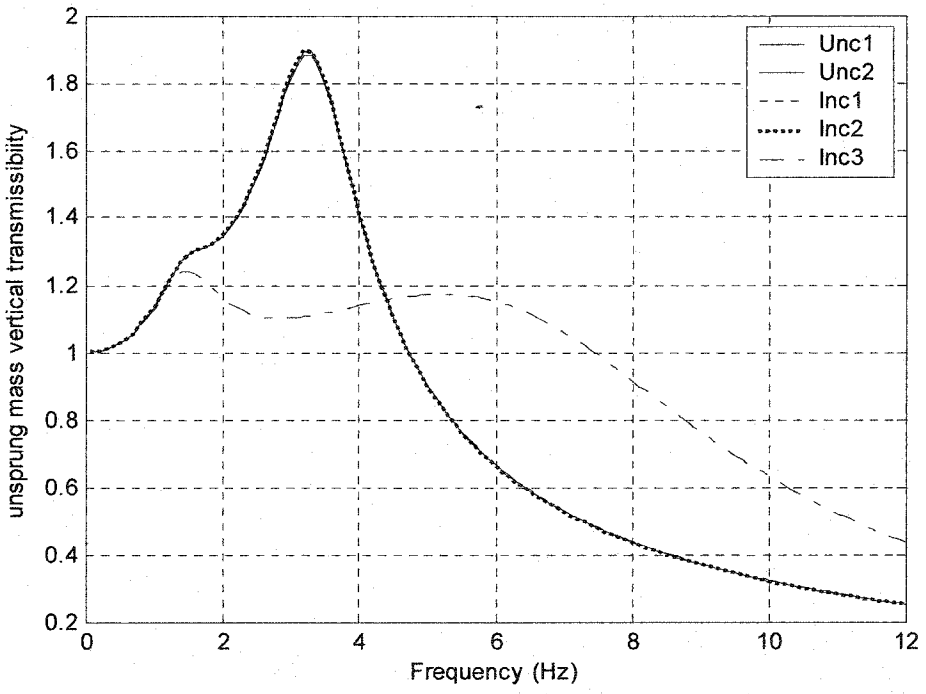

Figure 4.18: Comparison of unsprung mass vertical transmissibility of the vehicle model employing different suspension configurations.

Roll displacement transmissibility characteristics of sprung and unsprung masses of the vehicle with different suspensions are present in Figure 4.19 and 4.20. The roll frequencies of the sprung and unsprung masses of vehicle employing different suspensions under 0.01 m out-of-phase harmonic excitations are illustrated in Table 4.2. The roll mode sprung mass frequency is observed to be near 0.8 Hz, when used with Unc1 and Inc3 suspensions. The roll displacement response characteristic of Inc3 is lower than that of Unc1 and Unc2 suspension in the entire frequency range. This is attributed to their roll mode damping properties. While the resonant frequencies of Inc1 and Inc2 suspensions are observed to be 0.9 and 1.0 Hz, respectively. The Inc2 suspension yields lower peak magnitude of roll transmissibility. The addition of an anti-roll bar, however, deteriorates the ride performances of the vehicle by exhibiting large roll response in the frequency range of 0.8-3.0 Hz. A comparison of Figures 4.17 and 4.19 reveals that the vertical transmissibility of the sprung mass with Inc1 and Inc2 suspensions are identical to those with Unc1 and Unc2 suspensions, while the peak roll responses of the vehicle with Inc1 and Inc2 suspensions are much smaller. The sprung mass roll response of (Inc1 and Inc2) suspensions, however, exhibits poor attenuation of roll vibration beyond 1 Hz.

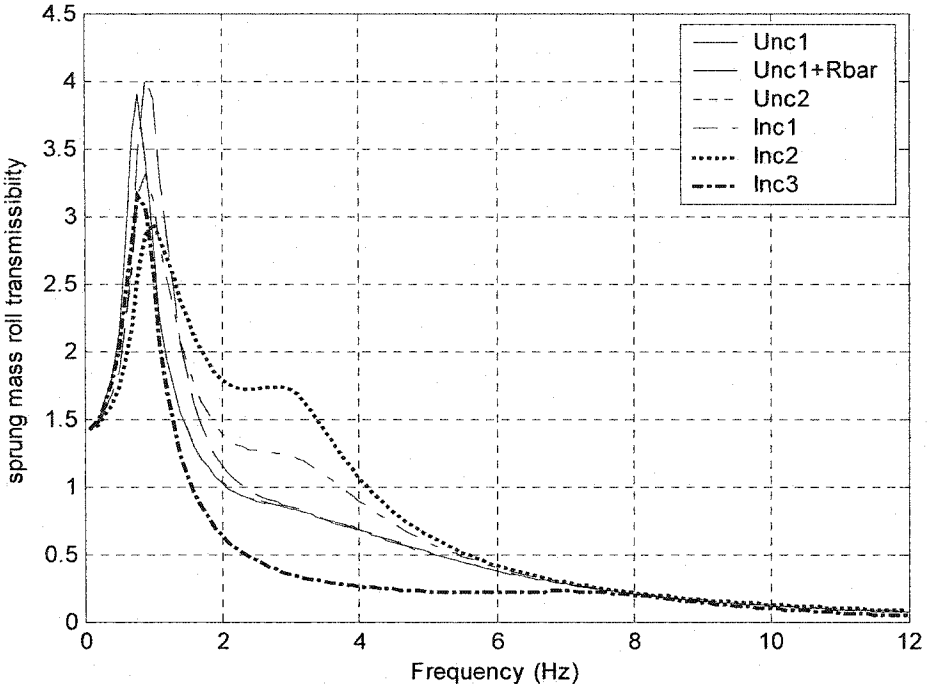

Figure 4.19: Comparison of sprung mass roll displacement transmissibility of the vehicle model employing different suspension configurations.

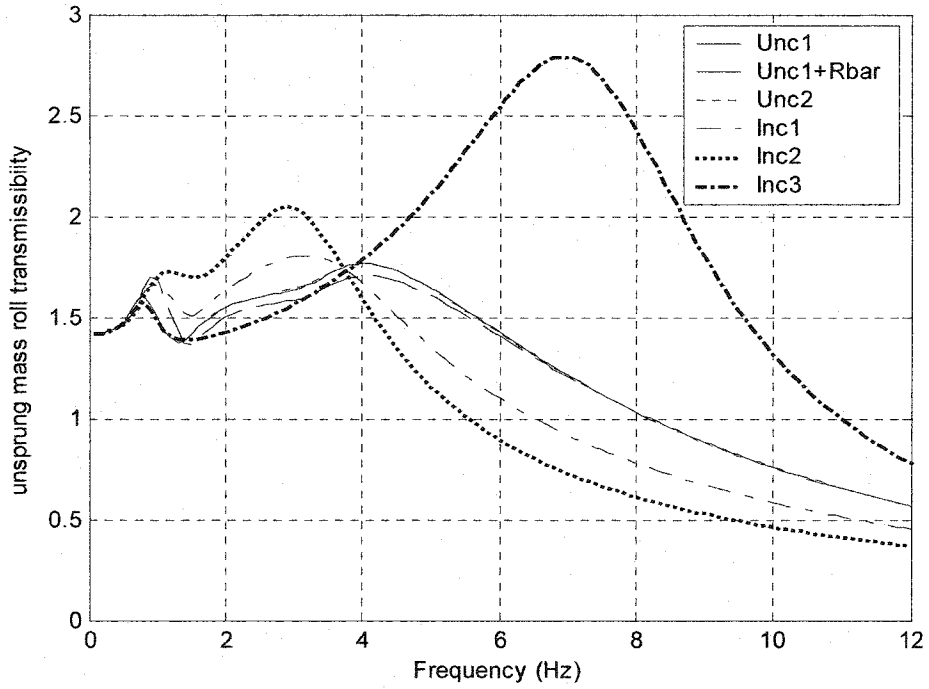

Figure 4.20: Comparison of unsprung mass roll displacement transmissibility of the vehicle model employ different suspension configurations.

4.6 SUMMARY

The ride and handling performance characteristics of different hydro-pneumatic suspension configurations are evaluated for deterministic excitations arising from both the steering inputs and tire-terrain interactions. The deterministic excitations include steady and transient lateral accelerations experienced by the sprung mass during steering maneuvers and in-phase and out-of-phase vertical excitations arising at the tire-terrain interfaces. The results clearly demonstrated that interconnected suspension (Inc2) in the roll plane effectively limits the body roll motion during steering maneuvers due to the enhanced coupling roll stiffness of the suspension. The damping characteristics of the suspension systems, illustrate a very important role in ride quality and road holding abilities. While high damping is desirable for improved road handling, light damping is preferred for adequate shock and vibration attenuation performance. Interconnected suspensions (Inc1 and Inc2) demonstrate larger damping forces in the roll mode than in the bounce mode. The interconnected suspensions (Inc1 and Inc2) thus offer a considerable potential to achieve a better compromise between handling performances and ride comfort. While the anti-roll bar suspension effectively limits the body roll during steering maneuvers, the vehicle ride quality is deteriorated. The comparison of vibration transmissibility characteristics of different suspensions also revealed that the interconnected suspension with identical suspension rate could provide improved vibration isolation performance. The Inc2 has identical roll stability with Inc1 suspension but it has more compact configuration, which eliminate the external

bladder (accumulator) and throttle restriction. The configuration also offers far more flexibility in realizing a larger working area than the Inc1 strut. Furthermore, the Inc3 suspension was found to have no significant effect to roll motion, the same dimension could offer lower damping force in bounce and roll mode.

CHAPTER 5

RESPONSE TO RANDOM ROAD EXCITATION

5.1 INTRODUCTION

The ride and handling performance characteristics of different suspension systems can be best evaluated under representative road excitation, which is random in nature. The random road roughness is often described in terms of its power spectral density (PSD) (Wong, 1991). The reported PSD of the road roughness properties, however, describe the mean roughness of the right-and-left tracks, while the presence of cross-slope or roll component is ignored. The assessment of roll-interconnected suspension would require the description of roughness properties of right- and left-tracks, including the variations in the elevations due to cross-slopes of the road. Furthermore, the reported road profiles are expressed in terms of spatial PSD, which can be expressed in terms of temporal PSD as a function of the forward speed. The simulations of the highly nonlinear models of the interconnected and unconnected suspension, however, require time histories of the road profiles. A time history of the road roughness could be synthesized by introducing a filter function (Carrier, 1999). The roughness profiles of various highways and secondary roads have been measured in many reported studies (Robson, 1979; Damien, 1992). A number of spectral functions have also been proposed to describe the average roughness spectra of different roads (Hac, 1987; Oueslati, 1995). The roughness characteristics of urban roads have been reported in a recent study (Rakheja, et al., 1999). This study describes the roughness characteristics of both the right

and left tracks of selected urban roads. The vehicle models formulated in chapter 2 are analyzed under the reported urban road excitation to study the suspension performance under a realistic road excitation.

5.2 ANALYSIS OF THE MEASURED ROAD ELEVATIONS

An urban road roughness measurement program was undertaken to characterize the roughness of urban roads in cities of Montréal and Longueuil (Carrier, 1999). The road elevation raw data was analyzed to generate temporal and spatial road roughness profiles in order to study the tire-terrain interactions and dynamics of urban buses (Rakheja, et al., 1999). Six different roads were considered for their roughness characterization over a total distance ranging from 538 m to 686 m. The average speed was maintained nearly constant over different segments, while the average speed over different segments varied from 43 km/h to 66 km/h.

The tire-terrain interactions and the forces developed by vehicle tires are strongly related to the macro- and micro-harshness of the road surfaces. It is thus vital to characterize roughness characteristics of the road surface at the macro- and micro-levels. The measured road elevations, however, include both the macro and micro roughness variations and the local gradient. A high-pass filter is often applied to eliminate the contributions due to low frequency variations associated with variations in the local gradients. In this study, the spatial elevation data is initially converted into its temporal history, which is then filtered through a high-pass (HP) filter. The temporal elevation history, $x_i(t)$, is obtained from the measured spatial profile, $x_i(d)$, by expressing the longitudinal

coordinate x in terms of the temporal coordinate t, ($d = vt$) as a function of forward speed v: The filtered profile is then converted back to its spatial form, as shown in Figure 5.1. The measured data is processed using the above algorithm in a digital signal processing software, (DADiSP, 1998). An HP filter is applied with cut-off frequency of 0.3 Hz.

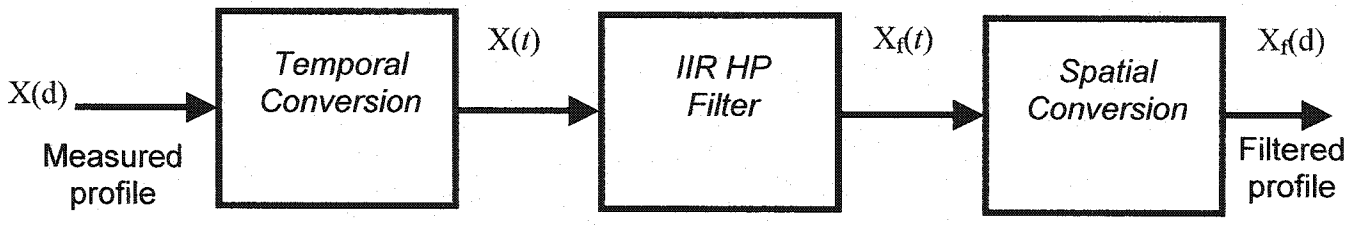

Figure 5.1: Elimination of local slopes from the measured profile.

5.3 POWER SPECTRAL DENSITY OF ROAD ROUGHNESS PROFILES

The road profile is usually considered to be a random process $x(d)$, where x is the road elevation corresponding to a certain distance along the road. The temporal variations in the road roughness, $x(t)$, is considered to be a stationary random process with zero mean. This can be characterized by its autocorrelation function (Davis, 2001):

$$R(\tau) = \langle x(t)x(t-\tau)\rangle = \lim_{T\to\infty}\frac{1}{T}\int_0^T x(t)x(t-\tau)dt[m^2] \qquad (5.1)$$

where $\langle\bullet\rangle$ is the time averaging operation.

The 'double sided' power spectral density $S(f)$ is derived from the Fourier transform of $R(\tau)$:

$$S(f) = \int_{-\infty}^{\infty} R(\tau)e^{-j2\pi f\tau}d\tau[m^2/Hz] \qquad (5.2)$$

$$R(\tau) = \int_{-\infty}^{\infty} S(f) e^{-j2\pi f\tau} df [m^2] \tag{5.3}$$

The power spectral density has the property such that if its integration over the entire frequency range yields the mean square value of $x(t)$.

$$\langle x^2(t) \rangle = R(0) = \int_{-\infty}^{\infty} S(f) df \tag{5.4}$$

Because $S(f)$ is an even function of f, it is sometimes defined in its 'single sided' form which is twice the value of the 'double sided' function. The road profile $x(di)$, with di being the distance along the road, can be characterized by an autocorrelation function $R(\delta) = \langle x(di) x(di - \delta) \rangle$, where $\langle \bullet \rangle$ is now a distance averaging operation. The power spectral density of $x(di)$ via the Fourier transform of $R(\delta)$ is then expressed in terms of a spatial frequency variable Ω in radians per meter. It is given by:

$$S(\Omega) = \int_{-\infty}^{\infty} R(\delta) e^{-j\Omega\delta} d\delta \tag{5.5}$$

$$R(\delta) = \int_{-\infty}^{\infty} S(\Omega) e^{-j\Omega\delta} d\Omega \tag{5.6}$$

where $S(\Omega)$ is the spatial spectral density of the road profile. The measured road profiles are invariably expressed in terms of the spatial power spectral density (PSD) of the roughness. It is more convenient to express the spatial PSD of the surface profiles in terms of the temporal PSD and temporal frequency in Hz rather than in terms of the spatial frequency since the vehicle vibration is a function of time (Wong, 1991). The spatial PSD, $S(\Omega)$, and spatial frequency,

Ω, of a roughness profile can be expressed in terms of temporal functions in the following manner:

$$\begin{cases} f = \Omega v; \\ S(f) = S(\Omega)/v \end{cases} \tag{5.7}$$

where f and $S(f)$ are temporal frequency and PSD of the road roughness, respectively.

The roughness data for an urban road were acquired from the CONCAVE database on road roughness (Carrier, 1999). The raw data acquired for left and right tracks were initially processed through a high-pass filter to eliminate the presence of slopes in the roadway. Figure 5.2 illustrates the filtered roughness profiles of left- and right- tracks of the selected road $x_{fi}(d), i = \ell, r$. The relative roll angle of the roadway roughness can be further derived from the filtered time histories in the following manner:

$$\theta(d) = \frac{x_{f\ell}(d) - x_{fr}(d)}{T} \tag{5.8}$$

where $x_{f\ell}(d)$ and $x_{fr}(d)$ are the time-histories of the left- and right-tracks, respectively, $\theta(d)$ is the relative roll angle of the road profile and T is the track width.

Figure 5.3 illustrates the resulting relative roll angle of the roadway. Figures show that the vertical road elevation could approach 2 cm for the left- track, while that of the right-track on the curb side could approach as high as 4.8 cm. The relative roll angle approaches as high as 0.023 radians.

A Hanning window function is applied to the filtered time-histories to minimize the leakage and PSD function available within MATLAB software is used to derive both the spatial as well as temporal spectral densities of the road profile. Figure 5.4 illustrates the spatial PSD of the left- and right- tracks of the road profile. The temporal acceleration PSD's due to road roughness of the two tracks corresponding to forward speeds of 50 km/h and 100 km/h are presented in Figures 5.5 and 5.6, respectively. These figures consistently show higher PSD magnitudes for the right track, which may be attributed to the presence of drain-covers and localized damages in the curb lane.

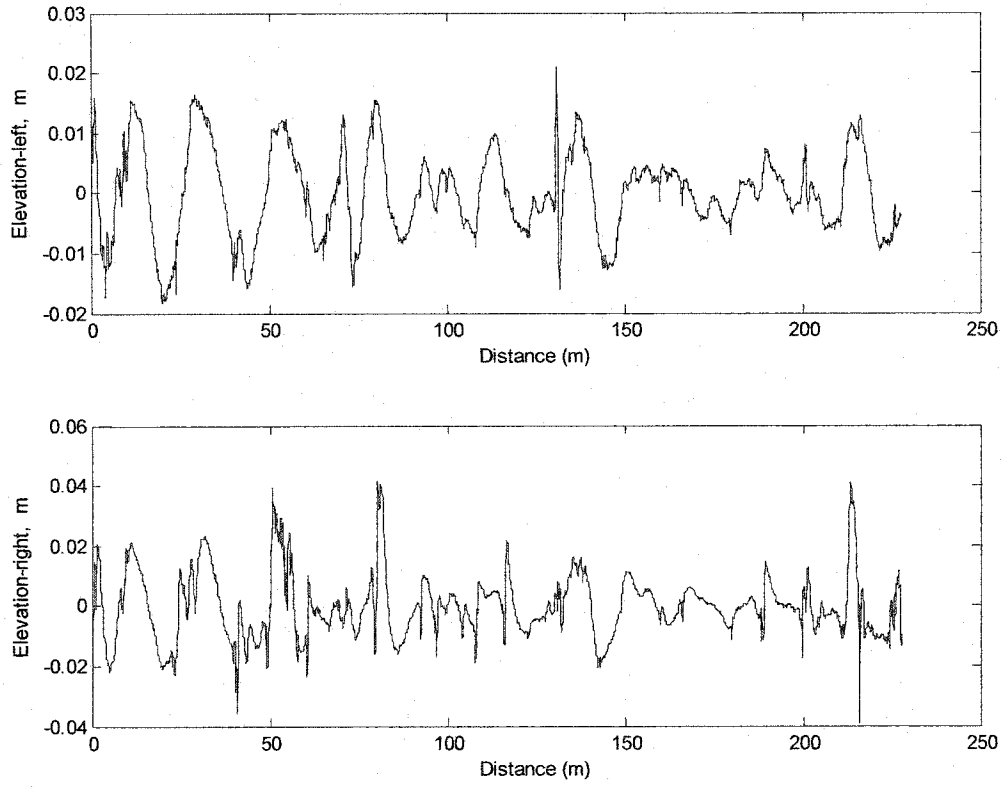

Figure 5.2: Filtered roughness profiles of the left- and right-tracks of the selected road.

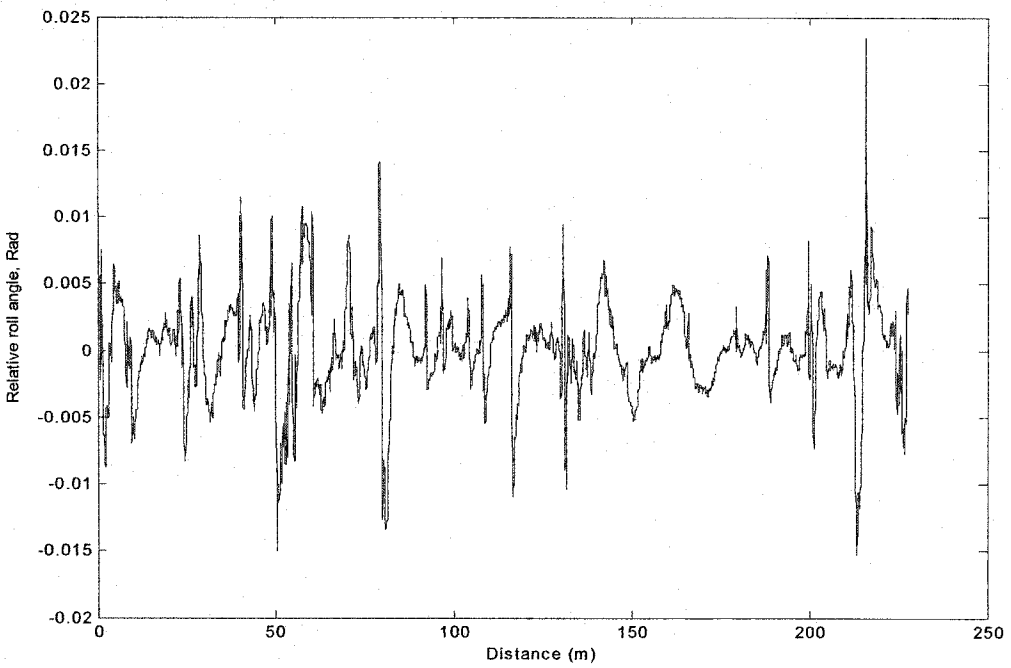

Figure 5.3: The relative roll angle of the selected roadway.

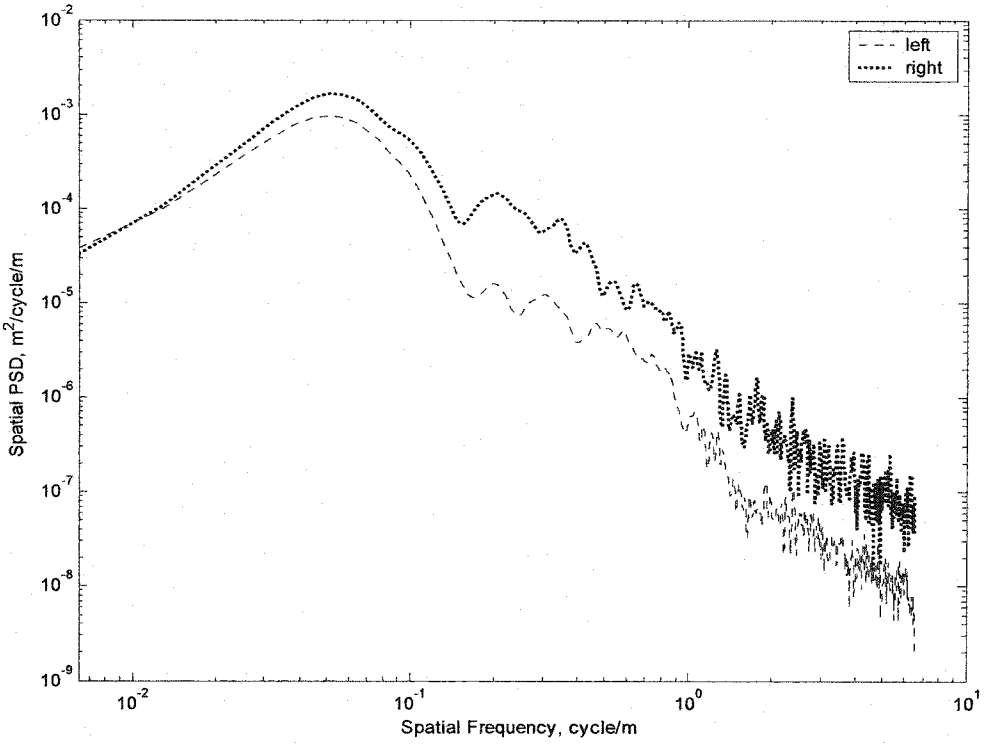

Figure 5.4: Spatial power spectral density of roughness of the right-and left-tracks

The spatial PSD of the roughness profile of the right track is considerably higher than that of the left-track, specifically at frequencies above 0.1 cycle/m. The spatial spectrum of the roughness profile, shown in Figure 5.4, exhibits trends that are similar to the reported spectra for rough runways, highways and gravel roads (Wong, 1991). The comparisons with the reported spectra revealed that the magnitudes of roughness spectral density of the selected urban road are considerably higher than those of highways but less than those of the gravel roads and rough runways.

The temporal acceleration PSD due to roughness of right-track is also considerably higher than that of the left-track, irrespective of the forward speed, as evident from Figures 5.5 and 5.6. The magnitude of acceleration PSD increases considerably as the speed is increased from 50km/h to 100 km/h.

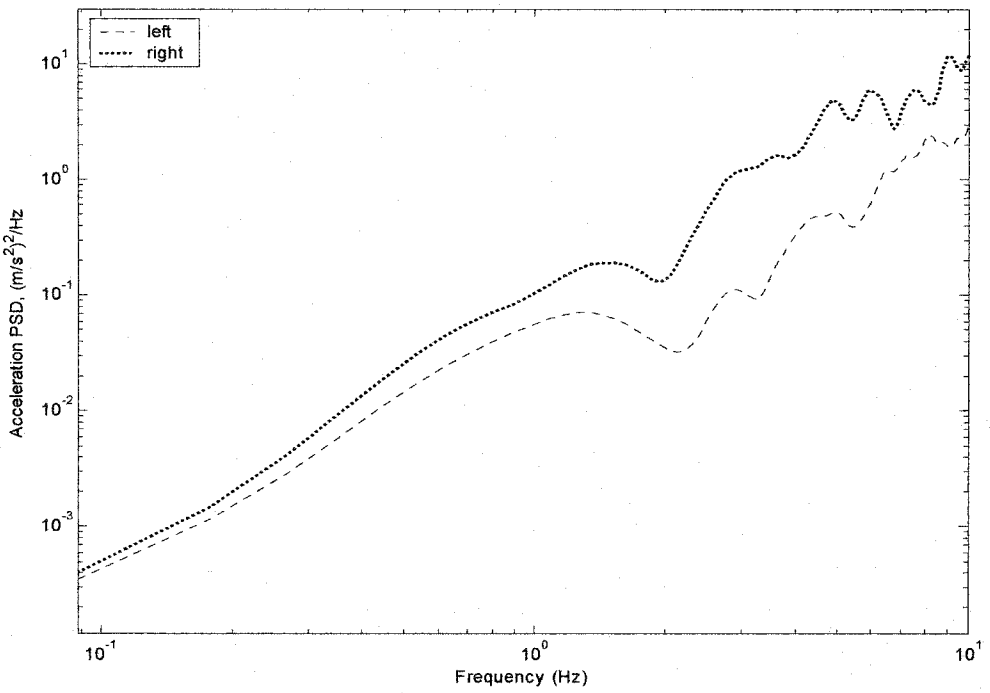

Figure 5.5: Acceleration PSD due to roughness of the left- and right-tracks (speed= 50 km/h)

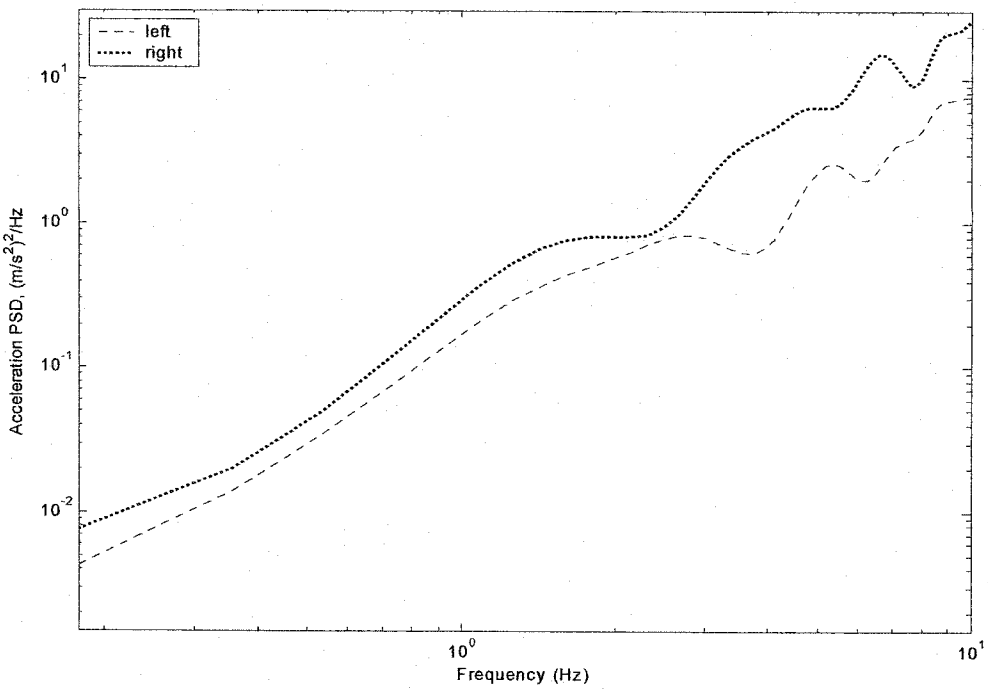

Figure 5.6: Acceleration PSD due to roughness of the left- and right-tracks (speed= 100 km/h)

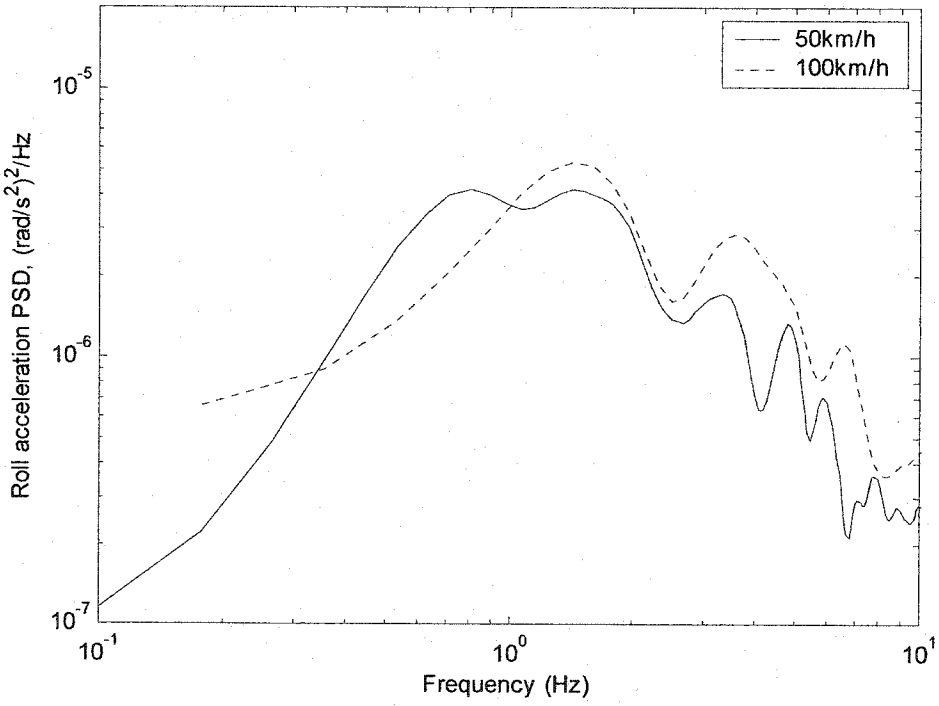

Figure 5.7: Roll Accelerations PSDs' due to cross-elevation of the left- and right-tracks under two constant speeds

Figures 5.7 illustrates a comparison of the temporal acceleration PSD's due to cross-elevation or roll component of the road profile corresponding to forward speeds of 50 and 100 km/h. The results show that the magnitudes of roll acceleration PSD of the road profile increase considerably as the speed is increased, specifically at frequencies above 1 Hz, as observed in the case of vertical acceleration. The peak magnitude increases from 4×10^{-6} to 5.5 $\times10^{-6}$ near 1.5 Hz. Higher roll acceleration PSD at the lower speed of 50 km/h, however, is observed in the 0.35 to 1 Hz range.

5.4 RIDE DYNAMIC RESPONSES OF VEHICLE MODELS

Equations of motion formulated for unconnected and interconnected suspension configurations in chapter 2 are solved under filtered road excitation described in Figure 5.2, while the forward speed is assumed constant. The ride dynamic responses of the roll vehicle model are evaluated in terms of vertical and roll accelerations of the sprung masses. Figure 5.8 illustrates the time-histories of vertical and roll acceleration responses of the sprung mass of the vehicle with Unc1 and Inc2 suspensions at a forward speed of 50 km/h, as an example. The responses obtained for unconnected (Unc1) and interconnected (Inc2) suspension reveal nearly identical vertical acceleration of the sprung mass, which is attributed to their identical vertical mode damping and spring rates. The peak of vertical acceleration approaches around 9 m/s^2 for both suspensions. The interconnected suspension (Inc2) yields slightly higher roll acceleration peaks of the sprung mass than the unconnected suspension (Unc1). The peak values approach 7.2 rad/s^2 and 6.8 rad/s^2 for the Inc2 and Unc1

suspensions, respectively, over the simulation period presented in Figure 5.8. The higher roll acceleration response of the Inc2 suspension is attributed to its higher effective roll stiffness and damping, which is evident from the properties and acceleration transmissibility presented in Figures 3.3 and 3.4. The high roll stiffness of the interconnected suspension is considered to be beneficial in limiting the roll motion of the sprung mass caused by the steering inputs, which occur at frequencies well below 0.5 Hz. The high roll stiffness and damping however would yield higher roll mode natural frequency and acceleration of the sprung mass.

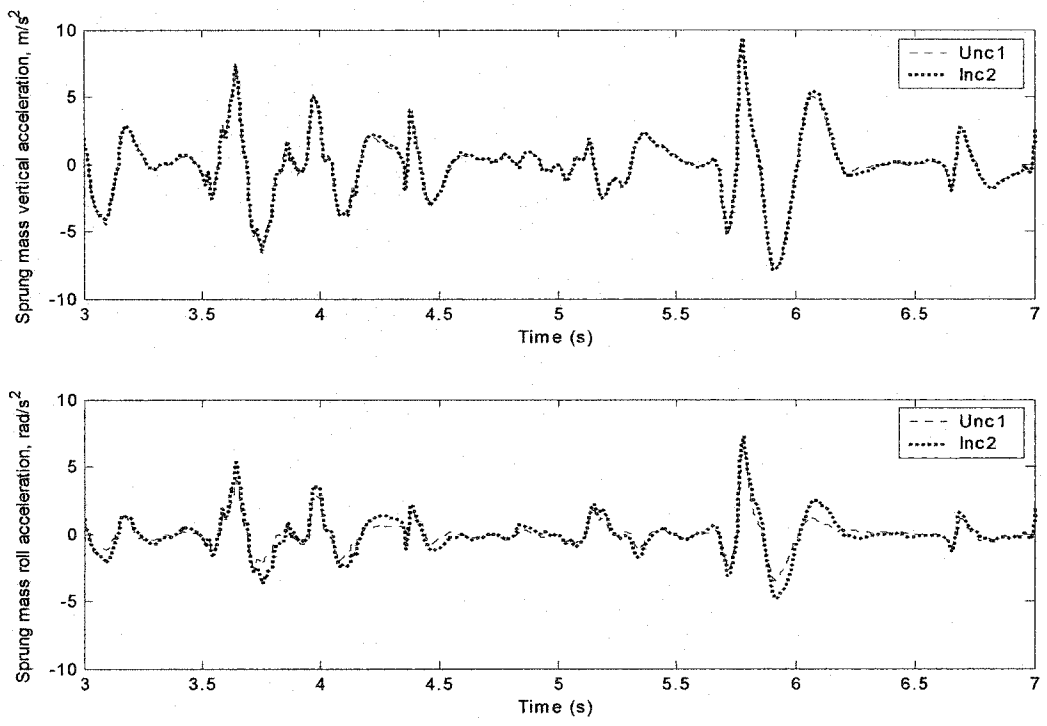

Figure 5.8: The vertical and roll acceleration of sprung mass of unconnected suspension (Unc1) and interconnected (Inc2) suspension (speed= 50 km/h)

The PSD of vertical acceleration response of the sprung mass supported on different suspension configurations are evaluated and compared in Figure 5.9 and 5.10 corresponding to two different constant speeds (50 and 100 km/h).

Owing to nearly identical spring rates and damping properties of the Unc1, Unc1+Rbar, Inc1, and Inc2 suspension systems, these suspensions yield almost identical vertical acceleration responses of the sprung mass. The acceleration PSD responses show peaks near the sprung mass bounce frequency near 1.4 Hz and that of the unsprung mass near 3.2 Hz. Such trends are also evident from the vertical acceleration transmissibility characteristics presented in Figures 4.17 and 4.18. The peak acceleration PSD of the sprung mass approach 1 $(m/s^2)^2/Hz$ for 50 km/h speed, and 5 $(m/s^2)^2/Hz$ at a speed of 100 km/h, near the unsprung mass resonant frequency. The high acceleration response and lower unsprung mass resonant frequency are attributed to relatively high damping forces generated by the suspension struts with constant orifice. Such peak responses can be considerably reduces by introducing lower damping trough design of multi-stage valve, which would lower the hydraulic resistance at higher relative velocity (Su, 1990). This is evident from the sprung mass acceleration response with Inc3 suspension configuration, which yields relatively lower damping. The results shown in Figures 5.9 and 5.10 suggest that lower damping of the Inc3 suspension tends to considerably suppress the peak response near the unsprung mass resonant frequency, irrespective of the vehicle speed. The response magnitude corresponding to the sprung mass resonance however increases. The results suggest that the Inc3 suspension configuration could provide improved vertical ride, which could be further improved by further reducing the damping and by introducing multi-stage variable damping through control valves.

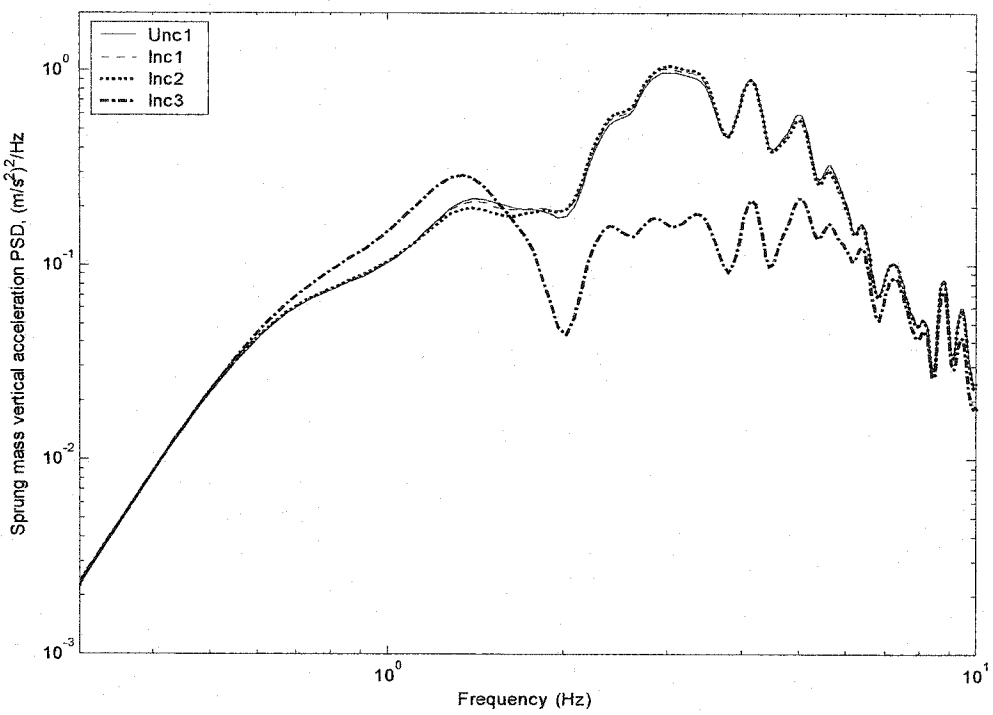

Figure 5.9: Comparison of vertical acceleration PSD responses of the sprung mass with different suspension systems. (speed= 50 km/h)

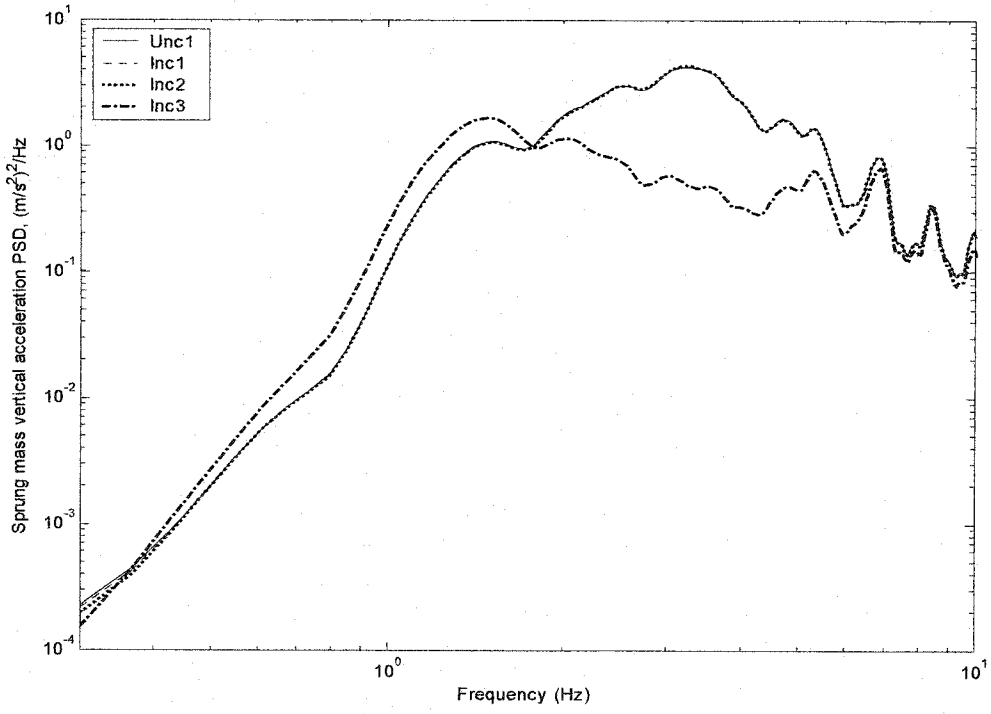

Figure 5.10: Comparison of vertical acceleration PSD responses of the sprung mass with different suspension systems. (speed= 100 km/h)

Figure 5.11 and 5.12 illustrate comparison of PSD of roll acceleration responses of the sprung mass of the vehicle with different suspension configurations at forward speeds of 50 km/h and 100 km/h, respectively. Unlike the vertical mode, different suspensions exhibit considerably different properties in the roll mode. The roll acceleration responses of the sprung mass with different suspensions thus differ. The addition an anti-roll bar to the unconnected struts increases the sprung mass roll frequency from approximately 0.8 Hz and 0.9 Hz, and reduces the magnitude of roll acceleration PSD at frequencies below the resonant frequency. High effective roll stiffness of the anti-roll bar, however, yields higher roll acceleration in the 0.8 to 2.5 Hz, irrespective of the vehicle speed. The Inc1 and Inc2 suspensions yield lower roll acceleration response prior to their respective roll mode frequencies, 0.9 Hz and 1.0 Hz, due to their high effective roll stiffness. The high roll stiffness coupled with high roll damping of these suspensions cause relatively higher roll acceleration response at higher frequencies. The Inc3 suspension yields higher roll acceleration at low frequencies but considerably lower acceleration response at higher frequencies. This response behavior is attributed to its relatively lower roll mode stiffness and damping, as discussed earlier.

The response characteristics of the vehicle model with different suspension systems subject to random urban road excitations are further evaluated in terms of the root mean square (RMS) values of the vertical and roll acceleration, and roll deflection of the sprung mass. The RMS values of the sprung mass responses are computed from:

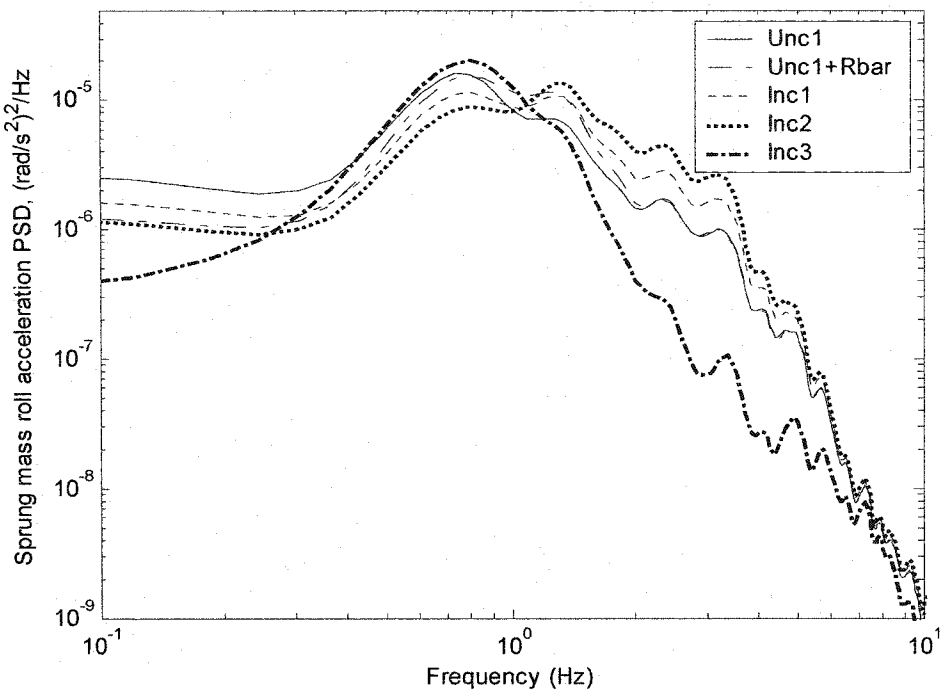

Figure 5.11: Comparison of roll acceleration PSD responses of the sprung mass with different suspension systems. (speed= 50 km/h)

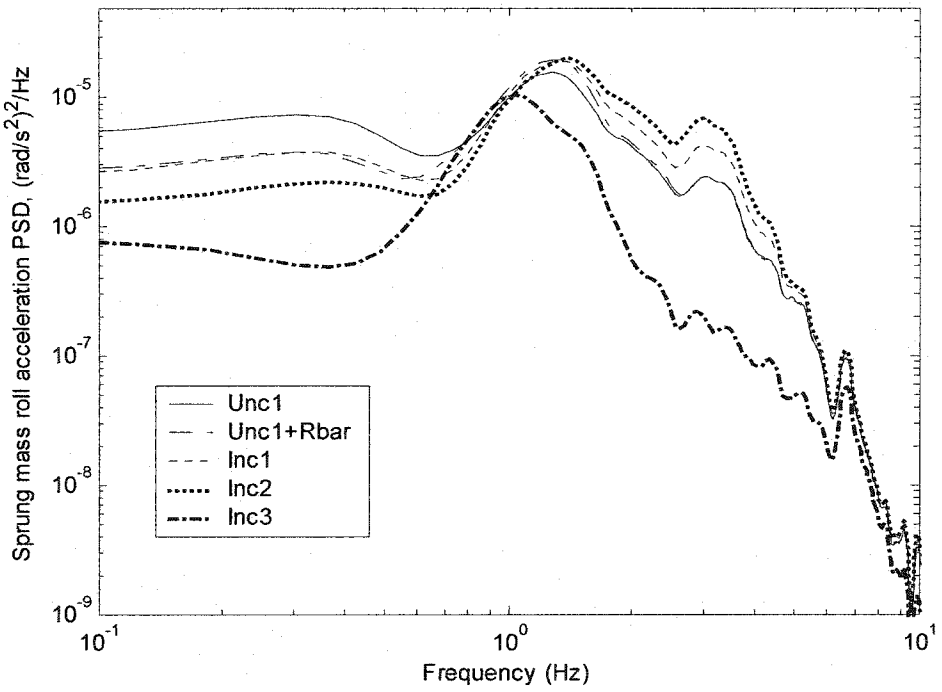

Figure 5.12: Comparison of roll acceleration PSD responses of the sprung mass with different suspension systems. (speed= 100 km/h)

$$\overline{\ddot{x}}_s = \sqrt{\frac{1}{T_s}\int \ddot{x}_s(t)dt} \tag{5.9}$$

$$\overline{\ddot{\theta}}_s = \sqrt{\frac{1}{T_s}\int \ddot{\theta}_s(t)dt} \tag{5.10}$$

$$\overline{\theta}_s = \sqrt{\frac{1}{T_s}\int \theta_s(t)dt} \tag{5.11}$$

Where $\overline{\ddot{x}}_s$ is the RMS value of the sprung mass vertical acceleration, $\overline{\ddot{\theta}}_s$ is the RMS value of the sprung mass roll acceleration, and $\overline{\theta}_s$ is the RMS value of the sprung mass roll angle, and T_s is the time duration of the response. Table 5.1 presents a comparison of the RMS values of the sprung mass responses corresponding to vehicle speeds of 50 km/h and 100 km/h.

Table 5.1: Comparison of RMS values of sprung mass vertical and roll acceleration, and roll deflection with different suspension systems

	50km/h			100km/h		
	$\overline{\ddot{x}_s}$ (m/s^2)	$\overline{\ddot{\theta}_s}$ (rad/s^2)	$\overline{\theta_s}$ (rad)	$\overline{\ddot{x}_s}$ (m/s^2)	$\overline{\ddot{\theta}_s}$ (rad/s^2)	$\overline{\theta_s}$ (rad)
Unc1	1.7799	0.7975	0.0038	3.1949	1.1815	0.0043
Unc2	1.7799	0.7975	0.0038	3.1949	1.1815	0.0043
Unc1+Rollbar	1.7791	0.8023	0.0040	3.1932	1.1842	0.0044
Inc1	1.7870	0.9491	0.0041	3.1868	1.3793	0.0047
Inc2	1.7873	1.0934	0.0044	3.1838	1.5391	0.0050
Inc3	1.1012	0.4257	0.0034	2.0254	0.6079	0.0026

The results show that the RMS values of vertical and roll accelerations increase considerably as the vehicle speed is increased from 50 dm/h to 100 km/h, irrespective of the suspension configuration employed. All the suspension configurations, with the exception of Inc3, yield nearly similar RMS values of the vertical and roll acceleration. The Inc3 suspension with lower roll stiffness and damping yields considerably lower values. Apart from the vertical and roll accelerations, the Inc3 suspension yields lower roll deflection of the sprung mass. The Inc3 suspension can thus be considered to provide improved ride and handling performance of the vehicle under rough urban road excitation.

5.5 SUMMARY

The ride and handling performance characteristics of different hydro-pneumatic suspension configurations are further evaluated under random excitations arising from an urban road. The roughness characteristics of the left- and right-tracks of the selected road are analyzed to derive the spatial and temporal PSD's of the vertical and roll excitations. The ride dynamic responses of vehicle models employed different suspension configurations are evaluate and presented in terms of vertical and roll acceleration PSD of sprung mass. The RMS values of the vertical and roll accelerations, and roll deflection of the sprung mass are further evaluated and compared. The result demonstrated that higher speeds yield higher response accelerations, irrespective of the suspension configurations. All the suspension systems, with the exception of Inc3, yield similar vertical acceleration responses due to their suspension with its lower damping yields considerably lower vertical acceleration response in the ride

zone. The RMS values of roll and vertical accelerations, and roll deflections of the sprung mass with Inc3 suspension are considerably lower than those attained with other suspensions.

CHAPTER 6

CONCLUSIONS AND RECOMMENDATIONS FOR FUTURE WORK

6.1 MAJOR HIGHLIGHTS

The passenger ride comfort and vehicle handling performances impose conflicting requirements on the suspension design, which often results in a compromise between the two design goals. The handling and directional control characteristics constitute the primary design considerations for heavy vehicle suspensions, while the ride quality receives the secondary consideration. The heavy vehicle suspensions are thus designed to yield high roll stiffness to enhance highway safety through improved handling and control performance. Such suspension designs, however, yield poor ride performance. In this dissertation, two types of hydro-pneumatic suspension interconnected by different chambers in the roll plane are thoroughly investigated to achieve improved compromise between the ride and roll performance characteristics of a heavy vehicle.

The primary objectives of this study included: (1) development of analytical models of the two types of unconnected hydro-pneumatic struts with and without an anti-roll bar, and three different interconnected suspension systems in the roll plane; (2) development of methodologies to evaluate the static and dynamic properties of the different suspension systems; and (3) evaluation of roll and ride dynamic potentials of the interconnected suspensions.

The major highlights of this investigation are summarized below:

1. The design concept of a compact hydro-pneumatic strut is explored to realize larger working area and thus reduced operating pressure to achieve desired load carrying capacity. Unlike the struts proposed in the literature, the type 2 strut described in this dissertation integrates the gas chamber within the strut thereby resulting in a compact design. This design allows for a relatively larger rod area when compared to those reported in the literature (Type I).
2. Two different methods of interconnections are proposed for the compact strut to realize enhanced roll stiffness and damping properties. Analytical formulations on the basis of fluid flows through orifices and interconnecting pipes are presented for both interconnections. Analytical formulation for the reported struts and interconnection are also derived in order to derive their relative properties.
3. The static and dynamic properties of different unconnected and interconnected suspension systems are derived analytically and compared in terms of load-carrying capacities, suspension rates, roll stiffness and vertical and roll mode damping characteristics. The fundamental bounce and roll properties of different suspension are discussed in view of their potential for achieved improved ride and handling performances.

4. The ride and handling performance characteristics of these hydro-pneumatic suspension systems are investigated under deterministic centrifugal force and transient road excitations.
5. The ride properties of different suspension properties are further investigated under in-plane and out-of-plane harmonic excitations, and random road excitations.

6.3 CONCLUSIONS

Following major conclusion could be drawn on the basis of simulation results obtained for the different suspension configurations considered in this dissertation research:

- A hydro-pneumatic suspension with integrated gas chamber (Type II) yields a compact design and increased working area thereby reducing the operating pressure requirement and the size.
- The Type II strut offers two different alternatives for realizing roll-plane interconnections.
- The interconnection between the left- and right-struts in the roll plane offer significant potential for tuning of roll stiffness and damping properties of the suspension.
- The interconnected suspensions yield a negative feedback effect associated with flows through the interconnecting pipes. This feedback could affect influences the roll mode damping alone most significantly.

- The contribution due to the feedback effect to the roll mode damping strongly depends upon the associated working area and size of the interconnecting tube. A large working area, as in the case of Inc3 suspension, yields considerable potentials for tuning the roll mode damping properties.
- The feedback effect is less pronounced when the associated working area is small, as in the case of Inc1 and Inc2 suspensions.
- The ride and handling performance characteristics of concepts in interconnected hydro-pneumatic suspension can be effectively investigated from the simplified roll plane model of the vehicle.
- An anti-roll bar can be modeled as a torsion spring, which introduces and auxiliary roll stiffness when sprung mass experiences a relative roll motion with respect to unsprung mass.
- Under pure vertical motions, the interconnected suspension yield spring rates identical to those of the unconnected suspension. The interconnected suspension, however yield considerably higher roll stiffness to realize improved handling performance.
- The interconnected suspension involving interconnections between the piston and rod chambers (Inc3) yield roll stiffness identical to that of the unconnected struts. This configuration however yields considerably superior damping properties to realize a better compromise between ride and handling performance.

- The roughness characteristics of right- and left-tracks of a road lane could be used to derive the random road excitation due to cross-slope of the road.
- The roughness of the right-track of an urban road is observed to be considerably higher than the left track due to presence of drain covers and road damage caused by frequent stopping and acceleration of urban buses in the curb lane.
- The ride dynamic responses of the vehicle to random excitations of an urban road revealed that Inc3 suspension with relatively light damping offers better ride quality than other suspension configuration.
- Unlike the unconnected suspensions, the interconnected suspension (Inc1 and Inc2) yield considerably higher stiffness and damping in the roll mode.
- High suspension damping tends to improve handling performance of vehicle, while light suspension damping yields improved shock and vibration attenuation performance.
- A vehicle suspension with identical bounce rate and enhanced roll stiffness can be achieved from the interconnected struts. The interconnected suspension can thus provide a better compromise between handling performances and ride comfort. Damping control valves, however would be required to achieve multi-stage damping for enhancement of vehicle ride quality.

- While an anti-roll bar effectively restricts the body roll motion, tends to increase the roll response of the vehicle when subject to a single-wheel bump.

6.4 RECOMMENDATIONS FOR FUTURE WORK

This thesis research is carried out to evaluate the roll and ride dynamic performance of different concepts in interconnected hydro-pneumatic suspension systems. In view of the significant potentials demonstrated in this study, it is recommended to undertake the further investigations to fully explore their performance potentials through integration of damping control valves, development of more comprehensive models, and development of more comprehensive models, and prototype development and testing.

The analytical model of the interconnected suspension needs to be validated through fabrication and testing of a prototype in a laboratory setting. Efforts are needed to incorporate fluid compressibility, inlet and outlet flow losses of interconnecting pipes and variable damping valves to achieve more desirable damping properties.

The stiffness and damping properties of interconnected struts are related to various geometric parameters in a highly complex manner. These configurations however offer ample possibilities for tuning of the suspension, which should be thoroughly explored through extensive parametric studies.

A more elaborate three-dimensional vehicle model, incorporating fluid flow interconnections in the roll and pitch planes, should be developed and analyzed

to assess the ride, anti-roll and anti-pitch characteristics of the vehicle suspension.

An optimal design of interconnected hydro-pneumatic system should be carried out to achieve a better compromise between the vibration isolation and handling performance.

Efforts should be made to incorporate self-leveling ability of interconnected hydro-pneumatic suspension to achieve even better ride comfort and handling performance of the vehicle.

The semi-active and active control methods could be integrated into the interconnected suspension to enhance the roll stability. It may be beneficial to provide the interconnections only for low frequency roll motions caused by centrifugal forces and moments, which influence the vehicle handling performance.

REFERENCES

0AHMCT Research Report. 2002. Simulation of cranes using a boom support vehicle. University of California at Davis, California Department of Transportation

Alleyne, A., and Hedrick, J.K. 1995. Nonlinear adaptive control of active suspensions. IEEE Trans. Control Syst. Technol., vol 3. no.1, pp. 94-101.

Alleyne, A. and Hedrick, J.K. 1992. Nonlinear control of a quarter car active suspension. Proc. Amer. Contr. Conf, pp, 21-25, Chicago.

Anders Forsén. 1999. Heavy vehicle ride and endurance-Modelling and model validation. Ph.D Dissertation. Department of Vehicle Engineering Royal Institute of Technology. Stockholm 1999

Anonymous. 1979. Agricultural wheeled tractors and field machinery – Measurement of whole-body vibration of the operator. ISO5008:1979. Geneva, Switzerland: International Organization for Standardization.

Bastow, B. 1987. Car suspension and Handling. Pentech Press Limited, London.

Beard, D, Karnopp D.C., Sahm, D., Scarpatetti, D. 1992. Hydraulically actuated suspension system for motor vehicles. Daimler-Benz AG German Patent DE 4231641A

Campos, et al. 1998. Active Suspension Control of Ground Vehicle Heave and Pitch Motions. Automation and Robotics Research Institute. A report prepared for the University of Texas at Arlington.

Cebon D. 1993. Interaction between heavy vehicles and roads. SAE SP–951, 1993, SAE paper No. 930001.

Cech,I. 1987. A slow-acting in-series' active suspension. Vehicle System Dynamics. 1987 vol. 16, No. 1, pp. 17-26.

Chon, Jae-Choon et. 2001. A new design of active suspension system for low energy vonsumption and good ride comfort. 8th IEEE Conference on Mechatrinics and Machine Vision in Practice. Hong Kong

Cotterell, M. 1975. Theoretical analysis of an active suspension fitted to a London transport bus. Chapter 14 of Stress, Vibration and Noise Analysis In Vehicles, Ed.Gibbs,H.G. and Richards, T.H. Applied Science Publications, London.

Cooperrider, N. K., Thomas, T. M., and Hammoud, S. A. 1990. Testing and analysis of vehicle rollover behavior. SAE Transactions, pp. 518–527, 1990.

Darling, J. and Hickson, L.R. 1998. An experimental study of a prototype active anti-roll suspension system. Vehicle System Dynamics. pp. 309-329.

Engelman, G.H., and Rizzoni, G. 1993. Inclosing the force generation process in active suspension control formulation. Proc. Amer. Contr. Conf. pp.701-705, San Francisco CA, June.

Ervin, R.D. 1983. The influence of size and weight variables on the roll stability of heavy duty trucks. SAE paper: 1983 No.831163, Society of Automotive Engineering, Warrendale PA.

Felez, J. and Vera, C. 1987. Bond graph assisted models for hydro-Pneumatic suspensions in Crane vehicles. Vehicle System Dynamics. vol 16, pp. 313-332.

Frank, R. Joo. 1991. Dynamic analysis of a hydro-pneumatic suspension system. A Thesis of Master Degree. Concordia University.

Fraser, I.H. 1982. Mathematical modeling of a passive and semi-active hydro-pneumatic suspension system applied to a single wheel station. Royal Military College of Science. Shrivenham

Gillespie, T.D. 1992. Fundamentals of vehicle dynamics. Society of Automotive Engineers, Warrendale, Pennsylvania.

Hac Aleksander,. 2002. Rollover stability index including effects of suspension design. SAE Technical Paper Series: 2002-01-0965.

Horton, D.N.L. and D.A. Crolla. 1984. Designing off-road vehicles with good ride behavior. Proceedings of the 8th International Conference of the ISTVS 1:171-184. Amsterdam, The Netherlands: Elsevier Science.

Horton, D.N.L. and Crolla, D.A. 1986. Theoretical Analysis of a semi-active suspension fitted to an off-road vehicle. Vehicle System Dynamics. vol 15, pp. 351-372.

Ikenaga S., F. L. Lewis, L. Davis, J. Campos, M. Evans and S. Scully. 1999. Active suspension control using a novel strut and active filtered feedback: Design and implementation. Proceedings of the 1999 IEEE International Conference on Control Applications

Jacobsen, L. S. and Robert S. 1958. Engineering Vibrations, McGraw-Hill Book Company, New York

King, R.I. and Crolla, D.A. 1998. Flexible and efficient model development and analysis for road vehicle dynamics using a modular approach. Proc, 4th International Symposium on Advanced Vehicle Control, pp. 547-551, Nagoya, Japan.

Kitching K.J., Cole D.J. and Cebon D. 1998. Performance of a semi-active damper for heavey vehicles. ASME Journal of Dynamic Systems Measurement and Control. June, 1998.

Lang, R. and Walz, U. 1991. Active roll reduction. Proc. EAEC 3rd International Conference On Vehicle Dynamics and Power Train Engineering. EAEC No.91059, Strabburg.

Lin, J.S., and Kanelladopoulos, I. 1997. Nonlinear design of active suspensions. IEEE Control Systems Magazine, vol. 17, no. 3, pp.45-59.

Liu Peijun. 1994. An analytical study of ride and handling performance of and interconnected vehicle suspension. A dissertation for master degree. Concordia University.

Michael W. Sayers and Steven M. Karamihas. 1998. The little book of prodiling (Basic information about measuring and interpreting road profiles). The regent of the University of Michigan.

Moulton, A.E. and Best, A. 1979. Hydragas Suspension. SAE Paper SAE-790374.

Newton, K. 1989. The Motor Vehicle. Butterworth, Eleventh edition, London.

Packer, M.B. 1978. Active ride control–a logical step from static vehicle attitude control. Society of Automotive Engineers, 780050.

Pevsner, J.M. 1957. Equlizing types of suspension. Automobile Engineer.

Pitcher, R.H., Hiller, H. and Curtis, C.H. 1977. Hydraulic suspensions with particular reference to public service vehicles. The Design Construction and Operation of Public Service Vehicles. Paper No C138/77, Mech.E. Conference.

Probert, S.T. 1984. Computer modeling investigation of a semi-active monocycle and vehicle suspension system. Branch Note VS1-6/84, Royal Armament Research and Development Establishment. Chertsey.

Rakheja, S. Sankar, S. and Ranganthan, R. 1987. Roll plane analysis of articulated tank vehicles during steady turning. Vehicle System Dynamics, vol 17, No. 2, pp. 81–104.

Rakheja, S. Sankar, S. and Ranganthan, R. 1989. Influence of tank design factors on the roll-over threshold of partially filled tank vehicles. SAE Transactions, pp. 536-547.

Rideout, G. & Anderson, Ronald J. 2003. Experimental testing and mathematical modeling of the interconnected hydragas suspension system. Society of Automotive Engineers.

Rosam, N. and Darling, J. 1997. Development and simulation of a novel roll control system for the interconnected hydragas suspension. Vehicle System Dynamics, 1997, 27 pp.1-18.

Sampson Matthew David, John. 2000. Active roll control of articulated Heavy vehicles. The degree of doctor of philosophy dissertation. Cambridge University Engineering Department.

Sanjeev Chaudhary. 1998. Ride and roll performance analysis of a vehicle with spring loaded interconnected hydro-pneumatic suspension. A thesis of master degree. Concordia University.

Sayers Michael W. and Karamihas Steven M.. 1996. Interpretation of interpretation of road roughness profile data. Federal Highway Administration. UMTRI 96-19

Sayers, M.W. and Riley, S.M. 1996. Modeling assumptions for realistic multi-body simulations of the yaw and roll behaviour of heavy trucks, SAE Transactions, pp.72-83.

Schmitz, G.W. 2000. Seal arrangement for a central tire inflation system. U.S. Patent No. 6,145,558

Schroeder, Jr, Donald W. 1985. A tutorial on pipe flow equations. Oil and Gas Journal. April 1, 1985.

Sharp, R.S. and Pan, D. 1992. On active roll control for automobiles. Vehicle System Dynamics. Swets and Zeitlinger, Lisse, Netherlands.

Sharp, R.S. and Pan, D. 1993. On the design of an active roll control system for a luxury car. Proc. Inst. Mech. Eng, vol. 207, pp.275-283.

Su, Hong. 1990. An investigation of vibration isolation systems using active, semi-active and tunable passive mechanisms, with applications to vehicle suspensions. A dissertation for doctor degree. Concordia University.

Suresh, B.A. and Gilmore, B.J. 1994. Vehicle model complexity-how much is too much? Automotive Simultaneous Engineering, number 940656 in SP-1035. SAE, Warrendale, PA, USA.

Wong, J.Y. 1991. Theory of ground vehicles. John wiley & Sons, Inc.

http://www.m-100.org/6point9/brochure/suspension/